UNCLASS
SECURITY CLASSIFICATION OF THIS PAGE (When Data Entered)

AFIT-CI-

REPORT DOCUMENTATION PAGE

READ INSTRUCTIONS BEFORE COMPLETING FORM

1. REPORT NUMBER	2. GOVT ACCESSION NO	3. RECIPIENT'S CATALOG NUMBER
81-6D	AD-A101627	627

4. TITLE (and Subtitle)
Lithium: Cryptand 2.1.1 Electrides: A Study of Some Magnetic and Optical Properties.

5. TYPE OF REPORT & PERIOD COVERED
THESIS/DISSERTATION

6. PERFORMING ORG. REPORT NUMBER

7. AUTHOR(s)
John Steven Landers

8. CONTRACT OR GRANT NUMBER(s)
Doctoral Thesis

LEVEL II

9. PERFORMING ORGANIZATION NAME AND ADDRESS
AFIT STUDENT AT: Michigan State University

10. PROGRAM ELEMENT, PROJECT, TASK AREA & WORK UNIT NUMBERS

11. CONTROLLING OFFICE NAME AND ADDRESS
AFIT/NR
WPAFB OH 45433

12. REPORT DATE
1981

13. NUMBER OF PAGES
208

14. MONITORING AGENCY NAME & ADDRESS(if different from Controlling Office)

15. SECURITY CLASS. (of this report)
UNCLASS

15a. DECLASSIFICATION/DOWNGRADING SCHEDULE

16. DISTRIBUTION STATEMENT (of this Report)
APPROVED FOR PUBLIC RELEASE; DISTRIBUTION UNLIMITED

DTIC ELECTE JUL 21 1981 S D F

17. DISTRIBUTION STATEMENT (of the abstract entered in Block 20, if different from Report)

18. SUPPLEMENTARY NOTES
APPROVED FOR PUBLIC RELEASE: IAW AFR 190-17
23 JUN 1981

Fredric C. Lynch
FREDRIC C. LYNCH, Major, USAF
Director of Public Affairs
Air Force Institute of Technology (ATC)
Wright-Patterson AFB, OH 45433

19. KEY WORDS (Continue on reverse side if necessary and identify by block number)

20. ABSTRACT (Continue on reverse side if necessary and identify by block number)
ATTACHED

DD FORM 1 JAN 73 1473 EDITION OF 1 NOV 65 IS OBSOLETE

UNCLASS
SECURITY CLASSIFICATION OF THIS PAGE (When Data Entered)

AD A101627

DTIC FILE COPY

81 7 16 006

Accession For
NTIS GRA&I
DTIC TAB
Unannounced
Justification
By
Distribution/
Availability Codes
Dist | Avail and/or Special
A

ABSTRACT

LITHIUM : CRYPTAND 2.1.1 ELECTRIDES: A STUDY OF SOME MAGNETIC AND OPTICAL PROPERTIES

By

John Steven Landers

Dark blue microcrystalline powders produced from lithium metal and the cation complexing agent cryptand 2.1.1 (C211) were prepared from ammonia and from methylamine solutions. The mole ratio of lithium to cryptand, R, was varied from 0.60 to 2.0 but there was no evidence for Li^-. The optical and magnetic properties indicate that $Li^+C211 \cdot e^-$ is an electride, a member of the class of materials in which the anions are electrons. Samples were studied by optical transmission spectroscopy, EPR spectroscopy, magnetic susceptibility, and microwave and D.C. conductivities. In many cases several methods were used to characterize samples prepared from the same solution; correlation among the various properties is high.

Solvent-free films consisting only of lithium metal

flecks deposited by ammonia or methylamine evaporation did not show any optical absorption. However, when the flecks are allowed to absorb solvent, the spectra show a plasma edge typical of concentrated metal-ammonia solutions. Solvent-free films from solutions containing both lithium and C211 have properties which depend upon the lithium to cryptand mole ratio, R. Films from solutions with R < 1.15 have an absorption spectrum with low absorbance below 4000 cm^{-1}, peaks at 5000 cm^{-1} and 7000 cm^{-1} and a high energy shoulder at $\sim$12,000 cm^{-1} indicating electron localization in several different non-equivalent environments. Annealing the films increases the infrared absorbance below 5000 cm^{-1}. On the other hand, spectra from films with R = 2 show a conduction electron plasma edge and high absorbance below 5000 cm^{-1}. Two $Li^{+}C211 \cdot e^{-}$ systems with R = 0.94 also showed metallic character, one throughout the range -35° to -70°C and the other above -45°C. This apparent metal-nonmetal transition at -45°C was confirmed by EPR spectroscopy and microwave conductivity. Why these two systems showed metallic character while three other systems at the same mole ratio did not is uncertain.

EPR spectra of $Li^{+}C211 \cdot e^{-}$ systems generally show the following: g-values at or near the free electron value, 2.00232; narrow spectra with ΔH_{p-p} $\sim$0.15 - 0.6 Gauss; A/B ratios less than 1.25; and no free lithium metal. Samples that showed multiple absorptions in the optical spectra

also showed multiple EPR peaks below about 30K. The number of unpaired spins in the samples was determined by comparison with a ruby spin standard. "Metallic" samples have significantly less than 1% of their spins unpaired whereas 30% to 100% of the spins are unpaired in nonmetallic samples at 235K. At least two reversible temperature-dependent spin-pairing processes were observed in several samples with pairing energies of approximately 30 cal/mole and 100 cal/mole. The pairing is virtually complete by 3K.

These results were verified by static magnetic susceptibilities which showed maxima in their temperature dependence. Maximum susceptibilities varied from 5. x 10^{-3} esu/mole at 20K to 0.7 x 10^{-3} esu/mole at 70K, depending upon the lithium content. In all cases the susceptibilities dropped sharply at liquid helium temperatures. At high temperatures the susceptibility curves fit the Curie-Weiss law rather well and indicate the presence of about one unpaired electron per lithium. This confirms that essentially all of the electrons in the samples participate in the spin-pairing process.

The optical spectra of solvent-free films of $K^+C222 \cdot e^-$ also showed metallic character while films of $Na^+C222 \cdot e^-$, $Rb^+C222 \cdot e^-$ and $Cs^+C322 \cdot e^-$ generally showed localized (nonmetallic) electron absorptions. Even with R < 1, the Rb/C222 system showed an anion absorption peak. The mixed alkalide systems $Li^+C211 \cdot Na^-$ and $Cs^+C322 \cdot Na^-$ showed strong Na^- absorptions at about 13,800 cm^{-1}.

AFIT RESEARCH ASSESSMENT

The purpose of this questionnaire is to ascertain the value and/or contribution of research accomplished by students or faculty of the Air Force Institute of Technology (ATC). It would be greatly appreciated if you would complete the following questionnaire and return it to:

AFIT/NR
Wright-Patterson AFB OH 45433

RESEARCH TITLE: Lithium: Cryptand 2.1.1 Electrides: A Study of Some Magnetic and Optical Properties

AUTHOR: John Steven Landers

RESEARCH ASSESSMENT QUESTIONS:

1. Did this research contribute to a current Air Force project?

( ) a. YES ( ) b. NO

2. Do you believe this research topic is significant enough that it would have been researched (or contracted) by your organization or another agency if AFIT had not?

( ) a. YES ( ) b. NO

3. The benefits of AFIT research can often be expressed by the equivalent value that your agency achieved/received by virtue of AFIT performing the research. Can you estimate what this research would have cost if it had been accomplished under contract or if it had been done in-house in terms of manpower and/or dollars?

( ) a. MAN-YEARS _____ ( ) b. $_____

4. Often it is not possible to attach equivalent dollar values to research, although the results of the research may, in fact, be important. Whether or not you were able to establish an equivalent value for this research (3. above), what is your estimate of its significance?

( ) a. HIGHLY SIGNIFICANT ( ) b. SIGNIFICANT ( ) c. SLIGHTLY SIGNIFICANT ( ) d. OF NO SIGNIFICANCE

5. AFIT welcomes any further comments you may have on the above questions, or any additional details concerning the current application, future potential, or other value of this research. Please use the bottom part of this questionnaire for your statement(s).

NAME GRADE POSITION

ORGANIZATION LOCATION

STATEMENT(s):

LITHIUM : CRYPTAND 2.1.1 ELECTRIDES : A STUDY OF SOME MAGNETIC AND OPTICAL PROPERTIES

By

John Steven Landers

A DISSERTATION

Submitted to
Michigan State University
in partial fulfillment of the requirements
for the degree of

DOCTOR OF PHILOSOPHY

Department of Chemistry

1981

to a speedy reunion

with Michael

ACKNOWLEDGMENTS

In the pursuit of a degree, one is indebted to many organizations and people for their assistance. My gratitude extends to a multitude with some deserving specific mention. Thanks go to the United States Air Force and the Air Force Academy Department of Chemistry for sponsoring this educational opportunity. Professor James L. Dye's ability to blend encouragement and direction were vital to my completing the program. Of the colleagues in the research group, Dr. Mike DaGue provided tutelage on low temperature, high vacuum techniques, while Brad Van Eck was extremely helpful as the backbone of the group. I also appreciated the aid and advice of Dr. Harlan Lewis, Dr. Long Dinh Le and Mike Yemen. The cheerful help of undergraduates Holly Lystad, Jeff Gulcher, Jim Anderson and Steve Hillson is acknowledged.

I appreciated the warm hospitality of Cornell University's Dr. Michael J. Sienko and his research group, especially Angy Stacy. Their aid with magnetic susceptibility measurements has proven very important in confirming what we believe about lithium-cryptand systems. Thanks also to Drs. William Pratt and Jerry Cowen of the M.S.U. Department of Physics who built a magnetic susceptometer for this study.

MSU's technical and clerical staff deserve thanks also, especially glassblowers Keki Mistry, Jerry DeGroot and Andy Seer for their excellent and timely service, the very skilled machinists Dick Menke and Len Eisle, electronics designer Marty Rabb, and secretary Naomi Hack for her care and concern.

Above, all Sherry's patience, help and understanding have been vital to me.

Last, and definitely least, thanks to MSU for all its power outages, each one carefully timed for the most inopportune moment, and for The Great Parking Hassle, ultimately (?) won by Professor Horne.

Research support from NSF under Grant Number PCM-78-15750 is gratefully acknowledged.

TABLE OF CONTENTS

LIST OF TABLES

LIST OF FIGURES

INTRODUCTION

The study of solutions and compounds prepared with alkali metal cations and cyclic polyethers is less than twelve years old, but it is based upon the nearly 120-year-old study of alkali metals in ammonia. From the original work of Weyl on the ammonia solutions of potassium and sodium (1) in the 1860s, the research has burgeoned, reaching the point in the past several decades that a number of international conferences have been held on the general subject. One series of five conferences whose proceedings have been published bears the title "Colloque Weyl" in honor of the original researcher. These and other conferences, review articles and important works in this field are listed in Reference 2.

A branch of this research was propagated in the early 1970s by Dye and coworkers who demonstrated the tremendous solubility enhancement that cyclic polyethers provide for alkali metals in amine and ether solvents (3-5). This work led to further growth: the isolation of solvent-free compounds of alkali metals and cyclic polyethers, including the single crystal *x*-ray structure of one such compound (6). The research presented herein is an offshoot of this rapidly growing and interesting branch concerning the effects of

cyclic polyethers on alkali metals.

A review of concentrated metal-ammonia solutions as well as metal-ammonia and metal-methylamine compounds provides some background for the current work. Because the subject compound, lithium : cryptand 2.1.1 electride, has electrons in its structure which are independent of the lithium cation core, the compound is somewhat similar to low temperature glasses containing trapped electrons. These glasses will be discussed, followed by a description of F-centers which consist of electrons trapped in anionic vacancies in crystalline salts. Lithium cryptand 2.1.1 electride may be thought of as an F-center material in which all anions are replaced by electrons. In some cases the electron density becomes sufficient to cause the compound to undergo a transition to metallic character, but it is not clear which factor(s) control the metal-nonmetal transition observed in this study. Several theories describing such a transition will be very briefly mentioned.

I.A. Metal-Ammonia Solutions

Metal-ammonia ($M-NH_3$) solutions can be divided, somewhat arbitrarily, into three classifications according to the concentration of the dissolved metal. Generally solutions of one mole percent metal (MPM) or less are electrolytic in nature, those between 1 and 8 MPM show variable character which places them in the metal-nonmetal (MNM)

transition region, and those above 8 MPM are metallic. The concentration region of the DND transition may vary depending upon the property being observed, but the crossover is generally complete by 8 MPM. Optical spectra of concentrated M-NH_3 solutions have generally been obtained by reflectance techniques. Figure 1 shows the reflectance spectra of Na-NH_3 solutions in the intermediate and concentrated regions (7). As the concentration of metal rises above 5.6 MPM, the reflectance spectra show a very sharp drop at the plasma frequency which is a collective resonance of the conduction electrons. Concentrated Li-NH_3 solutions show a similar response (8). The electrical conductivity of Li-NH_3 solutions in this region increases approximately as the cube of the metal concentration (9). At 20 MPM it reaches nearly 1.5×10^4 $(ohm\text{-}cm)^{-1}$, but not until this very concentrated region does $\partial\sigma/\partial T$ become negative as expected for a true metal.

Electron paramagnetic resonance (EPR) spectroscopy of M-NH_3 solutions shows an onset of metallic character at relatively low concentrations. In 1963 Vos noted a distinct change in the A/B ratio to that characteristic of metallic systems (10). Two years later Catterall determined that the A/B change occurs at 0°C in a 0.86 MPM solution of Cs in NH_3 and at higher temperatures in solutions of even lower concentration (11). (A and B are the respective amplitudes of the low and high field lobes of first derivative EPR

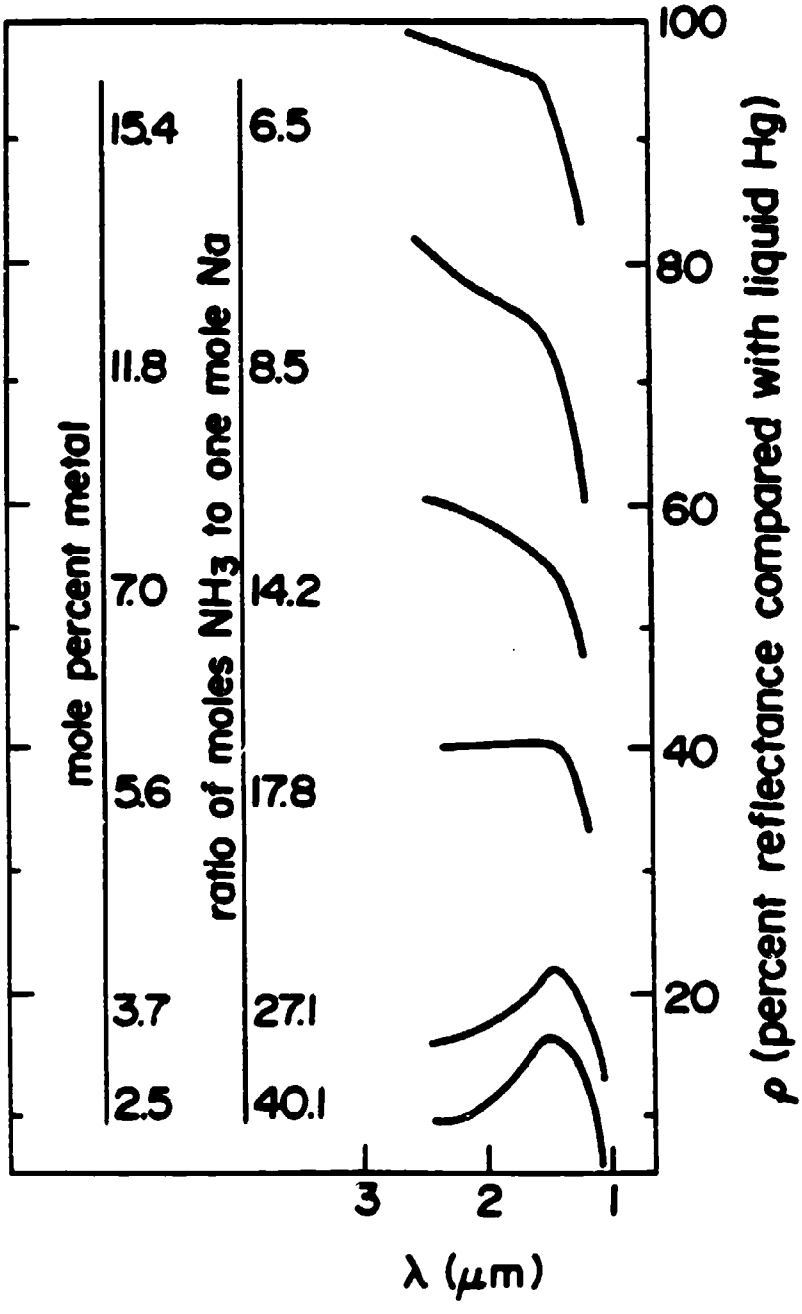

Figure 1. Reflectance spectra of Na-NH_3 solutions from Reference 7.

spectra which will be discussed in greater detail in Section I.B.) Lelieur showed that the linewidth, ΔH_{p-p} (where "$_{p-p}$" indicates the width in Gauss between the first derivative peaks) for Na-NH_3 increases from 30 mG in dilute solutions to about 5 G at 10 MPM (12). This rapid increase in ΔH_{p-p} may be due to the increase in electrical conductivity associated with the more concentrated solutions (13). Static susceptibilities are diamagnetic but become less so as the M-NH_3 solutions become metallic, although they never lose their weak temperature dependence (14-16). The effect of the concentrated metal is never sufficient to overcome ammonia's diamagnetism.

I.B. Metal-Amine Compounds

Of the alkali metal-ammonia systems which Marshall studied, only the saturated Li-NH_3 system showed a dramatic decrease in the solution vapor pressure as the lithium mole fraction was increased (17). This strongly implies the existence of a compound $Li(NH_3)_4$ since the mole fraction of lithium in the saturated NH_3 solution is 0.20. In fact a metallic compound with stoichiometry $Li(NH_3)_4$ is formed when a 20 MPM solution is frozen at ~89K. Compounds $M(NH_3)_6$ have also been identified where M is Ca, Sr, Ba, Eu and Yb (12). The $Li(NH_3)_4$ compound is face centered cubic between 82 and 88K, with a transition to a hexagonal structure below 82K. Magnetic susceptibility measurements

show that the hexagonal phase obeys the Curie-Weiss law to 15K. The optical spectra are similar to those of the liquid (12). Evidence suggests that, unlike the hexagonal phase, the cubic phase exhibits nearly-free-electron (NFE) behavior (18). By freezing a Li-NH_3 solution more dilute than 0.2 MPM, the cubic phase can be stabilized well below its normal 82-88K range. Studies over the expanded temperature range confirm the metallic character of the cubic phase (18).

In their studies of cubic $Li(NH_3)_4$ by EPR, Glaunsinger and Sienko used a theoretical lineshape equation derived by Dyson and extended by Webb to analyze the data for their metallic samples. In 1955 Dyson solved the theoretical equations accounting for the diffusion of conduction electrons into and out of the region penetrated by the EPR radio-frequency (rf) field (19). For a metallic sample which is thick compared to this rf skin depth, δ, the EPR lineshape assumes a characteristic asymmetric shape now commonly known as Dysonian in which $2.7 < A/B < 20$. The theoretical shape, which also depends upon the electronic diffusion (T_D) and relaxation (T_2) times, was confirmed experimentally by Feher and Kip, also in 1955 (20). Two years later Webb extended Dyson's derivation for use with spherical particles in the region of the normal skin effect (21). Several conclusions can be drawn from this extension: metallic particles whose radii, a, are large

compared to δ will still have a nearly symmetric EPR signal ($A/B \sim 1$) if $T_D >> T_1$ where $T_1 = T_2$ in a metal; and of more practical importance in the current study, even though the sample may be metallic, if the sample particle sizes are small compared to the skin depth ($a/\delta < 1$), the EPR signal will be very nearly symmetric. The Dyson theory was extended to the region of the anomalous skin effect by Kittel (20). In this case the mean free path of the conduction electrons is long compared to the skin depth, δ. Assuming $T_D << T_1$ then $A/B = 5$ invariably.

Glaunsinger and Sienko's $Li(NH_3)_4$ cubic phase data were in excellent agreement with Dyson's equation as extended by Webb and at 120K the liquid droplets of $Li(NH_3)_4$ dispersed in solid NH_3 yielded symmetric Lorentzian lineshapes. In both cases they were able to draw conclusions about T_1 relaxation times and mechanisms. Li-methylamine (MA) systems have also been studied in Sienko's laboratory and to date the existence of $Li(MA)_4$ has only been inferred (22). In that work the lineshapes had an asymmetry $1 < A/B < 2.7$, so the authors used a direct interpolation between Lorentzian and Dysonian lineshape functions to extract relaxation times (23,24).

Before leaving the metal-amine subject, an interesting result from $Ca(ND_3)_6$ studies is worthy of mention. The crystal structure of $Ca(ND_3)_6$ determined by powder neutron diffraction shows highly distorted ND_3 molecules arranged

in an exact octahedron around the Ca (25). One N-D bond is 0.94Å while the other two are 1.4Å. The ND_3 molecule is flatter than normal with D-N-D angles of 122° and 115° compared to the 110° angles of solid ND_3. Finally the pseudotrigonal axis of each ND_3 is not coincident with the Ca-N bond but makes a 13° angle with it. This result has subsequently been found true for $M(ND_3)_6$ where M is also Sr, Ba and Yb (26). Glaunsinger believes the novel ND_3 structure may somehow be stabilized by the presence of itinerant electrons (27). These structures are very interesting, but as Thompson has harshly remarked about $Li(NH_3)_4$ (which could apply equally well to all the metal-amine compounds), ". . . the considerable available data is rendered nearly useless by the absence of single crystals" (28).

I.C. Electrons in Low Temperature Glasses

For several decades, "excess" electrons injected into condensed phases have been studied in an attempt to understand electron localization and solvation processes. One branch of this work has involved glassy disordered media, generally at liquid nitrogen temperatures, but more recently in the liquid helium range on the pico and nanosecond time scales.

Electrons rapidly occupy nonequilibrium or presolvated positions in the disordered matrix within nanoseconds after

injection. A minimum trap depth seems to be 0.4 - 0.5 eV (3100 - 2500 nm) (29). Then depending on the temperature, the electrons attain solvated equilibrium positions on a microsecond scale (30). The mechanism is molecular reorientation of the solvent; the electrons apparently do not hop site-to-site in search of deeper equilibrium traps (31). In the optical spectra the presolvated electron absorption in the near infrared shifts into the visible as the electron forces molecular reorientation around itself. In the case of C_2H_5OD, the electron finally attains four tetrahedrally arranged solvent molecules at equilibrium (32). Willard has conducted a series of bleaching experiments in which the optical density in the near infrared is reduced at the bleaching wavelength and longer but the remainder of the spectrum is unaffected. However, at 1064 nm and shorter wavelengths, the entire spectrum is bleached uniformly because all e_t^- apparently have high energy tails. There is no subpopulation with sufficient nonoverlapping spectra to allow deep hole burning (33). In some cases molecular reorientation does not occur until the glass is annealed, typically at 77K. After the irreversible shift, the narrow singlet EPR signal with a g-value near that of the free electron does not change, indicating a symmetrical equilibrium environment for the electron. As the matrix becomes more polar, ΔH_{p-p} increases because of hyperfine interaction of the electron with atoms along the trap

walls (34).

Several solvated equilibrium structures in glasses have been reported. In 1975 Willard presumed that, because the optical spectrum of electrons trapped in 2-methyltetrahydrofuran (MTHF) had three distinct peaks, the structure probably contained three different discrete orientations of MTHF, each with a different trap depth (34). In 1980 Kevan reported the structure as an electron surrounded by three MTHF molecules whose planes are perpendicular to the electron. The MTHF molecules are oriented statistically with either side of the ring toward the center, causing multiple environments for the electron, with the closest proton at 3.4Å from the electron. Kevan also reports that electrons in an aqueous glass create an octahedral structure with one O-H bond of each molecule pointed at the electron 2.1Å distant. In methanol glass the solvation shell is 4 ± 2 molecules with an electron-to-hydroxyl proton distance of 2.28 ± 0.15Å. Again the O-H bond points at the electron (29).

In mixed matrix glasses, there is one optical peak which shifts position according to the mole fraction of the solvents if the solvents are composed of similar types of molecules. If the molecules are sufficiently different there will be two distinct optical peaks. Initially e_t^- is in a trap of the more abundant solvent, but it anneals to the more polar trap by stepwise changes in the solvation shell. Again this apparently occurs through solvent reorientation, not electron tunneling, although the mechanism

is not clear (29).

There are similarities in the characteristics of electrons trapped in glasses and those trapped in carbohydrate single crystals. The electron g-values are nearly those of the free electron and both systems react similarly to bleaching. On the other hand electrons trapped in carbohydrate or polyhydroxy single crystals show strong anisotropic hyperfine interactions with the hydroxyl protons 1.6 - 1.75Å distant. Also electron traps may not be as deep in these single crystals as in glasses (35). In monoclinic crystals such as rhamnose or sucrose, the electron is only in a single trapping site although many of the structures appear to offer more than one such site, according to Box (36).

There have been at least five major theoretical models proposed to describe solvated electrons in disordered systems. They have been reviewed by Feng and Kevan (37) and two of them will be briefly mentioned. In the continuum model first put on a sound theoretical basis by Jortner, a spherically symmetrical cavity is formed within a polarizable, continuous dielectric medium. In 1970 Copeland, Kestner and Jortner (CKJ) and Fueki, Feng and Kevan (FFK) proposed slightly different variations of the semicontinuum model which include both short and long range interactions. The electron is still located in the center of a spherical cavity, but it is surrounded by N solvent molecules arranged symmetrically. These molecules provide the short-range

attractive interactions with the electron necessary to account for the absolute value of the electronic energy levels (37). Outside the solvation shell is the dielectric continuum. These models as well as the others not discussed here are good to excellent in predicting optical absorption maxima as a function of matrix polarity, temperature and pressure. However the predicted optical peaks are too narrow and symmetrical compared to experimental peaks (37).

Shida et al empirically fit the absorption spectra of trapped electrons in over forty low-temperature matrices and then successfully applied the equation to the spectra of solvated electrons in liquids (38,39). The physical basis for at least one of their parameters is not clear, however. On the other hand a recent theoretical formalism has been developed by Banerjee and Simons based upon fundamental principles (40). They begin with a Hamiltonian which includes both electronic and vibrational motion of the system e_t^- plus solvent. The final absorption band shape is a function of three contributions: the largest is from a localized (bound-bound) transition and the other two arise from effects of electron hopping and fluctuations. Contributions from these nonlocalized transitions formally account for the asymmetry of the optical band (37). This model has been successfully applied to excess electrons in ethanol and in anthracene glass, indicating that perhaps it will have general application to condensed media (40).

However, Rice in a recent article concluded that EPR, photobleaching, photoconductivity, scavenger reactions and optical absorption relaxation evidence all argue strongly that electron migration from trap-to-trap does not occur (41). He did not specifically address Banerjee and Simon's formalism, nor has anyone else to date except Feng and Kevan (37).

I.D. F-Centers

An anion vacancy in an ionic lattice occupied by an electron is an F-center or color center. The most commonly studied centers are in the alkali halide single crystals, most of which have the face-centered-cubic (fcc) structure. In this NaCl-type structure the electronic wave function is shared by the six nearest-neighbor cations which are the walls of the vacancy and also to a slight degree by the twelve second-nearest neighbors (42). The room temperature optical absorption maximum varies from 250 nm for the LiF crystal which has the shortest interionic distance, to 785 nm for CsI which possesses the largest distance (43). The absorption peak is asymmetric with a high energy tail, but the asymmetry is quite minor compared to that of solvated electrons in polar and non-polar solvents. There is a slight positive shift of wavelength with temperature and a negative shift with pressure, reflecting the changes in lattice spacing.

Mollwo first recognized that the absorption wavelength was directly proportional to the square of the lattice spacing for fcc structures. Later Ivey refined the expression with a least squares computer fit of the data, yielding the Mollwo-Ivey relation: $\lambda_{max} = 703 \cdot d^{1.84}$ where d is the lattice parameter of the crystal. In the more than thirty years since this empirical formulation, others have attempted theoretical treatments. However to reproduce experimental energies, they invariably add an empirical parameter. The F-center is the simplest defect in ionic solids, yet the theoretical approach may have to include dynamic lattice effects and more detailed treatments of lattice distortion and ionic polarization before theoretically predicted energies closely approximate the experimental values (44).

The EPR linewidths are broad, typically 45 - 200 G depending upon the temperature and the system studied (45). The widths are functions of the significant hyperfine interaction of the trapped electron with the nuclear moments of the adjacent alkali ions. However, hyperfine splitting is evident only in crystals with short interionic distances. The g-values are generally 1.99 ± .02 with a much smaller deviation for a particular alkali halide. F-centers generally have a density of only 10^{16} - $10^{19}/cm^3$ so the centers only decrease the diamagnetism of the ionic lattice slightly in static susceptibility studies.

Schindewolf injected electrons into molten salts by electrolysis (46). These fluid "F-centers" are characterized by broad featureless absorption spectra with widths at half height of approximately 1250 nm (~1 eV). Peak positions undergo the expected shifts as temperature and ionic sizes are varied and the broad spectra are very similar to those of solvated electrons in polar fluids. The peak widths, three to four times greater than those in the solid, are due to the distribution of cavity sizes in the fluid (46).

I.E. The Metal-Nonmetal Transition

There is no doubt that a MNM transition occurs in many systems, for example in M-NH_3 solutions between the dilute and concentrated regions and in some metal-amine compounds. However there is disagreement about the mechanism(s) responsible for the electron delocalization/localization controlling the metallic character. Several theories will be very briefly described in simplified form.

Mott and Hubbard approached the problem from different perspectives, yet their conclusions were compatible, resulting in the Mott-Hubbard model for the MNM transition. Mott's approach (47) considers the long-range Coulombic attraction of electron-hole pairs. When screening reaches a certain magnitude, the electron is no longer bound by the attraction and it becomes itinerant. Using a screening

constant that must be smaller than the inverse Bohr radius for localized states to exist, Mott calculated his criterion for metallic conduction:

$$n^{1/3} a_H > 0.25$$

where n is the electron density and a_H is the Bohr radius. Empirically Edwards and Sienko (48) showed that this relationship is applicable to a large number of systems when using an effective Bohr radius a_H^* and a critical density n_c:

$$n_c^{1/3} \, a_H^* = 0.26$$

A system with an effective Bohr radius of 2.6Å would be at the MNM transition when its electron density reaches $10^{21}/cm^3$.

Hubbard (49) viewed the problem based upon electron repulsion at a particular site. The bandwidth of energies from the overlap of atomic wavefunctions is given by $W = 2zI$ where z is the number of nearest neighbors and I is the overlap integral of wavefunctions for adjacent electron centers. If U is the single site Coulombic repulsion energy, then when $W/U \geq 1.15$, the electrons will be itinerant. Mott concluded through another approach that $W/U \sim 1$ was indeed appropriate for the prediction of the MNM

transition, hence the theory has advanced as the Mott-Hubbard model.

Anderson's approach is one based on disorder (50). Suppose that the lattice is composed of potential energy wells of variable depth where V_o is the spread in energy. If W is the bandwidth as described in the Hubbard model, then the Anderson MNM transition occurs at $V_o/W = 5$ for $z = 6$. More recently others have placed the ratio at 2 - 4 (47). Essentially, an electron without phonon assistance is unable to find another site with the same energy within a given distance and it therefore remains localized. Possibly the MNM transition can also occur through a spatial disorder as well as or in addition to a potential energy disorder (47). Some have used a combination of Mott-Hubbard and Anderson models to explain the MNM transition in Li-CH_3NH_2 solutions (24).

I.F. Alkali Metal - Cryptand Systems

One class of macrocyclic polyether complexing agents, the macrobicyclic diamines, was synthesized by Lehn in 1969 (51). Because they are three-stranded, the molecules create their own cavity, hence the name cryptands. They are depicted in Figure 2. The numbers refer to the quantity of ether oxygens in each strand and the trival names are based upon these numbers. For example, the polyether in Figure 2 with two oxygens in each strand would

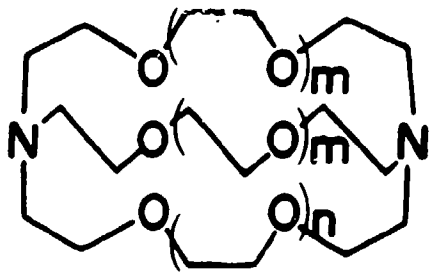

I. m = 0; n = 1 (C211)
II. m = 1; n = 0 (C221)
III. m = n = 1 (C222)
IV. m = 1; n = 2 (C322)

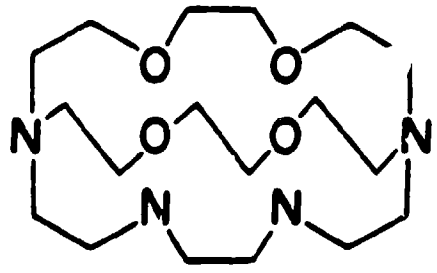

Tetraza C222 or C2N22

Figure 2. Cryptand molecular structures.

be cryptand 2.2.2 or more simply C222. IUPAC names are listed in Section II.A.1.

The large number of nitrogen and oxygen atoms lining the cryptand cavity provides a prime environment for complexing a cation. The number of ether linkages in each strand dictates the cavity size which in turn dictates the size of cation which can be readily complexed in the cavity. Figure 3 shows this selectivity as well as the high complexation constants when a cation is of optimum size for a particular cryptand cavity. The lack of selectivity among large cations by C322 (and other large cryptands) seems to result from the flexibility of the larger molecules (52).

By proper choice of alkali metal, cryptand and solvent, a solution of controlled stoichiometry can be prepared which may contain either alkali metal anions or simply electrons as the counterions for the encrypted cations. Dye has discussed the considerations and strategies for these preparations in numerous articles (53-57). When a cryptand contains a cation, the complex will be referred to as a "cryptate". When a cryptate in a solution or solid has an alkali metal counterion, the complex, $M^+C \cdot N^-$, is called an "alkalide" where N may be the same as M or different (54). An example is the alkalide $Cs^+C322 \cdot Na^-$, cesium C322 sodide. When a cryptate has a counterion which is an electron, the complex, $M^+C \cdot e^-$, is called an

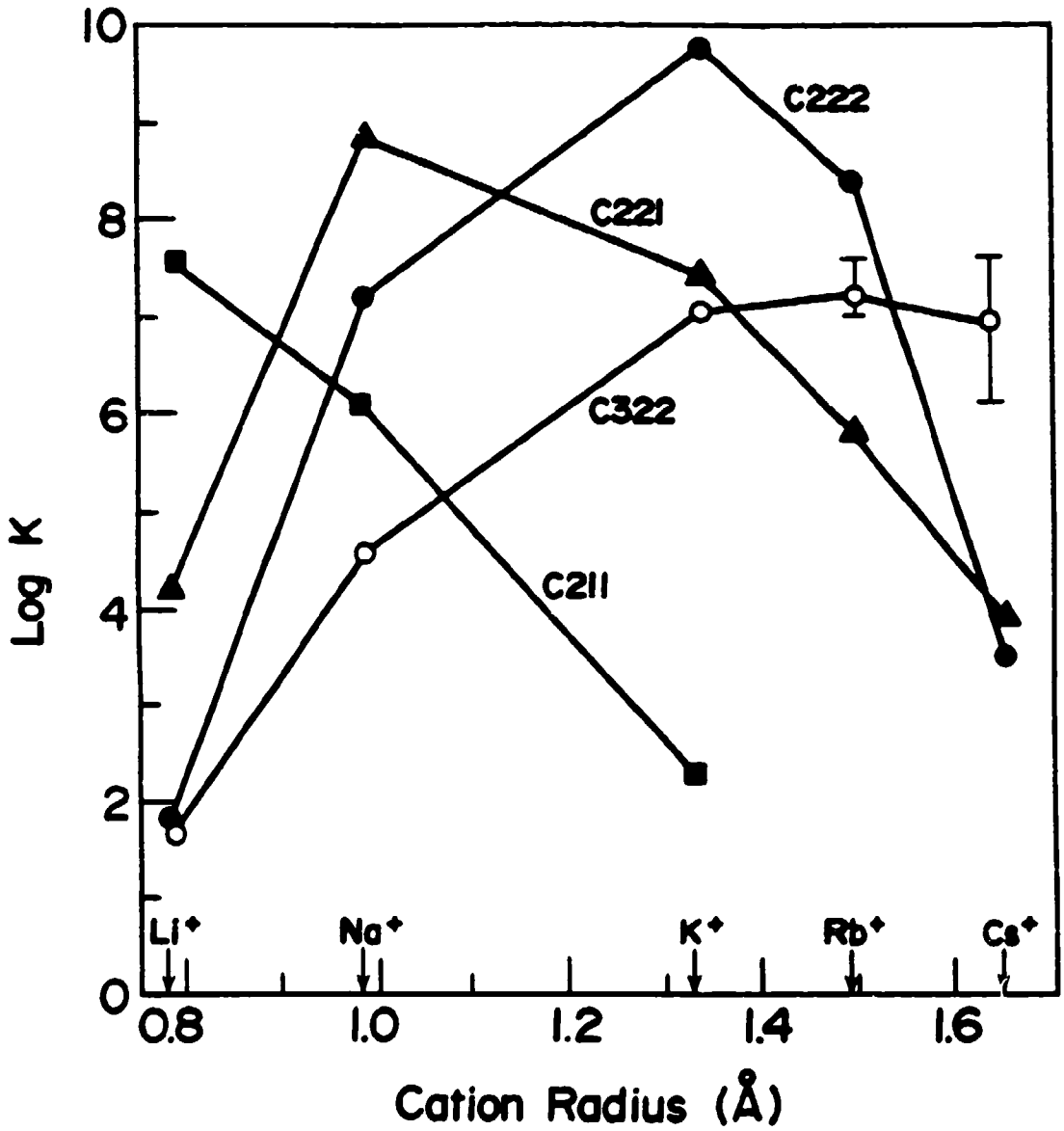

Figure 3. Selectivity and stability of various cryptand complexes with alkali metal cations in 95% methanol.

"electride" (58). The electride of importance in this study is $Li^+C211 \cdot e^-$, lithium C211 electride.

Crystals of $Na^+C222 \cdot Na^-$ were first reported in 1974 (6). An x-ray structural determination of these thin, gold-colored plates showed cubic closest-packing (59). Essentially the crystal contains closest-packed cryptate complexes with anions in the octahedral holes. The Na^- - Na^- intraplane distance is 8.8Å while the interplane Na^- - Na^- distance is 11.0Å, leading to a probable anisotropy of properties dependent upon the anion-anion distance (54). No crystal structures of electrides have been determined although paramagnetic blue powders of probable stoichiometry $M^+C \cdot e^-$ have been prepared (58,60,61). If a single crystal of $Na^+C222 \cdot e^-$ could be isolated, it is possible that its structure would also be hexagonal but with electrons occupying the octahedral holes. The effect that an unsymmetrical cryptand such as C211, C221 or C322 might have on hexagonal packing is uncertain. However, the structure of $Li^+C211 \cdot I^-$ is tetragonal, space group $P4_12_12$, with four molecular species in a unit cell of dimensions $a = b = 8.72$Å and $c = 24.36$Å (62). The iodide ion with a radius of 2.16Å would be too large to occupy the octahedral hole if the Li^+C211 cryptates were to pack hexagonally like hard spheres, but an electron could fit, of course.

The deep blue paramagnetic solid $Li^+C211 \cdot e^-$ is the primary subject of this dissertation. It is probably

more ordered than a molecular glass and it certainly has a greater density of trapped electrons. On the other hand the electride, a fully substituted F-center, is more disordered than an alkali halide F-center single crystal, but once again its trapped electron density is much higher. Because of the size of the cryptate, the electron density of the electrides is about an order of magnitude lower than that of simple metals. In this respect the electride is similar to $Li(NH_3)_4$ or $M(NH_3)_6$ compounds, which are low electron density (expanded) metals, and to the $Li(CH_3NH_2)_4$ system which undergoes a MNM transition. The majority of this thesis is devoted to the characterization of $Li^+C211 \cdot e^-$ which is nearly metallic and which upon occasion has shown a MNM transition. The remainder of the dissertation focuses on the optical spectra of alkalides and other electrides.

CHAPTER II

EXPERIMENTAL

II.A. Reagents

II.A.1. Complexing Agents

Generally the complexing agents listed below were stored in a freezer (-20°C) prior to purification. Afterwards they were stored in the dark under mechanical pump vacuum at room temperature.

2,1,1-Cryptand - (C211 or IUPAC: 4,7,13,18-tetraoxa-1,10-diazabicyclo-[8.5.5]eicosane). C211 (manufactured by E. Merck, purchased from PCR, Inc.) was purified by dynamic high vacuum distillation with the apparatus shown in Figure 4. The light-sensitive impure cryptand was placed in the apparatus below the cup. In semidarkness the cryptand was heated with an oil bath to 65 - 68°C while the cold finger was maintained at -50 ± 10°C with chilled nitrogen gas. After completion of the distillation and upon warming to 30 - 35°C, the C211 liquified and dripped into the cup attached to the cold finger. Upon cooling to room temperature, the C211 crystallized. The arms attaching the cup to the cold finger were broken and the cup was removed

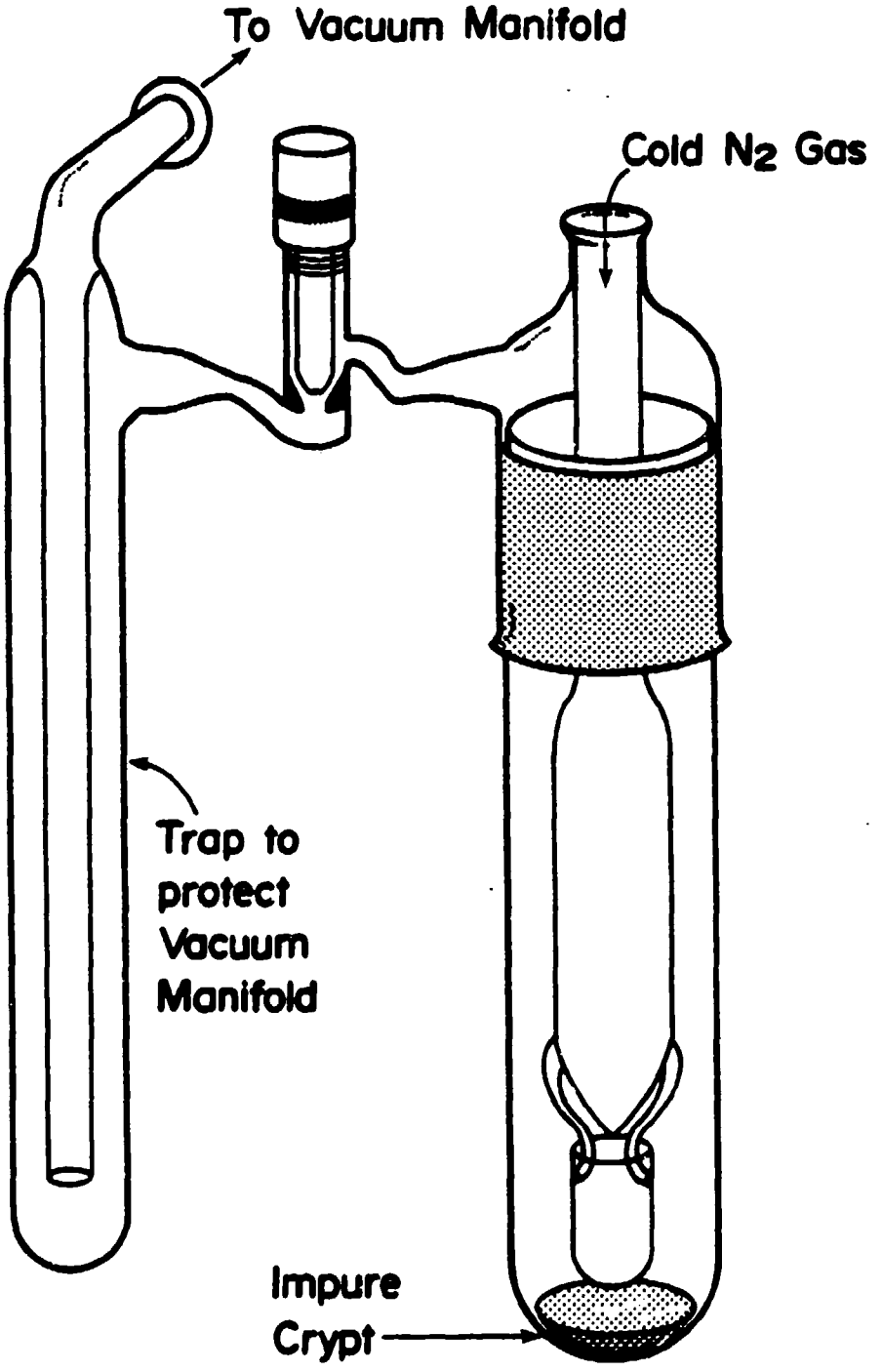

Figure 4. Liquid cryptand purification apparatus.

to storage.

2,2,1-Cryptand - (C221 or IUPAC 4,7,13,16,21-pentaoxa-1,10-diazabicyclo[8.8.5]tricosane). C221 (manufactured by E. Merck, purchased from PCR, Inc.) was only purified *in situ* in the solution preparation vessel (Figure 5). The mass of the small tubing used as a C221 weighing container increased by 2.0% of the original C221 mass after the *in situ* distillation, presumably due to C221 residue.

2,2,2-Cryptand - (C222 or IUPAC 4,7,13,16,21,24-hexaoxa-1,10-diazabicyclo[8.8.8]hexacosane). The purification of C222 (manufactured by E. Merck, purchased from PCR, Inc.) was nearly identical to that for C211. However, the symmetrical cryptand remains a white solid at room temperature, so it was scraped from the cold finger into a vacuum storage vessel.

3,2,2-Cryptand - (C322 or IUPAC 4,7,10,16,19,24,27-heptaoxa-1,13-diazabicyclo[11.8.o]nonacosane). C322 (prepared by Dr. Patrick B. Smith and Michael R. Yemen following Lehn's method (51)) was purified in the same manner as the other liquid cryptands, except that it was distilled at 145 - 150°C. After distillation C322 appeared to slowly decompose, as indicated by its slowly increasing yellow-brown hue, despite being stored in an evacuated storage device inside a desiccator which was kept in the dark.

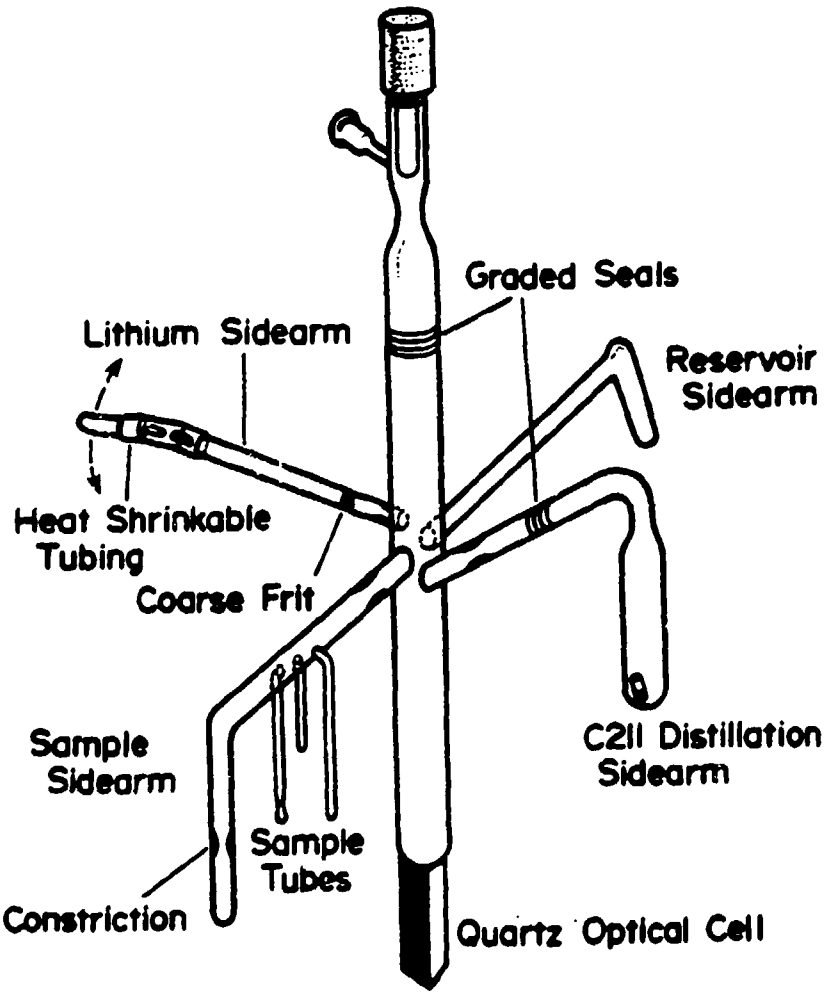

Figure 5. $Li^{+}C211 \cdot e^{-}$ multiple sample preparation apparatus.

2N,2,2-Cryptand - C2N22 or IUPAC 4,7,13,16-tetraoxa-1,10,21,24-tetrazabicyclo[8.8.8]hexacosane. C2N22 or tetraza C222 (gift from Professor J. M. Lehn, Institut de Chemie, Strasbourg, France) was purified by a method similar to that of Lehn (63). However the sublimation conditions he reported (50°C and .01 mmHg) were modified to increase the rate of purification. The solid was melted (m.p. = 69°C) and held at 75 - 78°C and 8 x 10^{-6} torr as vapor condensed on the cold finger. The white powder was stored in an inert atmosphere over Drierite (W. A. Hammond Drierite Co.).

1,4-Diazabicyclo[2.2.2]octane (DABCO) - This white compound (Aldrich Chemical, 97%) is not a complexing agent like those described above because of its oxygen-free rings. However it is similar in size and shape to the cryptands and it was purified in a similar manner. The DABCO was twice recrystallized from 45°C acetone. After sublimation, the compound was stored in the dark in a nitrogen atmosphere.

II.A.2. Metals

Lithium - Several methods were employed to produce reasonably pure 0.5 - 1.0 mg ($\sim$1 x 10^{-1} millimole) pieces of lithium. Most methods were judged unsatisfactory because the lithium mass could not be determined with sufficient

accuracy.

The initial attempt used small pieces of lithium cut from a long ribbon (Alfa Ventron, metal purity 99.9%) in an argon-filled dry box described elsewhere (64). Each piece of lithium was loaded into a preweighed 5 mm O.D. tube sealed at one end. A preweighed cap, to which polyolefin heat-shrinkable tubing (Alpha Wire Corporation) had been previously attached, was sealed onto the sample tube, providing a gas-tight seal. After removal from the box, the end of the tubing containing the lithium was placed in liquid nitrogen while the tubing was flame sealed. The heat-shrinkable tubing was removed with a razor blade and the three pieces of glass were reweighed on a Mettler model B6 balance with 3 - 5 x 10^{-5} g precision. The difference between pre- and post-weights after bouyancy corrections and a correction for sealed argon should have yielded the lithium sample masses. However, the amount of sealed argon was difficult to determine. Since the argon mass was approximately the same as the lithium mass, the poorly determined argon mass may have spoiled the potential accuracy of this sample preparation method.

The next attempt was very similar, except that the sample tubes were evacuated before being flame sealed. Although a correction for argon was no longer necessary, the lithium sample masses were once again quite poor.

The third attempt was to mass produce lithium disks

by punching them out of a sheet with an appropriately sized sheet metal punch. However, in the argon atmosphere, the freshly cut lithium tended to stick to the metal punch. Upon removal from the end of the punch, the lithium tore into irreproducibly shaped disks.

A modified borer was built of stainless steel with a "Delrin" core ("Delrin" is the trademark of E. I. DuPont de Nemours & Co. for its acetal resin, purchased from Cadillac Plastic & Chemical Co.) to push the disks off the steel cutting edge. After determination of the lithium ribbon thickness with a micrometer of 3×10^{-5} mm precision, disks were punched which appeared to be very similar in shape. Some samples were vacuum sealed while others were sealed under argon. From the measured I.D. of the steel bore and the measured thickness of the lithium ribbon, all samples should have been 2.18×10^{-4} moles. One lithium sample sealed under argon was randomly selected and subjected to decomposition in a hydrogen evolution apparatus (74): $2Li + 2H_2O \rightarrow H_2(\uparrow) + 2LiOH$. By the ideal gas law, the evolved hydrogen was released by 1.91×10^{-4} moles of lithium, an amount 14.1% lower than that predicted by the lithium measurement. The lithium ribbon was probably of nonuniform thickness and/or the sample could have been slightly decomposed before hydrogen evolution.

As an interim measure, rectangular lithium samples were cut with scissors in an inert atmosphere glove bag.

Sample dimensions were measured with a micrometer and calibrated microscope scale before the glass tubing was sealed under vacuum.

The most satisfactory lithium sample preparation method used a helium atmosphere Dri-Lab (Vacuum Atmospheres Company) at Cornell University. A clean knife was used to cut small chunks of lithium (Lithium Corporation of America, 99.99%) which were then weighed on a model G2 Cahn Electrobalance inside the Dri-Lab. Each sample was then transferred into evacuable glass tubing and a flame seal was accomplished at approximately 5×10^{-5} torr. At Michigan State University a sample was sacrificed in the hydrogen evolution apparatus. By weight the sample was nominally 2.67×10^{-4} moles while hydrogen evolution indicated 2.72×10^{-4} moles or 1.85% higher. The sample contained three chunks of lithium, two of which had been weighed together. Since the masses of most samples were determined in one weighing, it seems likely that the error in the sample masses would be no worse than the cumulative error of two weighings. If so, 2% may represent an upper limit on lithium mass inaccuracy with this preparation method.

Sodium, potassium and rubidium - These metals (Alfa Ventron, total purity 99.95%, 99.95% and 99.93%, respectively) were supplied in five gram ampoules under argon. Distribution to smaller tubing was by DaGue's method (64). Storage in the tubing was under vacuum. After measuring

the I.D. of the smaller tubing, it was possible to obtain accurate quantities of metal by seal-offs of appropriate lengths of the tubing.

Cesium - The metal (donated by Dow Chemical) was distributed in the same manner as sodium, potassium and rubidium. A more detailed description of cesium purification, as well as preparation and analysis techniques discussed in some of the following sections, is available (53).

II.A.3. Solvents

Ammonia (NH_3) and dimethylamine - Ammonia (Matheson, anhydrous, 99.99%) and dimethylamine (Matheson, anhydrous, 99.0%) were individually placed over sodium-potassium alloy (NaK_3) twice with numerous freeze-pump-thaw cycles while in each bottle. When the solution remained blue and when evolved gas was no longer evident during freeze-pumping, each solvent was presumed dry and transferred to a thick-walled vacuum storage bottle.

Methylamine (MA), Ethylamine (EA), 1,2-dimethoxyethane (DME), isopropylamine (iPA) and t-butylamine - Methylamine (Matheson, anhydrous, 98.0%), ethylamine (Matheson, 98.5%), DME (Matheson, 98%), isopropylamine (Eastman Kodak) and t-butylamine (Eastman Kodak) were individually stirred over calcium hydride for several days with accompanying

freeze-pump-thaw degassing. Each was transferred over NaK_3 twice with additional freeze-pump-thaw cycles, and finally distilled into a vacuum storage bottle.

Tetrahydrofuran (THF) - Tetrahydrofuran (Burdick and Jackson) was stirred over barium oxide before transfer into a storage bottle containing benzophenone and an excess of NaK_3, with the purple color of the benzophenone ketyl indicating dryness.

Benzene - Benzene (Fisher, spectrograde) was agitated over calcium hydride for several hours before storage over benzophenone and excess NaK_3.

II.B. Glassware Cleaning

It is extremely important that glass which contacts alkali metal solutions be thoroughly clean to inhibit solution decomposition. To this end, the following ritual was faithfully observed. First, the apparatus was rinsed with a hydrogen fluoride cleaning solution composed of 5% HF (28M), 2% detergent, 33% HNO_3 (16M) and 60% distilled water by volume. To minimize etching of the optical cell windows by the cleaning solution, the apparatus was quickly rinsed with distilled water, followed by five more distilled water rinses. Next the glassware was partially filled with aqua regia, a three-to-one mixture of HCl and HNO_3, and allowed to stand overnight. Alternatively, the

aqua regia was heated to promote the liberation of Cl_2 and allowed to stand for several hours. At the end of either cleaning period, the aqua regia was poured out and the vessel was rinsed six times with distilled water, followed by a minimum of six rinses with conductivity water (distilled water which had been deionized and redistilled through a high reflux ratio column to less than 1 ppm impurity). Finally the apparatus was dried in a 125°C oven.

The only glass not cleaned by this ritual was the lithium sample tubing at Cornell University. For those tubes, the HF/detergent step was omitted; otherwise the procedure was identical.

II.C. Solution and Sample Preparation

II.C.1. $Li^+C211 \cdot e^-$ Preparation

Because the bulk solution and sample preparation of $Li^+C211 \cdot e^-$ is more complex than that for most metal-cryptand systems (53,58,60,61), it is described in detail here. A description of modifications to incorporate other alkali metals and non-liquid cryptands follows.

The basic apparatus for $Li^+C211 \cdot e^-$ preparation was made of fused silica (Figure 5). To preclude the possibility of sodium exchange into alkali metal-amine solutions in contact with sodium borosilicate glass, only

portions of the vessel which would not normally contact the solution were of sodium borosilicate (65). It should be noted however, that to date, this exchange has not been reported in NH_3 solutions.

The initial step of a $Li^+C211 \cdot e^-$ solution preparation was to thoroughly clean the appropriate fused silica apparatus with the ritual detailed in the previous section. An appropriate-size lithium metal sample was selected and its thin wall tubing was lightly scored to facilitate breaking the tubing later. A piece of heat-shrinkable tubing (Flo-Tite tubing, Pope Scientific, Inc.) was sealed with a cool flame onto the open end of a short length of glass tubing. The scored lithium sample was placed into this device which was then sealed onto the metal sidearm (Figure 5).

The liquid cryptand, C211, was drawn from its vacuum storage vessel with a disposable pipette and placed into a short cup fashioned from 3 mm O.D. thin-wall NMR tubing. With the cup held upright on a balance pan, it was possible to introduce the desired stoichiometric amount of C211 into the cup to within tenths of milligrams. The vertical portion of the liquid cryptand sidearm (Figure 5) was then scored and removed, the cup of C211 was placed inside and the vertical portion was butt sealed back onto the sidearm. At this point the apparatus was evacuated on a greaseless vacuum system (64) with a liquid nitrogen trap on the

tee to protect the vacuum manifold from contamination. While most liquid cryptands appear to have a low vapor pressure, the dynamic pumping time was limited to about three hours as a precaution. The apparatus usually stood under static vacuum overnight, followed by a rapid return to $\sim 2 \times 10^{-5}$ torr. With the valve closed and the apparatus removed from the vacuum tee, the lithium sample tube was broken as depicted in Figure 5. With careful shaking, the lithium was moved down the sidearm to the frit while the shattered glass was separated and trapped near the heat shrink tubing. The sample sidearm was then flame sealed 6 - 8 cm from the frit while under dynamic pumping. Asbestos tape wrapped near the frit protected the lithium sample from possibly reacting with hot fused silica during the sealoff.

The C211 was then distilled *in situ* at $\sim 8 \times 10^{-6}$ torr in semidarkness. A paraffin oil bath was raised on the liquid cryptand sidearm and heated to approximately 50°C to rid the cryptand of volatile impurities. At this temperature the main stem from the optical cell to above the liquid cryptand sidearm branch was chilled to -78°C. The oil bath was then raised to a final temperature of 74 - 76°C where the distillation progressed slowly. Most of the purified C211 collected at the main stem which was at -78°C, however a significant amount remained in the unheated sloping sidearm. Therefore, at the conclusion of

the distillation a heat gun was gently used to clear the sidearm of C211, followed by a dynamic vacuum flame seal-off of the sidearm at the constriction.

Ammonia was distilled into the main stem of the apparatus from the solvent bottle connected to the opposite side of the tee. Because the tee and apparatus were pumped to high vacuum before the tee valve was closed, the solvent transfer was accomplished in the tee only, thus protecting the vacuum manifold. The NH_3 bottle was chilled to $< -50°C$ before its valve stem was opened to reduce ammonia's high vapor pressure.

Once sufficient NH_3 had been distilled into the apparatus to make a solution $2 - 3 \times 10^{-2}$ M in C211, the valve was closed and the apparatus was removed to an isopropanol bath maintained at -40° to -45°C with dry ice. No attempt was made to determine the solubility of C211 in NH_3. Rather the solvent was poured over the lithium and the resulting blue solution was used to dissolve the C211. Dissolution required only a few minutes at -45°C. Encrypting Li inside C211 is quite another story, however. NMR work has determined that forming the Li-C211 cryptate in water is fairly slow: $k_f = 0.98 \times 10^3$ sec^{-1} for $Li^+ + C211 \rightarrow Li^+C211$ (66). Empirically it was determined that encryptation was substantially complete if the $Li/C211/NH_3$ solution was held at $-40 \pm 3°C$ for a minimum of two hours with occasional agitation (see Section III.A.3. for further

details of encryptation kinetics).

Once the $Li^+C211 \cdot e^-$ solution had been prepared, the solution was poured gently into the sample sidearm. Depending upon the particular experiment, there may have been a combination of up to three different sample tubes on the sidearm from among the following: EPR, microwave conductivity, magnetic susceptibility tubing for use at Cornell University and/or a susceptibility tube for use at Michigan State University, in addition to a powder sample reservoir. Care was required to rotate the apparatus during pouring to fill the desired tube with the proper amount of solution. Many small pours were generally required so the tubes would not be overfilled and so the apparatus could be constantly returned to the cold isopropanol bath. The sample tubing I.D. had been measured with a calibrated microscope before construction of the apparatus. Combined with a measurement of the initial solution height in the tubing, it was then possible to estimate the amount of $Li^+C211 \cdot e^-$ in the sample.

Ammonia was removed slowly to avoid bumping by holding the bulk solution in the main stem at -78°C and the sample tubes and sample reservoir at -70°C initially. As the evaporation progressed, it was necessary to return the apparatus to a cold isopropanol bath and recondense NH_3 in the upper portions of the sample tubes to wash the $Li^+C211 \cdot e^-$ residue into the bottom of the tubes. After

several cycles the material was in the bottom several millimeters of the tubes, at which time the bulk solution was transferred to the reservoir sidearm, the main stem and sidearm were washed clean, and the bulk solution was frozen with liquid nitrogen. All samples were then dynamically pumped for 30 - 45 minutes before the first sample was sealed. Samples were then stored at 77K. After all sample tubes and the adjacent reservoir were sealed off, the sidearm was removed at the constriction near the main stem, leaving an apparatus consisting only of the main stem with its optical cell and the reservoir sidearm. This was the configuration used for optical spectroscopy.

Other reagents - Many preparations used reagents other than Li/C211/NH_3. All solvents were handled essentially as described above for NH_3. However, a minor modification was made for metals other than Li: no frit was necessary. Instead, an appropriate length of metal in 2 or 3 mm O.D. tubing was flame sealed following the method of DaGue (64). The metal ampoule was scored and placed in a cup which was connected to the apparatus with heat shrink tubing. After the apparatus was evacuated, the scored tubing was broken, the two pieces of metal ampoule were gently moved down the sidearm, and the heat shrink tubing end of the sidearm was sealed away. The only metal requiring a modification of this procedure was Cs. It was necessary to chill the cesium ampoule before cracking it to prevent the cesium

from melting due to finger heat and sticking to the shrink tubing. The metal was then distilled under dynamic pumping into the main stem and the sidearm was sealed off at the constriction near the main stem.

Other liquid cryptands were handled similarly to C211. C221, however, was not prepurified, but merely distilled *in situ*. By weighing the cryptand cup before use and again after use and *aqua regia* cleaning, the residue was found to be 2.0% of the original C221 mass. To compensate for cryptand impurity, subsequent preparations used a slight excess of liquid cryptand (1 - 4%, depending upon its shade of light yellow or amount of probable decomposition) over the stoichiometry desired.

C322 was more difficult to distill. An oil bath at 155 - 160°C was necessary to complete the distillation. A noticable deepening of the light yellow color of the cryptand in the distillation cup may have indicated that thermal decomposition was occurring at this temperature. After the distillation, the heat gun was unsuccessfully used to move C322 out of the unheated portion of the sidearm. So a cool flame was used to distill the C322 into the main stem. A very light yellow color was noted in the cryptand in the main stem, probably a result of the flame distillation. Therefore, in subsequent preparations with C322 the cryptand was not distilled, but rather the metal-solvent solution was poured into the cryptand

sidearm, dissolving the C322. The sidearm was thoroughly rinsed with solvent and then sealed away. Optical spectra of solutions prepared this way did not indicate increased decomposition and crystals were even grown after one such solution was used for optical spectra (Section II.C.2.f.).

Solid cryptands such as C222 were introduced carefully through the top of the apparatus before the valve stem was screwed into place. Therefore, no distillation sidearm was necessary for preparations using cryptands which are solid at room temperature.

II.C.2. Sample Preparation and Instrumental Description

After the metal and cryptand were dissolved in the solvent, and sufficient time had elapsed for metal cation complexation to occur, appropriate amounts of solution were poured into various sample tubes for magnetic susceptibility, EPR, or microwave conductivity. The solvent was evaporated and these tubes were sealed off. Then the bulk solution was used for optical spectra, followed by either a crystal growth attempt or an evaporation to prepare a packed powder conductivity sample. A main thrust of this study was to characterize $Li^{+}C211 \cdot e^{-}$ by multiple means on the same solution to minimize variances between different sample preparations. However, that caused some problems due to instrumental sensitivity: it was often difficult to produce a magnetic susceptibility sample sufficiently large

while simultaneously producing an EPR sample sufficiently small from the same solution.

Once the solvent was distilled into the apparatus, the cryptate concentration was fixed, and with the apparatus in Figure 5, the sample tubes were filled at the same time with the solution of fixed concentration. It would have been difficult to use an apparatus with multiple sample arms in order to pour solutions of different concentrations into different tubes. So a decision was made to continue with the same design at the possible expense of optimum EPR and/or susceptibility data on a given preparation.

II.C.2.a. Magnetic Susceptibility

Two different types of susceptibility samples were prepared: one for use in a Faraday balance at Cornell University and the other for use in a superconducting quantum interference device (SQUID) at Michigan State University. In the Faraday method, the force, f_x, on a powdered sample is

$$f_x = m \cdot \chi_g \cdot H_z \cdot \frac{\partial H_z}{\partial x} \qquad (1)$$

where m is the sample mass, χ_g is the magnetic susceptibility per gram of sample and H_z is the magnetic field strength in the z direction between pole faces. For a sample of unknown susceptibility, χ_g is normally determined

by comparison with a standard and by assuming that both the sample and standard hang in an identical location in which the field gradient is essentially constant. To make this assumption valid, it was necessary to construct the sample capsule from the same material as those at Cornell University in addition to making the capsule length as similar as possible. Therefore, susceptibility sample buckets were made of 4 mm O.D. Spectrosil fused silica (Thermal American Fused Quartz). When the bucket was built, 4 mm O.D. tubing was blown to give a round end and then constricted slightly 0.75 cm to 1.25 cm above that end. After the sample was dried in the bottom 0.4 - 0.5 cm of this tube, the end was immersed in liquid nitrogen and carefully sealed with a tiny hot flame approximately 1.0 cm above the end of the tube. A small fused silica hook was then attached to the top of the bucket prior to storage at 77K. Care was taken to avoid grasping the bucket or its hook with metallic forceps while the fused silica was hot in order to minimize ferromagnetic impurities.

At Cornell University the cold bucket was wiped fairly clean, then carefully hung on the "V" shaped end of a delicate fused silica fiber cut to such a length that the bucket would hang at exactly the correct height in the magnetic field. Once the bucket was lowered into the pre-cooled Faraday balance Dewar, it was protected from de-composition due to warming. It was difficult to make this

transfer without collecting some frost on the chilled bucket, so while the balance system was vacuum pumping, the sample chamber temperature was raised to approximately 200K to more quickly rid the bucket of frost which would interfere with force measurements. Once the bucket was clean, force was measured from 2.5 - 230K in magnetic field strengths of 10 kG to zero in 2 kG increments. The magnetic fields were produced by an electromagnet (Eastern Scientific Instruments) and forces were measured with a Cahn RG Electrobalance (Cahn Instruments Division, Ventron Corporation). In this instrument, the field gradient in the sample region was studied; $H_z \frac{\partial H_z}{\partial x}$ varied less than 2% (67). Temperature was controlled to 0.1K with an Oxford Digital Temperature Controller Model DTC2 (Oxford Instruments, Inc.) fitted for use with a gold + 0.07% Fe/chromel P thermocouple. The temperature was monitored in the range 2.5 - 100K by a germanium resistance thermometer (Cryocal, Inc.) and in the range 100 - 230K by a copper/constantan thermocouple.

Before the sample susceptibility could be calculated by comparison with a $HgCO(SCN)_4$ standard, it was necessary to subtract the diamagnetic force on the empty bucket from that of the bucket loaded with sample. Previously this bucket force had been obtained after the sample force measurements by cracking the bucket, cleaning and reconstructing it, rehanging it on the balance and obtaining the force measurements. The problems with this method were

significant, the greatest of which was probably the introduction of ferromagnetic impurities with forceps on the hot fused silica during bucket reconstruction. Professor J. L. Dye suggested a far superior method of subtracting the empty bucket force: decomposing the temperature-sensitive paramagnetic sample in situ with heat. After an hour at room temperature, the decomposed sample was diamagnetic and the "empty" bucket force measurements were made without the previous problems.

At Michigan State University, magnetic susceptibility was measured in a SQUID apparatus designed by Professors J. Cowen and W. Pratt. They followed a basic SQUID design but increased the length of each counter-wound coil to 2.5 cm to minimize the effect of variable geometry between samples. After a field of up to 10 Gauss had been trapped inside a superconducting niobium shield, sample introduction caused a change of magnetic flux in the pickup coils which was detected by a highly sensitive SQUID detector and displayed as a digital voltage (68). Theoretically the SQUID should detect changes as small as one quantum of flux. The instrument was designed for operation between 4.2 and 1.5K; however, samples were only measured at 4K in this study.

Samples were prepared by the usual method in 4 mm O.D. fused silica Spectrosil tubes which were about 10 cm long. This length insured that the tubes would extend between both coils simultaneously and thus compensate for the

diamagnetic tubing. Samples of 1 - 2 mg were confined to the bottom 0.8 cm or less of the tubes. Sample sizes several times larger would have been preferable but were unattainable with the current apparatus design. Susceptibilities were determined by comparison with a ferric ammonium alum standard.

II.C.2.b. EPR

EPR spectra were recorded on an X-band spectrometer (Varian model E4 with E-4534 sample cavity) using either a liquid nitrogen or liquid helium cryostat. The nitrogen system provided temperatures above 100K with a variable temperature controller (Varian); temperatures were confirmed with a copper-constantan thermocouple with digital readout (Doric model DS-350). Temperatures from 3.3 to 160K were provided by a continuous flow liquid helium system (Oxford Instrument Co., Ltd. model ESR 9) with a digital temperature readout based upon an Au + 0.03% Fe/chromel thermocouple immediately below the sample.

EPR is a sensitive technique for detection of paramagnetic species, perhaps capable of detecting fewer than 10^{11} centers (69). Most samples in this study contained $\sim 2 \times 10^{17}$ spins, and when combined with their often highly conductive, nearly metallic character, the samples were occasionally too large for proper automatic frequency control (AFC) response. Similar effects have been observed

in M-MA solutions (23). According to Catterall, electron spin precession changing over very small fields (as in a narrow EPR signal) is sufficient to break the AFC control and drive the microwave frequency off resonance while approaching the center of the signal. Once past the center, the frequency apparently flips over suddenly giving very rapid crossover and resulting in an artificially narrow EPR spectrum (70). Buntaine countered this effect in his Li-MA study by reducing the number of spins in the sample to 10^{19} - 10^{20} and then pulling the sample tube as far out of the cavity as necessary to stabilize the microwave frequency at resonance (23). In this study in which the sample sizes were already 2-3 orders of magnitude smaller than Buntaines, some samples were reduced further by tapping the tubing sharply and breaking loose some of the cold powder. The tube was then inverted and the loose powder was allowed to decompose on warm tubing. Some quantitative information was lost this way in order to attain true spectral shapes with a stable AFC.

II.C.2.c. Optical Spectra

All optical spectra were recorded on a double beam recording spectrophotometer (Beckman DK-2A) modified to permit sample compartment temperatures between -65° and 0°C. An ethanol cooling bath (Neslab model LTE-9) provided rough temperature control for the compartment while nitrogen gas

flowing through a coil immersed in liquid nitrogen provided the fine adjustment. A copper-constantan thermocouple near the optical cell supplied the input for temperature readout (Doric model DS-350). Spectra were recorded from 4000 cm^{-1} (2500 nm) to 30,000 cm^{-1} (333 nm) for standard fused silica cells or 3125 cm^{-1} (3200 nm) to 28,000 cm^{-1} (357 nm) for Infrasil cells (Markson Science, Inc.). The reference beam passed through air.

Spectra were normalized to a scale of zero to 1.0 by subtracting a baseline correction, setting the lowest absorbance to zero and the maximum to 1.0, and scaling the absorbance at 500 cm^{-1} intervals. The baseline correction was made by using the spectrum of the empty cell. It was necessary to use a new baseline correction for each solution because of an apparent baseline shift for each cell with successive preparations. There appeared to be increased light scattering from each cell with use, possibly as a result of cleaning the cell between preparations with an HF solution (Section II.B.).

Films for optical spectra were formed in an apparatus that consisted only of the main stem and reservoir sidearm, all other arms having been sealed off in the preparation. With 0.1 - 0.2 ml of solution in the optical cell, the bulk solution in the reservoir sidearm was frozen in liquid nitrogen. Simultaneous with the freezing, the optical cell, immersed in a cold isopropanol bath, was

agitated rapidly about the axis through the reservoir sidearm. This agitation splashed the solution onto the cell walls where the film formed during flash evaporation of the solvent. Repeat attempts were sometimes necessary to form films of the proper thickness (absorbance).

Due to this method of film preparation, the films were often of non-uniform appearance. As the ammonia was evaporating from the cryptate/NH_3 solution splash site, the least soluble species probably was deposited first and the most soluble last. The most pronounced case of film inhomogeneity was observed with $K^+C222 \cdot e^-$. The optical "films" appeared to consist of partially overlapping dots of variable thickness. To assess the effect of such irregular film thickness on absorption curve shape, a study detailed in the Appendix was undertaken. An absorption peak of Lorentzian shape from a cone-shaped film filling the entire beam cross section would have its maximum amplitude decreased 1.3% and its width at half height increased 2.0% compared to a uniform film of the same average thickness with a nominal 1.5 absorption maximum. The same cone shape filling only 81% of the beam cross section would have a nominal 1.5 absorption maximum reduced 54% and its width at half height increased 68%. Generally films of non-uniform thickness and films not filling the entire sample beam cross section have decreased and broadened absorption peaks. Peak position should be

unaffected while relative amplitudes in multipeak spectra should be affected only slightly.

Many spectra were recorded of films containing some solvent. A film was prepared in the usual way and its solvent-free or "dry" spectrum was recorded. The temperature of the sidearm reservoir was then raised from -196°C to between 5° and 30°C below the film temperature. Depending upon the solution vapor pressure and the film's solvent affinity, the film acquired sufficient solvent to alter its "dry" spectrum. A film so altered will be referred to as "damp". The film could then be washed from the optical cell walls through the combination of solvent affinity and increased reservoir temperature. "Wet" will refer to a film just prior to its being washed down. A study was conducted to confirm the dryness of a solvent-free, "dry" film (Section II.D.).

Homogeneity of a non-uniform film could sometimes be improved by a dry-damp-dry cycle. A non-uniform dry film which acquired a moderate amount of solvent seemed to become noticeably more uniform if it were redried slowly. On several occasions, the maximum peak absorption jumped significantly after such a cycle, as expected for a film increasing in uniformity. The Appendix contains a detailed discussion of the spectral effects of spot size and film non-uniformity.

II.C.2.d. Microwave Conductivity

The conductivity of several samples was studied in the microwave region (X-band) by comparing the relative power absorptions of the samples with those of known conductors, semiconductors and insulators. The method used was that of Lok (71), except that the signal not attenuated in the TE_{103} cavity was measured by a power meter (Hewlett-Packard Model 432A) attached to a 10 db coupler.

Microwave samples were prepared in the usual way in 3 mm or 5 mm O.D. fused silica tubes and were stored in liquid nitrogen until the measurements. Initially samples and standards were studied in 5 mm O.D. tubes. However metallic standards and highly conducting samples spoiled the sample cavity Q so thoroughly that it became necessary to use the smaller 3 mm O.D. sample tubes. All standards were commercially available and no further purification was attempted. Metallic standards were used whose particle sizes were less than their respective skin depths at approximately 10 GHz. Because cryptate sample skin depths are unknown and because the cavity filling factor varied between samples and standards, this conductivity method produced non-quantitative results. However, it certainly did distinguish qualitatively between conductors and insulators.

II.C.2.e. Pressed Powder Conductivity

An apparatus designed by Michael R. Yemen was used to determine powdered sample D.C. conductivity and band gap (72). In this voltmeter-ammeter (V-I) method, a powdered sample was confined between two stainless steel electrodes inside a 2 mm I.D. heavy wall fused silica tube. Pressure on the sample was applied by a steel spring whose spring constant had been measured. Temperature in the sample region was controlled by a variable temperature controller (Varian model V-4540) using chilled nitrogen gas. In addition, boil-off from a liquid nitrogen Dewar helped maintain the temperature while bathing the sample cell in an inert atmosphere.

Powdered samples were prepared in the sample sidearm reservoir (Figure 5) by evaporating the solvent and then dynamically vacuum pumping on the sample for a minimum of 30 - 45 minutes before the tubing was flame sealed. The conductivity sample chamber was filled while it was colder than -40°C to prevent sample decomposition. The entire operation took place inside an inert atmosphere glove bag to prevent sample decomposition and to prevent frost growth on the cold sample chamber. After the sample was loaded, its ohmic response was checked. Then as the temperature was varied, the current through the sample was measured at a constant voltage.

II.C.2.f. Crystal Growth Attempts

An excellent method for definitive characterization of $Li^+C211 \cdot e^-$ would be to isolate a single crystal of the compound and complete an x-ray study of its structure. While not the primary thrust of this program, preliminary studies were nevertheless accomplished to determine possible solvents or solvent combinations favorable to crystal growth. In all cases such attempts were made in the original solution preparation apparatus (Figure 5) after the metal, cryptand and sample sidearms had been sealed off and after the optical spectra were recorded.

The NH_3 was removed from $Li^+C211 \cdot e^-$ preparation V (mole ratio Li/C211 = 0.97) and 4.1 ml of methylamine (MA) were added. The 5×10^{-3} M blue solution was stored for two days at -78°C before the MA was removed to near dryness. Then 3.2 ml of isopropylamine was distilled in and the apparatus was shaken for several minutes at -57°C to dissolve the electride powder. The solution was stored for several hours at -78°C before being warmed slowly from -60° to -51°C. At -51°C the solution was colorless and was discarded.

$Li^+C211 \cdot e^-$ (VI) with R = 1.15 was first studied in a mixed solvent of equal parts NH_3 and ethylamine (EA) at a molarity of 7×10^{-3}. After storage overnight at -78°C, one-third of the solvent was removed, leaving a solvent approximately two-thirds EA. After storage overnight,

2.3 ml of t-butylamine was added, making a dark blue viscous solution. Again the solution was stored overnight at -78°C. Several milliliters of solvent were then removed, leaving a solution with 20% EA and 80% t-butylamine which was stored for several days at -78°C. At the end of that period the solution was very light yellow.

$Li^+C211 \cdot e^-$ (VII) with R = 0.60 was short-lived also. A 1 x 10^{-2} M dark blue viscous solution resulted when dimethylamine was added to the electride powder. After storage at -78°C for two days, half the solvent was removed. The following day, the solution was a very light blue and was discarded.

No crystals were ever noted in any of these solutions. The general method was to reduce solvent polarity until crystals precipitated, but this shows little hope of success. Instead, it seemed that as the dielectric constant of the solvent was reduced, the solution could not support the ionic cryptated cation and bare electron. The electron probably increasingly localized on the cryptand, finally destroying the cryptand. It should be noted that when NH_3 was removed from the original solutions, the distillations were from a -60°C solution into a -78°C trap. It is significant that at these temperatures there is still NH_3 present in the nearly dry electride powders. Potentially the NH_3 could serve as sites for electron localization in the presence of nonpolar solvents, possibly helping prevent

solution decomposition. Solution VII, however, decomposed under these circumstances and solution V decomposed despite potential stabilization from MA. The method, though, bears further investigation.

Two other crystal growth attempts were successful in the original apparatus, though neither compound was an electride. After this author completed optical spectra of the solutions, Mr. Bradley Van Eck grew crystals having the apparent formula $Cs^{+}C322 \cdot Na^{-}$ and Dr. Long Dinh Le grew crystals which were apparently $Li^{+}C211 \cdot Na^{-}$.

II.D. Sample Analyses

Bulk solutions and the samples evaporated from them presumably contained the reactants in the same stoichiometries as were initially introduced into the preparation vessels. Lithium samples appeared to have only tiny amounts of surface oxidation, and perhaps 1-2% of the cryptand remained as residue from the *in situ* distillation. The apparently homogeneous solutions and powdered samples, then, should have had nearly the original stoichiometry. A suitable analysis, though, would define the stoichiometry and in addition would reveal the amount of reducing power still present in the sample at the time of analysis. Thus the analysis could confirm, for example, the presence of electrons in an electride EPR sample as a majority species, not merely a minority constituent.

In the analyses, samples were decomposed with water and the evolved hydrogen was collected and measured. The decomposed material was then titrated with a standardized acid. The titration solution was evaporated to dryness and the residue was made into an aqueous solution for metal ion flame emission. Finally, the unreduced water from the hydrogen evolution was analyzed for NH_3 to determine the solvent content of the sample. Other samples were analyzed solely for their NH_3 content.

II.D.1. Hydrogen Evolution

The cold sample tube was scored and sealed into a glass apparatus with shrink tubing. This apparatus was then connected to a vacuum system for hydrogen collection (73). The entire system was evacuated to $\sim 10^{-5}$ torr and the conductance water for decomposing the sample was degassed through four or more freeze/pump/thaw cycles until no detectable gas remained. The sample tube, maintained at -78°C with dry ice, was then cracked and the water was condensed onto the sample. Very slowly the ice was warmed so as to prevent pyrolysis of the sample with an accompanying low indication of reducing power. Eventually a controlled reaction of the following type occurred:

$$2Li^+C211\cdot e^- + 2H_2O \rightarrow H{:}H(\uparrow) + 2C211 + 2Li^+ + 2OH^-$$

The evolved hydrogen was manually pumped into a 10.00 ml burette with repeated cycles of a mercury leveling bulb. The height of the mercury, the atmospheric pressure and the temperature at the burette were measured and the moles of evolved hydrogen were calculated with the ideal gas law.

Several samples were quite small, yielding only a few torr of hydrogen pressure. Because the gas pressure was the difference between the measured atmospheric pressure and the height of the mercury column, there was potentially a one torr error in the hydrogen pressure, a large percentage error for small samples.

II.D.2. pH Titration

After the hydrogen evolution, the sample tube was rinsed to remove the cryptand and lithium hydroxide residue. The aqueous solution was then titrated with a standardized HCl solution using a pH electrode (Corning, catalog number 476050) and digital meter (Orion Research Model 701A) which had been calibrated with pH buffer solutions. The cryptand residue preparation and the titration were completed in a glove bag with a nitrogen atmosphere to minimize the effects of CO_2 on the titration. End points were determined graphically.

II.D.3. Flame Emission

After the titration, the solution was evaporated to dryness in a partially evacuated desiccator with Drierite as the drying agent. An aqueous solution was remade using a pipetted quantity of conductance water. The flame emission instrument (Jarrell Ash) was adjusted for the estimated parts per million (ppm) concentration of the unknown sample. Lithium salt standards were then run, followed by the unknown solution. Instead of reading an instantaneous or an estimated average from the instrument's output scale, the emission value was read from a digital signal averager which was conceived by Mr. Bradley Van Eck and designed by Mr. Martin Rabb. The instrument analog signal was averaged for 10, 20 or 30 seconds, converted to a digital value and then displayed until the end of the subsequent averaging cycle. The reading from conductance water was determined between all standards, yielding background emission or noise levels. A plot of relative emission output versus ppm gave a nearly straight line from which sample lithium concentrations were determined.

II.D.4. Ammonia Content of Samples

To determine the solvent content of various samples, an ammonia analysis was performed based upon indophenol blue formation (75). After the sample tube was cracked

open, a measured amount of conductance water was quickly added. Two drops of this solution were placed in a micro test tube and one drop of a phenol/sodium nitroferricyanide solution and one drop of a sodium hypochlorite solution were added. All reactants were reagent grade and were used without further purification. The test tube was placed in a 50°C water bath and the intensity of the resulting blue was compared to those of ammonium chloride solutions of known concentration which had been treated similarly. Unknown solutions yielding an intense blue were retested after dilution of the original solution.

Feigl and Anger state that the limit of identification for ammonia in samples of the size tested here should be ~1 picogram (75). This would correspond to a solution approximately 1×10^{-6} molar in ammonia. However, over a ten month period, the experimental limit of detection in this study was consistently an ammonia concentration of 1×10^{-4} M. This apparent decrease of two orders of magnitude in the limit of detection was judged to have no effect on the accuracy of this study.

CHAPTER III

LITHIUM CRYPTAND 2.1.1 ELECTRIDES

The subject material, first reported elsewhere (60,61), seemed to be metallic: its optical spectrum was quite similar to that of a concentrated MAS, although the cryptate film was virtually free of solvent. Further investigation of this curious response of a solvent-free solid produced from an organic cryptand and an alkali metal led to the studies which are the major topic of this dissertation.

Lithium 2,1,1-cryptand electride is abbreviated $Li^+C211 \cdot e^-$ to indicate the materials from which it is made (Li and C211) and its electride nature (the alkalide Li^- was not evident in this study). The symbol $Li^+C211 \cdot e^-$ is generic, representing material from Li and C211, regardless of the nominal stoichiometry or the metallic or insulator character of the electrons. R, the ratio of moles of metal to moles of cryptand, will identify the stoichiometry of a particular preparation.

The study of $Li^+C211 \cdot e^-$ soon branched from optical spectroscopy, in which the electride electrons appeared to be in quite different environments than the electrons in low temperature glasses or in F-centers, to microwave

conductivity, EPR, magnetic susceptibility and packed powder conductivity. In some cases the characteristics are similar to those of metal-ammonia compounds, though there are many differences. The various methods of study and their results are detailed below.

III.A. Optical Spectroscopy

For the optical range scanned in this work (4000 cm^{-1} to 30,000 cm^{-1} or 2500 - 333 nm), the atomic or molecular phenomena generally observed are electronic transitions. For alkalide anions (M^-) this can be considered an ns → np or bound-bound transition (54) with some contribution from a bound-continuum transition (76). Electrides (e_t^-) showing locally trapped character can be thought of as undergoing similar transitions. In both cases it is sometimes useful to refer to the bound-continuum transition as a contribution due to electronic promotion from the valence to the conduction band in a semiconductor. As noted in Section I.C., the Banerjee and Simons model for locally trapped (solvated) electrons would attribute the high energy skewness of the absorption peak to transitions from the ground state of one trapping site to the excited states of neighboring sites (40). The distinct similarity of solvated electron peaks and the solvent-free thin film absorption peaks of e_t^- and M^- suggest that the asymmetry on the high-energy side for these two species may also be caused by site-to-site

electron hopping. For electrides with delocalized (metallic) character, the optical spectrum is the result of a collective or plasma resonance of the conduction electrons.

Because the optical scanning range extends into the infrared, electronic transitions are not the only phenomena present. When the optical films are wet with ammonia, small peaks appear in the spectra which correspond almost precisely with those due to NH_3 combination vibrations in the liquid phase as reported by Burow and Lagowski (77): 4386 cm^{-1}, $\nu_1 + \nu_2$; 4470 cm^{-1}, $\nu_2 + \nu_3$; and 5000 cm^{-1}, $\nu_3 + \nu_4$. Shortly after the appearance of these peaks, the films wash off the optical cell walls.

III.A.1. Li with Ammonia and with Methylamine

The optical transmission spectra of lithium metal in NH_3 and in CH_3NH_2 (MA) in the absence of any complexing agent are similar. When the bulk solution in the apparatus sidearm reservoir (Figure 5) is frozen with liquid nitrogen, the liquid on the optical cell walls loses its characteristic blue color as the solvent evaporates. The result is a gray "film" of heterogeneous metal spots which yields no absorbance spectrum. Therefore, dry uncomplexed lithium metal should make no contribution to the absorbance spectra except, perhaps, for a higher background.

When the metal "films" contain solvent, however, there are definite spectral features. Curve A of Figure 6 shows

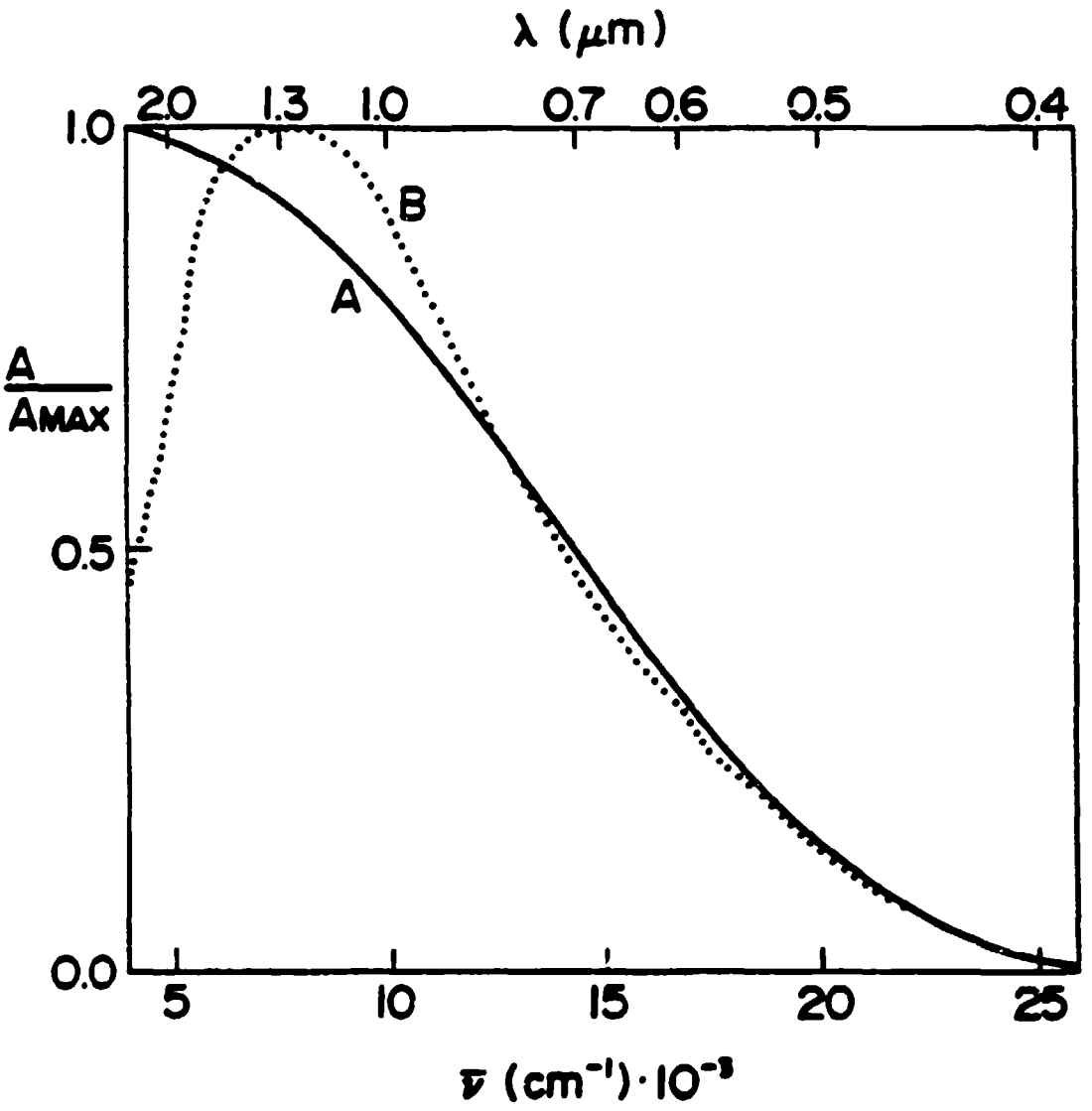

Figure 6. Spectra of lithium metal films which contain methylamine: A - damp film; B - wet film. Lithium films containing ammonia are virtually identical.

the spectrum of a damp film which contains only a small amount of MA. In other words this is the spectrum of a concentrated metal-methylamine solution. Since the lithium films with NH_3 were similar, spectrum A will also be referred to as a typical spectrum of a concentrated metal-ammonia solution (MAS). Section IV.A.1. contains a more detailed discussion of optical transmission spectra of MAS in which it is concluded that curves such as spectrum A of Figure 6 are typical of MAS and show the plasma edge due to conduction electrons. Spectrum B of Figure 6 was taken just before the wet film washed off the cell walls and is typical of MAS which have become more dilute by addition of solvent. The electrons are becoming more localized and the absorption gradually decreases on the infrared side of the peak. Spectra which show this decreased yet significant infrared absorption at 4000 cm^{-1} (2500 nm) will be referred to as having plasma character.

It is interesting to note the temperatures at which these metal films are considered damp and wet. The lithium film which gave spectrum A in Figure 6 was held at -47°C as the liquid nitrogen on the sidearm was replaced by a dry ice/isopropanol bath. The absorption began appearing within several minutes, reflecting the acquisition of methylamine. Spectrum A was taken when the bulk solution was at -73°C, a 26°C temperature differential. Spectrum B was taken with another film held at -46°C while the bulk

solution was at -56°C, shortly before the film washed off the walls. Both spectra demonstrate lithium's high affinity for methylamine and the possible formation of $Li(CH_3NH_2)_4$. Lithium and NH_3 show similar effects, reflecting the likely formation of $Li(NH_3)_4$. This solvent affinity is in stark contrast to that for Na and K detailed in Section IV.A.1. In those two cases the bulk solution was within 3 - 5°C of the film temperature before there was enough solvent in the film to cause significant absorption.

III.A.2. Li/C211 Films from Ammonia

Lithium electride systems have shown several major responses. These are described below and then discussed later in the chapter. The system $Li^+C211 \cdot e^-$ with R = 2 from NH_3 is reported elsewhere (61). The apparent metallic character of thin optical films of that preparation stimulated interest in determining the nature of lithium electride. The next preparation, $Li^+C211 \cdot e^-$ (I) with R = 0.93, showed almost identical features to the initial preparation with R = 2. Both systems showed a plasma edge due to delocalized electrons in dry films and in films damp with NH_3, similar to spectrum A of Figure 6. When wet with NH_3, both films gradually shifted to more localized character with high infrared absorbance as in spectrum B of Figure 6. However, the maximum in the R = 2 system was at 8650 cm^{-1} (1155 nm) (61) while the R = 0.93 maximum was

at 5900 cm^{-1} (1695 nm).

Because these preparations showed metallic character for the $Li^+C211 \cdot e^-$ system with an R value of 0.93, as well as for R = 2, a system with R · 0.95 was prepared in the apparatus of Figure 5 so that EPR and microwave samples from the same solution could be studied in addition to optical spectra. The purely metallic character of system I was replaced by a metallic - nonmetallic (MNM) transition in $Li^+C211 \cdot e^-$ (II). When a film was made while the optical apparatus was in a dry ice/isopropanol bath colder than -50°C, the spectra contained localized electron peaks. Warming this film did not cause a MNM transition, but merely gave decreased absolute absorption and indistinct character. In contrast, when the film was made and observed above -48°C, the spectrum was a plasma edge, curve A of Figure 7. Spectrum B is of the same film 27 minutes later at -53°C. The MNM transition was completed over a 5°C range while all other parameters apparently remained constant. Thirty minutes later and 7°C lower, the spectrum had evolved further into what was later considered a "typical" Li^+-$C211 \cdot e^-$ spectrum. An example of this typical spectrum when R is between 0.60 and 1.15 is curve C of Figure 7 where there are two low energy e_t^- peaks at 5000 and 7000 cm^{-1} (2000 and 1430 nm) and a high energy shoulder at 12,000 cm^{-1} (830 nm). This film was further chilled to -77°C and then warmed over a period of 50 minutes to -34°C.

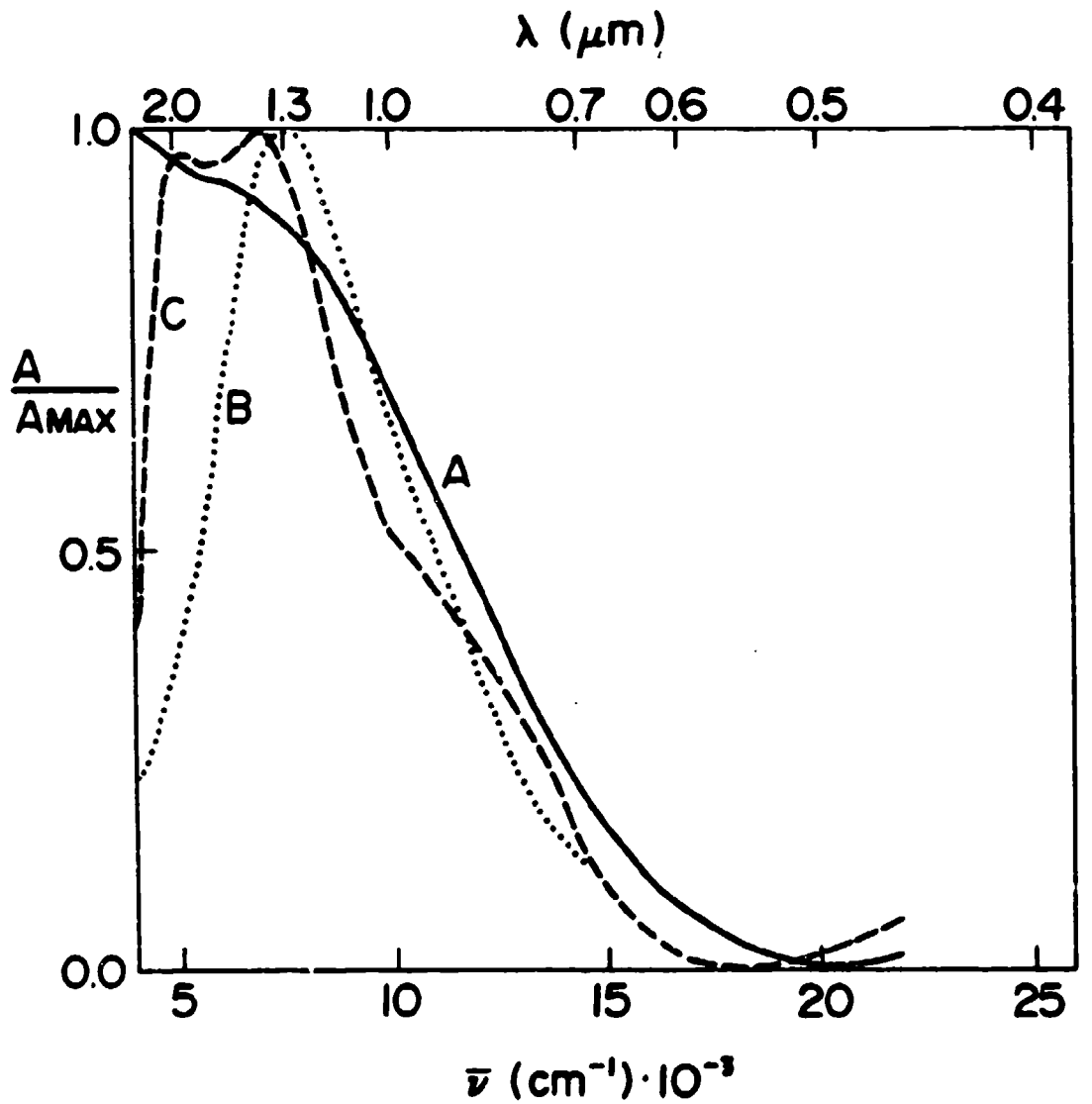

Figure 7. Spectra of a solvent-free $Li^{+}C211 \cdot e^{-}$ (II) film from ammonia with R = 0.95: A -48°C; B -53°C; C -61°C. Elapsed time from A to C: 57 minutes.

There was no change in the spectrum. The same film was then dampened with NH_3 and dried at -48°C, regenerating the plasma edge as in spectrum A of Figure 7.

In attempts to reproduce and further characterize the MNM transition of system II, systems III (R = 0.98), IV (R = 0.99) and V (R = 0.97) were studied. All three give the same general response but the definite MNM transition of II was never reproduced. Spectra A and B of Figure 8 show the response of warm and cold dry films. Spectrum A was taken with the film at -39°C and shows the typical e_t^- peaks at 5000 and 7000 cm^{-1} and the 12,000 cm^{-1} shoulder. Spectrum B at -70°C has the same general features though the relative heights of the low energy peaks fluctuate as does the absorbance at 4000 cm^{-1} (2500 nm). The differences between spectra A and B are typical: there is a slight decrease in plasma character as films are cooled.

Spectrum C of Figure 8 was taken after the bulk solution in the sidearm was thawed for a few minutes and then refrozen. The NH_3 vapor apparently caused annealing to a more homogeneous film with increased plasma character. The 7000 cm^{-1} peak and 12,000 cm^{-1} shoulder are significantly decreased. This is a typical response to the annealing process noted throughout the $Li^+C211 \cdot e^-$ study.

Although the mole ratios of VI and VII were varied to R = 1.15 and 0.60, respectively, their optical response is virtually identical to previous systems, as shown by curve

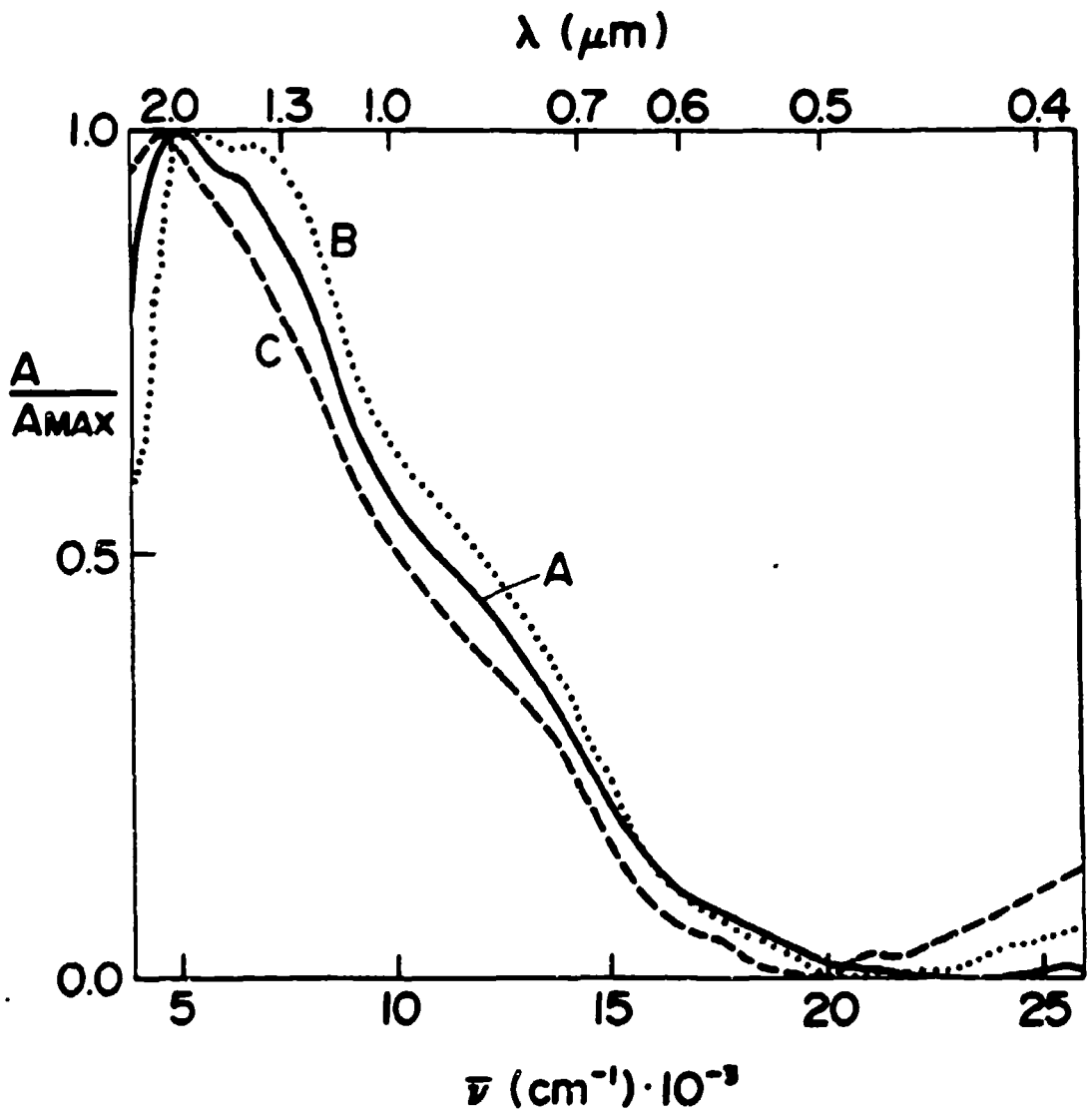

Figure 8. Spectra of solvent-free $Li^{+}C211 \cdot e^{-}$ (V) films from ammonia with R = 0.97: A -39°C, unannealed; B -70°C, unannealed; C -36°C, annealed.

A of Figure 9 for sample VII. By R = 1.57 in system VIII, however, there is a definite change. The spectrum of a dry, unannealed film is depicted as curve B of Figure 9, showing fairly homogeneous character and high infrared absorption. Annealing this film caused a shift to a plasma edge at -37°C, and a continued high infrared absorption at -70°C similar to spectrum B of Figure 9.

To ascertain the effect of ammonia on the character of optical spectra, a vapor pressure study was conducted. Based upon his study of activities in MAS (17), Marshall determined that a Li-NH_3 solution was saturated at 0.2110 mole fraction of Li at -35.00°C. If P° is the pure NH_3 vapor pressure at that temperature, P' is the solution vapor pressure and $\Delta P = P° - P'$, then $\Delta P/P° = 0.9958$ for the saturated solution. Assuming the same ratio for $\Delta P/P°$ at -65°C and using pure ammonia vapor pressure data (78), it is possible to calculate the NH_3 pressure necessary to give a saturated Li-NH_3 solution at -65°C. Assuming that the dilute bulk solution (mole fraction < .001) approximates pure NH_3, the temperature can be determined which would give this required vapor pressure. A slush bath table (79) shows the solvent which can be cooled with liquid nitrogen to give the proper temperature to yield a saturated optical film if lithium electride solvent affinity is nearly identical to that of lithium metal. By varying $\Delta P/P°$, temperatures for unsaturated and

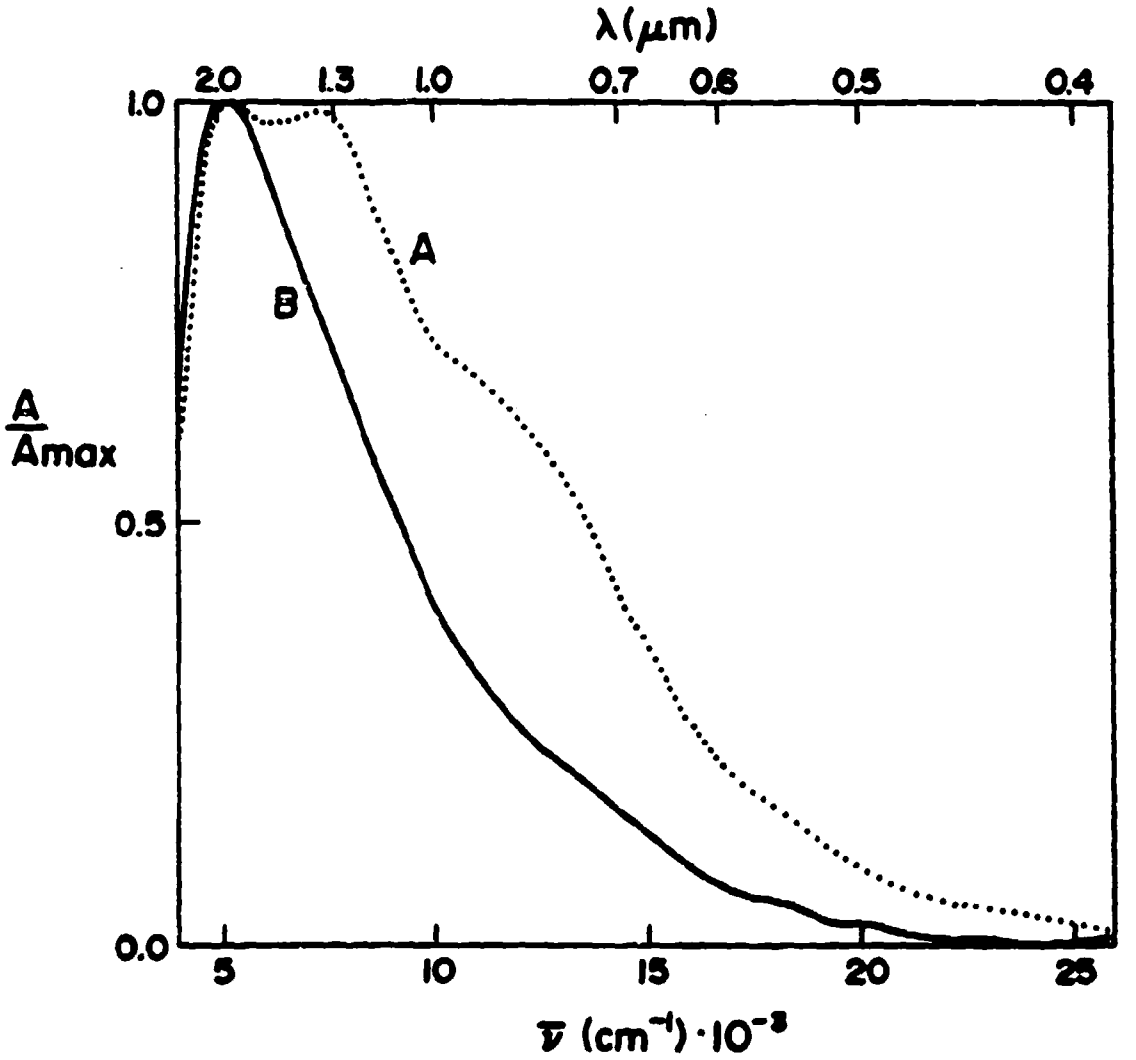

Figure 9. Spectra of solvent-free $Li^{+}C211 \cdot e^{-}$ films from ammonia: A - VII with R = 0.60; B - VIII with R = 1.57. Spectra of system VI with R = 1.15 were virtually identical to spectrum A.

supersaturated films can be calculated. Table 1 summarizes these calculations and the optical results.

Table 1. $Li^+C211 \cdot e^-/NH_3$ vapor pressure study[a].

Bulk Temp (°C)	P' (torr)[b]	$\Delta P/P°$	Condition if film were Li°	Optical Result
-196	$\sim 10^{-12}$	~1.000	dry	dry
-127	.070	.9994	dry	dry
-116	.50	.9958		dry
-91	11.3	.905	unsaturated	transition
-78	44.1	.630	wet	damp

[a]Predicated upon the film being at -65°C where P° = 119.05 torr.[b]

[b]Data from Reference 78.

One film from a solution with R = 0.96 was used for all spectra in this study and the results are shown in Figure 10. The NH_3 was removed from the film and the very typical spectrum C resulted. This spectrum was virtually unchanged from beginning to end whenever the bulk solution was frozen. In addition it was unchanged when the bulk solution was at -127°C for 52 minutes and at -116°C for 20 minutes. As indicated by spectrum B, however, noticeable effects of NH_3 vapor appeared about eight minutes after the temperature of

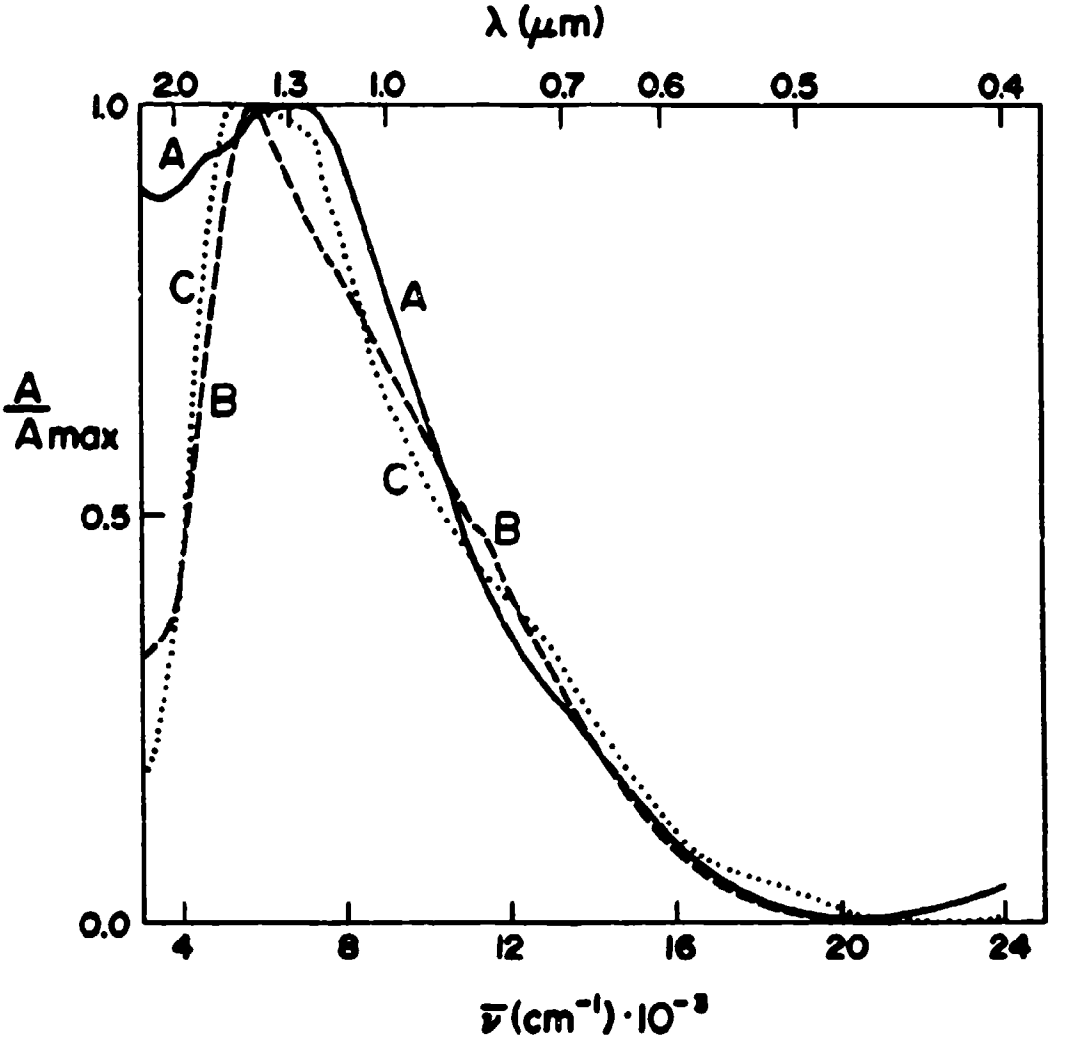

Figure 10. Spectra of a single $Li^{+}C211 \cdot e^{-}$ (X) film from ammonia with R = 0.96. The film was held at -65°C and the bulk solution temperature was varied: A -78°C, damp film; B -91°C, film in transition: C -116°C and lower, dry film.

the bulk solution was raised to -91°C. The spectra underwent no further change for the next ten minutes before the bulk solution was refrozen. In spectrum B, the 7000 cm^{-1} peak and 12,000 cm^{-1} shoulder are gone, and a fairly sharp e^- peak at 5650 cm^{-1} (1770 nm) and a rising absorbance in the infrared are present (out to 3125 cm^{-1} (3200 nm) in this figure). With the bulk solution at -78°C for eight minutes, spectrum A resulted. This is a typical film referred to as damp in this study.

III.A.3. Li/C211 Films from Methylamine

Because spectra of films from MA often lack shoulders and/or peaks found in comparable films from NH_3 (61), Li^+-C211·e^- films from MA were studied to determine if they might appear more homogeneous. The NH_3 was removed from system V (R = 0.97) and replaced with MA, resulting in the fresh film whose spectrum is curve A of Figure 11. There is only one broad peak, at 5800 cm^{-1} (1720 nm), with a high energy shoulder at 13,500 cm^{-1} (740 nm). Annealing simplifies the spectrum even more, resulting in a broad, asymmetric single peak at 5700 cm^{-1} (1750 nm) with only the hint of a high energy shoulder (spectrum B, Figure 11). Both films were at -36°C and for this temperature the amount of plasma character is lower than in similar unannealed and annealed films from NH_3, spectra A and C of Figure 8, respectively.

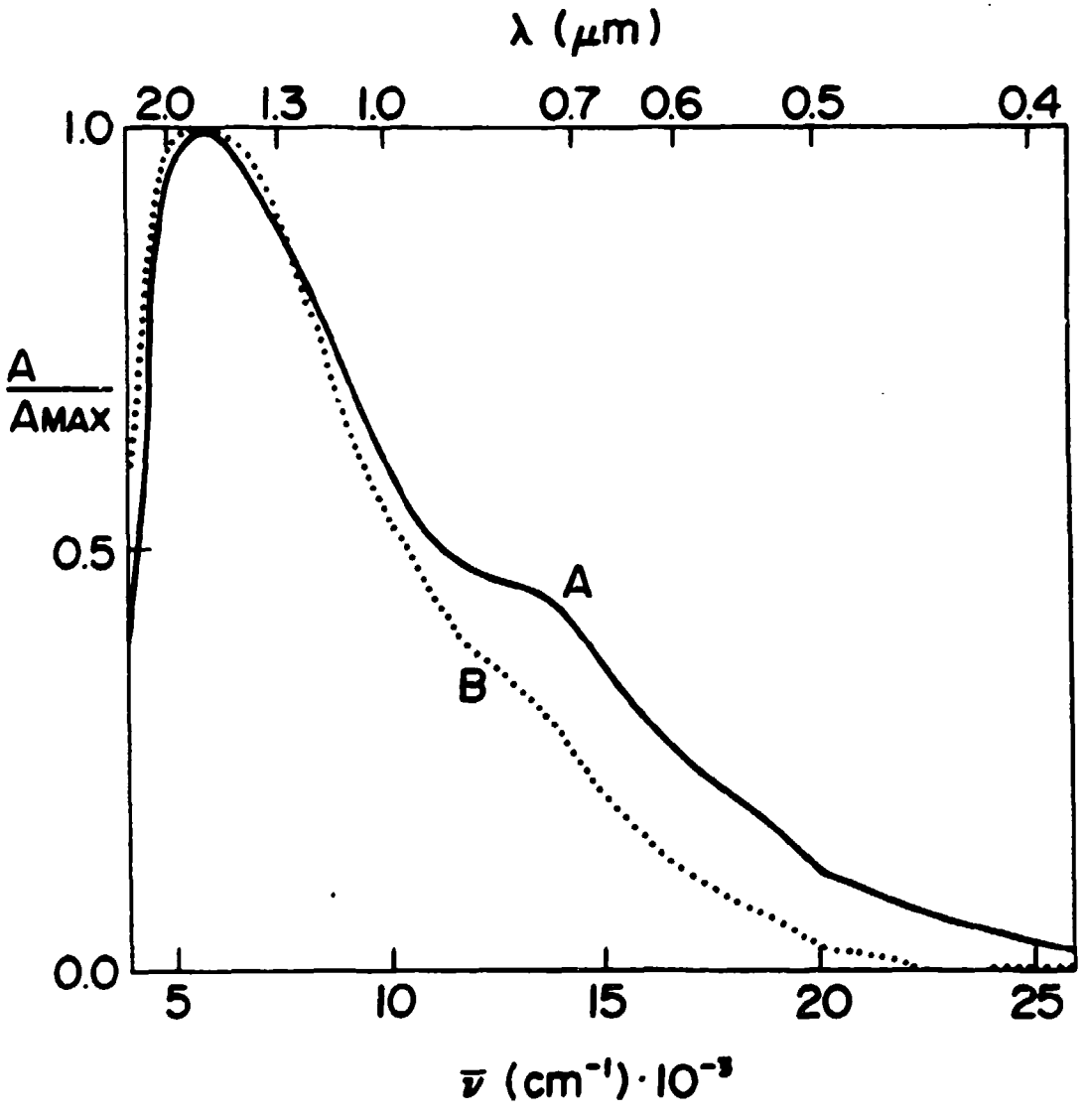

Figure 11. Spectra of a solvent-free $Li^+C211 \cdot e^-$ film from methylamine with R = 0.97: A -36°C, unannealed; B -36°C, annealed. The solution was made by replacing the ammonia of $Li^+C211 \cdot e^-$ (V) with methylamine.

Spectra of films from MA with R = 2, displayed in Figure 12, show metallic character. Curve A is the spectrum of an unannealed film at -76°C while curve B is the spectrum of the same film at -28°C after annealing and conversion to a plasma edge. For comparison, curve C depicts the spectrum of an annealed R = 2 film from NH_3. Spectra B and C both show metallic character, but it appears that the film from MA provides a much more homogeneous environment for the electrons.

The first preparation of Li/C211 with R = 2 from MA did not produce any optical spectra but there was an observation which should be noted. The cryptand, metal and solvent were introduced into the apparatus in the usual manner. Then the components were mixed and held at -40°C for 1.5 hours to allow Li^+ complexation. Since this was strictly a preparation for optical spectroscopy, the first film was made at the end of that ninety minute period. Repeatedly these films went virtually colorless within 5 - 15 seconds as the bulk blue solution was frozen in the sidearm. The resulting optical spectra were nearly featureless with only a very low peak in the infrared. The presence of MA vapor when the bulk solution was thawed produced a sizable plasma edge, but immediately when the optical film was redried, the very low e_t^- peak was reproduced almost exactly. Apparently the lithium complexation had not proceeded significantly and as the MA was removed, previously solvated

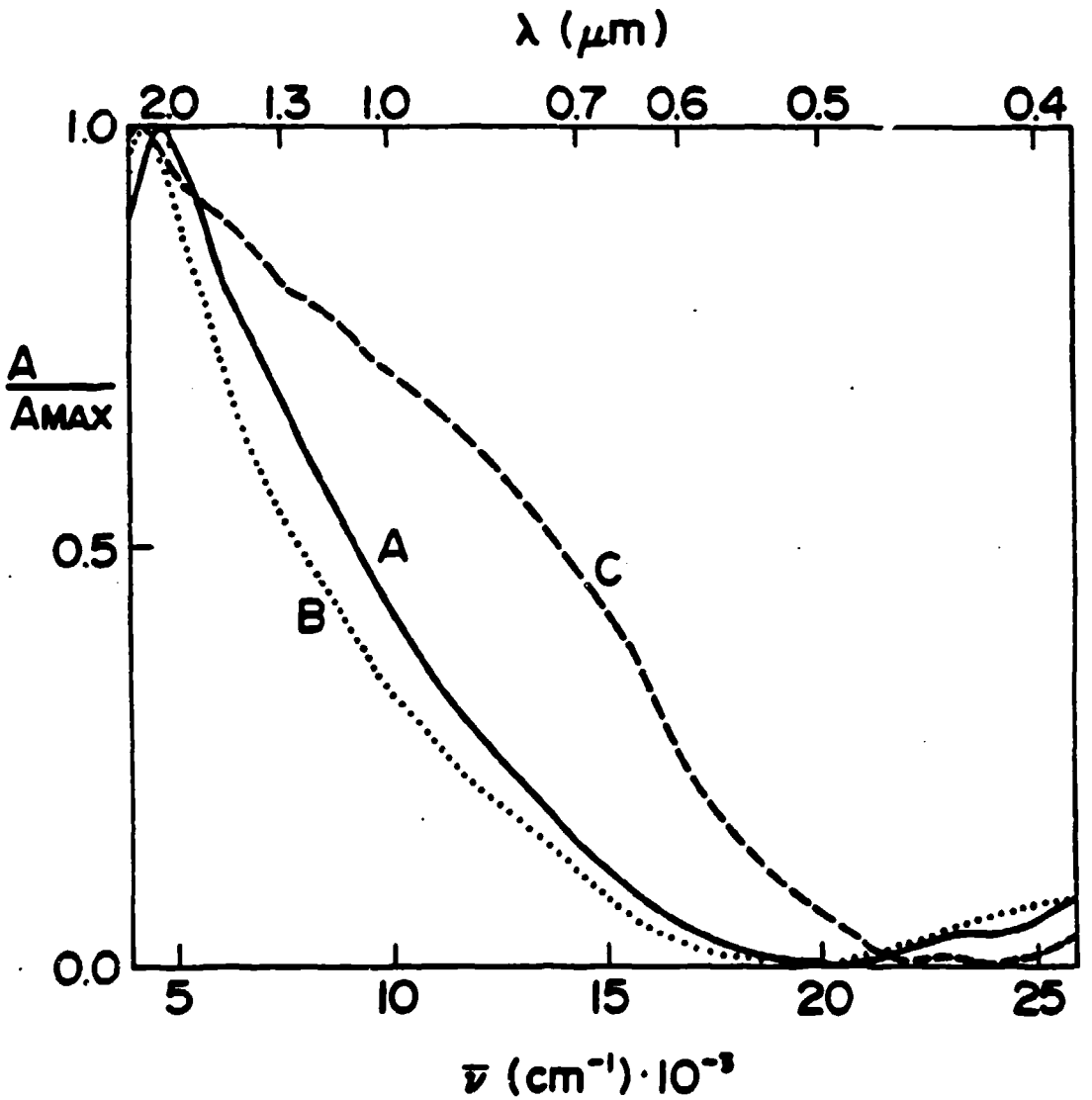

Figure 12. Spectra of solvent-free $Li^{+}C211 \cdot e^{-}$ films with R = 2: A - unannealed film from methylamine at -76°C; B - same film at -28°C; C - annealed film from ammonia, from Reference 61.

electrons were recombining with uncomplexed lithium to give spots of lithium metal.

The Li/C211 solution was held for an additional 4 - 5 hours at or slightly above -40°C to allow more complete encryptation of the Li^+. At the end of that period a new optical film was made which remained a robust blue when the bulk solution was frozen. Due to accidental breakage of the glassware, no optical spectra were produced. However the apparent effects of the two encryptation periods allow some kinetic comparisons. Suppose the temperature was constant at -40°C for this equilibrium:

$$Li^\circ + C211 \underset{k_b}{\overset{k_f}{\rightleftharpoons}} Li^+C211 + e^- \qquad (1)$$

From the data reported by Cahen, et al (66) for $\Delta G^{\neq}_o$, $\Delta H^{\neq}_o$ and $\Delta S^{\neq}_o$ for equilibrium 1 in water, $\Delta G^{\neq}$ at -40°C can be calculated, followed by k_f. Using log K = 5.3 in water (52), $k_f = 4.6 \times 10^{-2}$ sec^{-1}. The equilibrium constant in methylamine may be less than in water, so if log K = 4.5, then $k_f = 2.9 \times 10^{-1}$ sec^{-1}. Now presume the complexation was 25% complete after the initial 90 minute period and 75% complete after the additional 5 hours. Using a two component, second order, integrated rate equation gives an average rate constant of 1.6×10^{-3} sec^{-1}. Thus the observed half-life ($t_{1/2}$) is ~2.8 hours, compared to an average $t_{1/2}$ of ~3 minutes calculated by extrapolation of

the aqueous solutions. It should be noted that this was the slowest encryptation observed. All others were presumed to be substantially complete within 3 - 4 hours at -40°C and no experimental evidence indicated otherwise. In the absence of specific data for NH_3 or MA, these rates and times must be considered very crude approximations. Encryptation may proceed at a moderate rate, but it is evident that once complexed, the lithium cation is likely to remain trapped barring decomposition of the cryptand.

III.A.4. Summary and Discussion

Lithium electride systems with R = 2 have metallic character. The electrons show no evidence of being localized on lithium cores. That is another way of stating that Li^- apparently does not exist in solvent-free or damp wet films from NH_3 or MA: there was no peak corresponding to the reported 440 nm band attributed to Li^- in a lithium-ethylamine solution (80). While films with R = 2 from both NH_3 and MA are metallic, spectra of those from the latter solvent are considerably more homogeneous in appearance with fewer peaks and shoulders.

Systems with a nominal R = 1 have shown a variety of responses from metal to insulator. System I was predominately metallic, II was metallic but had an irreversible preference for non-metallic character at low temperatures,

and systems subsequent to II were non-metallic but approached metallic character under annealed, high temperature conditions. Because of the irreproducibility of the metallic character of system I and the distinct MNM transition of system II, only systems III-X will be considered typical of lithium elec' ide.

If the progressive change from metallic character to a MNM transition to nonmetallic character in the first three $Li^{+}C211 \cdot e^{-}$ preparations were the result of some systematic change of reactants or laboratory procedure, it must have been a subtle deviation, indeed. Lithium for the three preparations was from three different sources and the metal purity and accuracy of mass determinations surely varied. However in systems III - VIII where R varies from 0.60 to 1.15, the optical spectra as summarized in Table 2 show very similar character, thus discounting slight variations due to the amount of metal present. During the initial solution preparation, systems III - X were held at -40 ±3°C to promote lithium encryptation for from two to six hours. The spectra give no reason to believe that variable encryptation time has any effect on the metal-insulator character. In solid state studies it is not uncommon for slight changes in composition, inhomogeneity, grain boundary effects, etc., to have a significant impact on the nature of the solid. Composition effects can be discounted as readily as they were above because of the similarity of the

Table 2. Summary of optical spectra for Li/C2ll systems.

System	Solvent	R	Film Condition[a]	Peak Positions[b] (cm^{-1}) e_t^-	Others
(no C2ll)	NH_3	----	damp	----	plasma edge
		----	wet	∿6200	plasma character
(no C2ll)	CH_3NH_2	----	damp	----	plasma edge
		----	wet	∿7700	plasma character
----[c]	NH_3	2	dry	----	plasma edge
			damp	----	plasma edge
			wet	8650	plasma character
I	NH_3	0.93	dry	----	plasma edge
			damp	----	plasma edge
			wet	5900	plasma character
II	NH_3	0.95	dry, > -45°C	----	plasma edge
			dry, < -51°C	6000	----------
			dry, < -60°C	5000, 7000	∿12,000 (s)
			dry (re-formed)	----	nearly plasma edge
III	NH_3	0.98	dry	∿5000, ∿7000	∿12,000 (s) plasma character
IV	NH_3	0.99			

Table 2. Continued.

System	Solvent	R	Film Condition[a]	Peak Positions[b] (cm^{-1})	
				e_t^-	Others
V	NH_3	0.97	dry(fr)	∿5000, ∿7000	∿12,000 (s), plasma char.
			dry(ann)	4700	nearly plasma edge
VI	NH_3	1.15	dry	∿5200(m), ∿7000	plasma character
VII	NH_3	0.60	dry	∿5300, ∿7400	plasma character
VIII	NH_3	1.57	dry (fr)	∿5200	plasma character
			dry (ann), -37°C	----	plasma edge
			dry (ann), -70°C	5000	plasma character
X	NH_3	0.96	dry (fr & ann) and -65°/-127°C	∿5300, ∿7000	∿12,500 (s)
			-65°/-91°C	5650	increasing plasma char.
			-65°/-78°C	7000	nearly plasma edge
V	CH_3NH_2	0.97	dry (fr)	5800	∿13,500(s), plasma char.
			dry (ann)	∿5700	plasma character

Table 2. Continued.

System	Solvent	R	Film Condition[a]	Peak Positions[b] (cm^{-1}) e_t^-	Others
----	CH_3NH_2	2	dry (ann)		
			-76°C	~4800	nearly plasma edge
			-28°C	----	plasma edge

[a] fr = fresh, ann = annealed; where two temperatures are listed, the first is the film temperature, and the second is the bulk solution temperature.

[b] m = major peak, s = shoulder.

[c] Data from Reference 61.

optical spectra while the relative amount of metal was varied. Grain boundary effects or sample thickness are dismissed as a major factor because of the consistency of results from thin optical films to thicker films in EPR samples to bulk samples for magnetic susceptibility, typified by systems VII and VIII to be discussed later in this chapter.

One fairly obvious rationale for the discrepancy among the R = 1 preparations is the possible presence of solvent. The ammonia analyses of Chapter V and the vapor pressure study of systems IX and X were attempts to determine the possible effects of solvent. The results of Chapter V indicate that a "dry" electride optical film may still contain approximately one mole of NH_3 for every ten moles of cryptand. Chapter V results also argue that the mole ratio C211 : NH_3 increases (more NH_3 is removed) for longer static pumping times. However the optical spectra do not show annealing effects unless the bulk solution is warmed considerably above liquid nitrogen temperature. Therefore it is concluded that, for optical films in this research exposed to a bulk solution at -196°C, the films were essentially dry within several minutes of freezing the bulk solution and that any subsequent decrease of the film's NH_3 content had a negligible effect on the film, its spectra and its metallic or nonmetallic character. This conclusion is reinforced by the vapor pressure study wherein the

NH_3 vapor pressure was raised approximately thirteen orders of magnitude before any effect was noted in the optical spectra, at -116°C < Temp < -91°C for the bulk solution with the film at -65°C.

To summarize the above discussion, the reasons for the differences in behavior of $Li^+C211 \cdot e^-$ samples I and II from those of later samples remain unknown.

Several general trends are noted among the other lithium electride systems. As film temperatures are raised, the infrared absorbance increases, probably reflecting an increase in the conduction band population that is typical of thermal promotion in a small band-gap semiconductor. As the mole fraction of Li is raised from 1.15 to 1.57 to 2, the optical spectra appear to become more homogeneous. Only three systems with R values of 1.57 or 2 were studied so there is a possibility that these spectra are not representative. However if they are, then the increase in uncomplexed lithium cations (no evidence for Li° or Li^-) must be causing or helping create a more homogeneous environment for the electrons. Possible explanations follow.

It appears from optical spectra that somewhere between mole ratios 1.15 and 1.57 the high energy e_t^- peak and shoulder begin to disappear. It is possible, but it has not been demonstrated, that Li and C211 may form inclusive-exclusive complexes as in the case of Cs and C222 (81). Then the electrons would feel at least two

different environments (the cryptand asymmetry may create more), one in which the electron is in the vicinity of an inclusive Li/C211 complex and the other in which the electron may be forming some variety of loose ion pair (EPR shows no hyperfine splitting) with a protruding or exclusive cryptated lithium cation. It is possible that the higher energy peak of the two typical e_t^- absorption peaks is due to some form of ion pair, analogous to the 8475 cm^{-1} (1180 nm) peak attributed to the ion pair (Li^+, e^-_{solv}) in tetrahydrofuran (82). Then as the mole ratio is increased, free lithium cations begin to fill enough interstices to homogenize the environment for the electrons, progressively decreasing the effect of some quantity of exclusive Li^+.

A second and equally speculative possibility is that NH_3 is such a powerful solvating agent that the equilibrium

$$Li^\circ + C211 \rightleftarrows Li^+C211 + e^-$$

does not lie far to the right as with many other solvents (52). Perhaps competing equilibria

$$Li^\circ + 4NH_3 \rightleftarrows Li(NH_3)_4$$

or

$$Li^\circ + xNH_3 \rightleftarrows Li^+(NH_3)_x + e^-_{solv}$$

are so energetically favorable that the first equilibrium above is shifted somewhat to the left. Then when the solvent is removed by flash evaporation during optical film formation, some lithium is trapped outside the cryptand. The increase in the mole ratio, as in the previous hypothesis, homogenizes the solid structure and the electronic environment. It should be noted, however, that at R = 2 there are many more octahedral and tetrahedral holes than there are tiny lithium cations to occupy them. But before the structure is homogenized physically, it is homogenized by promotion of the electrons into the conduction band. Some critical minimum of Li^+ concentration is passed after which the electrons are metallic, with the transport process possibly being site-to-site hopping on Li^+ centers in the minimally metallic regime.

The spectra of damp and wet films show that electride films have a fairly high ammonia affinity, but considerably lower than that of lithium metal. With the bulk solution at -116°C there should have been enough NH_3 present to saturate a -65°C Li° film, yielding a typically metallic spectrum. However, this metallic spectrum did not appear for the electride until the bulk solution was at ∿-78°C where the vapor pressure was a factor of ∿90 higher than at -116°C.

III.B. EPR

Electron paramagnetic resonance (EPR) probes the change of the local environment of an unpaired spin, as opposed to methods which monitor bulk properties such as magnetic susceptibility and conductivity which will be discussed later. In the EPR experiment, degenerate spin energy levels are split by application of a magnetic field. Transitions between the Zeeman levels can be induced by radiation of the appropriate frequency. Since the Zeeman splitting is proportional to the applied magnetic field, field strength and/or radiation frequency can be varied to induce the resonance according to the equation

$$\Delta E = h\nu = g\beta H$$

where h is Planck's constant, ν is the frequency of the electromagnetic radiation, g is the Landé g factor, β is the Bohr magneton and H is the magnetic field strength. In practice, microwave radiation of a fixed frequency is generated and the magnetic field is swept through the resonance value. The Landé g factor is

$$g = \frac{3}{2} + \frac{S(S + 1) - L(L + 1)}{2J(J + 1)}$$

where S, L and J are spin, orbital and total angular momentum quantum numbers, respectively (83). For an electron with no orbital angular momentum, S = 1/2, J = 1/2 only and therefore g = 2. Systems similar to this, with the free electron g-value of 2.0023, will be considered in this study.

Two theoretical lineshape expressions are commonly used to describe spin systems which have symmetrical lineshapes (45). For a homogeneous environment where the spin system maintains thermal equilibrium during resonance and relaxation is dominated by spin-lattice interactions, the lineshape is normally Lorentzian. The Guassian shape usually applies to systems in which the spins are in different environments. If spin-spin relaxation is the predominant relaxation mechanism, both Lorentzian and gaussian shapes can be fit by normalized expressions involving T_2. To simply extract the spin-spin relaxation time for a Lorentzian line, $\Delta H_{1/2} = \hbar/g\beta T_2$ can be used where $\hbar = h/2\pi$ and $\Delta H_{1/2}$ is the half width at half height for the absorption curve. For a first derivative EPR lineshape, ΔH_{p-p} is the width between the maxima of the two lobes (peak-to-peak linewidth) and equals $2\Delta H_{1/2}/\sqrt{3}$. Therefore

$$\Delta H_{p-p} = 2\hbar/\sqrt{3}g\beta T_2 \qquad (2)$$

and T_2 can be determined from the readily attainable experimental value ΔH_{p-p}.

In this study neither purely Lorentzian nor purely gaussian expressions fit the experimental lineshapes. However, by using both lineshape functions and applying them to the widest and narrowest signals studied, the true spin-spin relaxation times for all $Li^+C211 \cdot e^-$ samples should be bracketed.

Equation 2 and ΔH_{p-p} values from Figure 19 yield the T_2 values of Table 3 in the high temperature region 100K < T < 240K and at approximately 4K.

Table 3. $Li^+C211 \cdot e^-$ spin-spin relaxation time extrema.

	VIII		VI	
Sample	High Temp.	4K	High Temp.	4K
ΔH_{p-p} (G)	0.60	2.2	0.175	0.50
Lorentzian T_2 (sec)	1.1×10^{-7}	3.0×10^{-8}	3.7×10^{-7}	1.3×10^{-7}
Gaussian T_2 (sec)	8.2×10^{-8}	2.2×10^{-8}	2.8×10^{-7}	9.9×10^{-8}

The fairly narrow linewidths correspond to long relaxation times which are due to weak spin-spin coupling (45).

Webb's extension (21) of Dyson's theory (19) for the EPR lineshape due to conduction electrons (discussed in Section I.B.) was perused for its applicability to the $Li^+C211 \cdot e^-$ system. The first derivative asymmetry

parameter A/B is independent of T_D/T_1 if $a/\delta \leq 1.60$, where: A and B are the low and high field lobe amplitudes of the first derivative curve, respectively; T_D is the time for a spin to diffuse across the material's skin depth, δ; T_1 is the spin-lattice relaxation time which equals T_2 for a metal; and a is the spherical particle radius for the material. Therefore, in the absence of independently determined values to allow a fit with Webb's lineshape equation, no fit was attempted. The $Li^+C211 \cdot e^-$ systems must be marginally- or non-metallic or else the effective particle radii (or sample thickness) must be approximately equal to the skin depth for A/B to be <2.5. Others have employed a direct interpolation between the classical Lorentzian lineshape (A/B = 1.0) and the lower limit of Dyson's theory (A/B ∿2.7) to extract spin relaxation times (24). No such interpolation was attempted in this study.

III.B.1. Results

Only minimal EPR information was gathered for $Li^+C211 \cdot e^-$(I) with R = 0.93, which showed metallic character in its optical spectra. At -152 ± 3°C, A/B was ∿1.0, ΔH_{p-p} = 0.37 G and the g-value = 2.00223. This g-value was determined by placing the electride sample and a small sample of α,α'-diphenyl-β-picrylhydrazyl (DPPH) in the EPR cavity at the same time and determining the spectrum. The same DPPH sample was then calibrated by comparison with the benzene

radical anion septet spectrum, giving g_{DPPH} = 2.00370 at -102°C (Section III.B.4.). Finally the g-value of the electride was calculated.

A search for free lithium metal was conducted. The lithium metal g-value is only slightly different from that for the free electron: $\Delta g = -6.1 \times 10^{-5}$ (84). Therefore the electride and lithium signals should overlap. A maximum first derivative amplitude is obtained when the spectrometer modulation amplitude is adjusted to approximately twice the value of the signal ΔH_{p-p} (69). In selected scans, the modulation amplitude was increased to aid the search for a free lithium signal with ΔH_{p-p} of 4 - 5 Gauss at the expense of a true electride lineshape. No free metal signal was observed.

$Li^{+}C211 \cdot e^{-}$ sample II was an interesting EPR specimen. Not only did it show the MNM transition upon cooling that was evident in the optical spectra, but the transition appeared to be completely reversible at -45 ± 1°C in either direction. There was a severe disruption of the cavity Q as well as significant changes in the spectra. Figure 13 shows spectra taken a few minutes apart on either side of the transition. Particularly note the change from 0.95 to 1.77 in the A/B ratio. Figure 14 depicts the ratio A/B for the range 4 - 240K obtained in three separate runs on the same sample. Besides the fairly sharp rise in the region 210 - 230K, A/B also appears to drop significantly

Figure 13. EPR spectra of $Li^{+}C_{211}\cdot e^{-}$ (II): upper spectrum at -59°C with A/B = 0.95; lower spectrum at -45°C with A/B = 1.77 after transition.

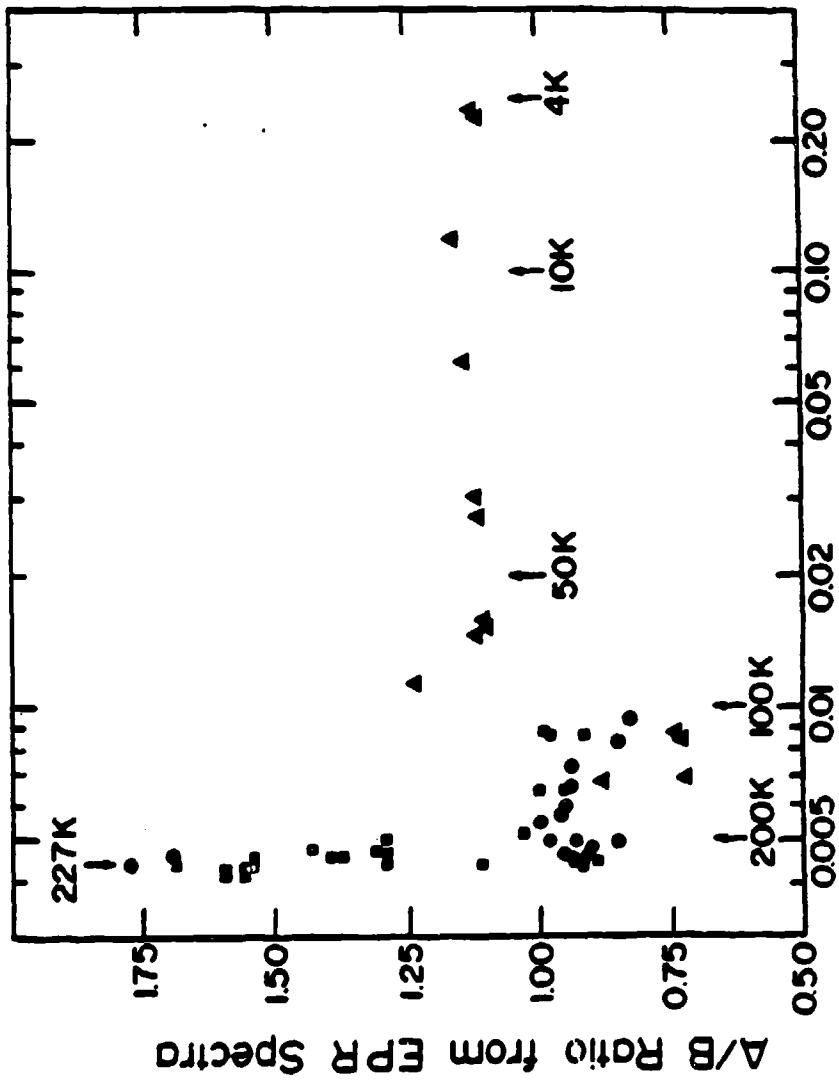

Figure 14. Semi-log plot of A/B vs. reciprocal temperature from $Li^{+}C211 \cdot e^{-}$ (II) EPR spectra. The three different kinds of symbols represent data collected on separate occasions during a three month period.

at about 100K. The plot of ΔH_{p-p} against temperature in Figure 15 shows definite changes in the same temperature regions. Hysteresis is evident in both figures. The significant change in ΔH_{p-p} near 5K was not an artifact. As the temperature was raised above ~3.5K a broader signal diminished and a narrower one increased. During an increase of 3 - 4K the low temperature signal became negligibly small compared to that of the high temperature species. This same phenomenon was noted in many other $Li^{+}C211 \cdot e^{-}$ systems. From -160°C up to the transition temperature the g-value was a constant 2.00200, but from -45°C to -41°C it was 2.00167.

It is of interest to determine the number of paramagnetic centers giving rise to the observed signals. This can be done absolutely or by comparison with a spin standard. The area under the absorption curve is proportional to the number of spins, so tedious double integration of the first derivative curves of the sample and the standard would give the desired information. However, the intensity of a Lorentzian or gaussian signal is proportional to $Y'_{max} \cdot (\Delta H_{p-p})^2$ where $2Y'_{max}$ is the derivative curve peak-to-peak amplitude (69). So in this study, the sample and a National Bureau of Standards crystalline $Al_2O_3:Cr^{3+}$ (ruby) rod were placed in the EPR cavity adjacent to one another. The intensity of each curve at a given temperature was approximated by $2Y'_{max} \cdot (\Delta H_{p-p})^2$ and the absolute number

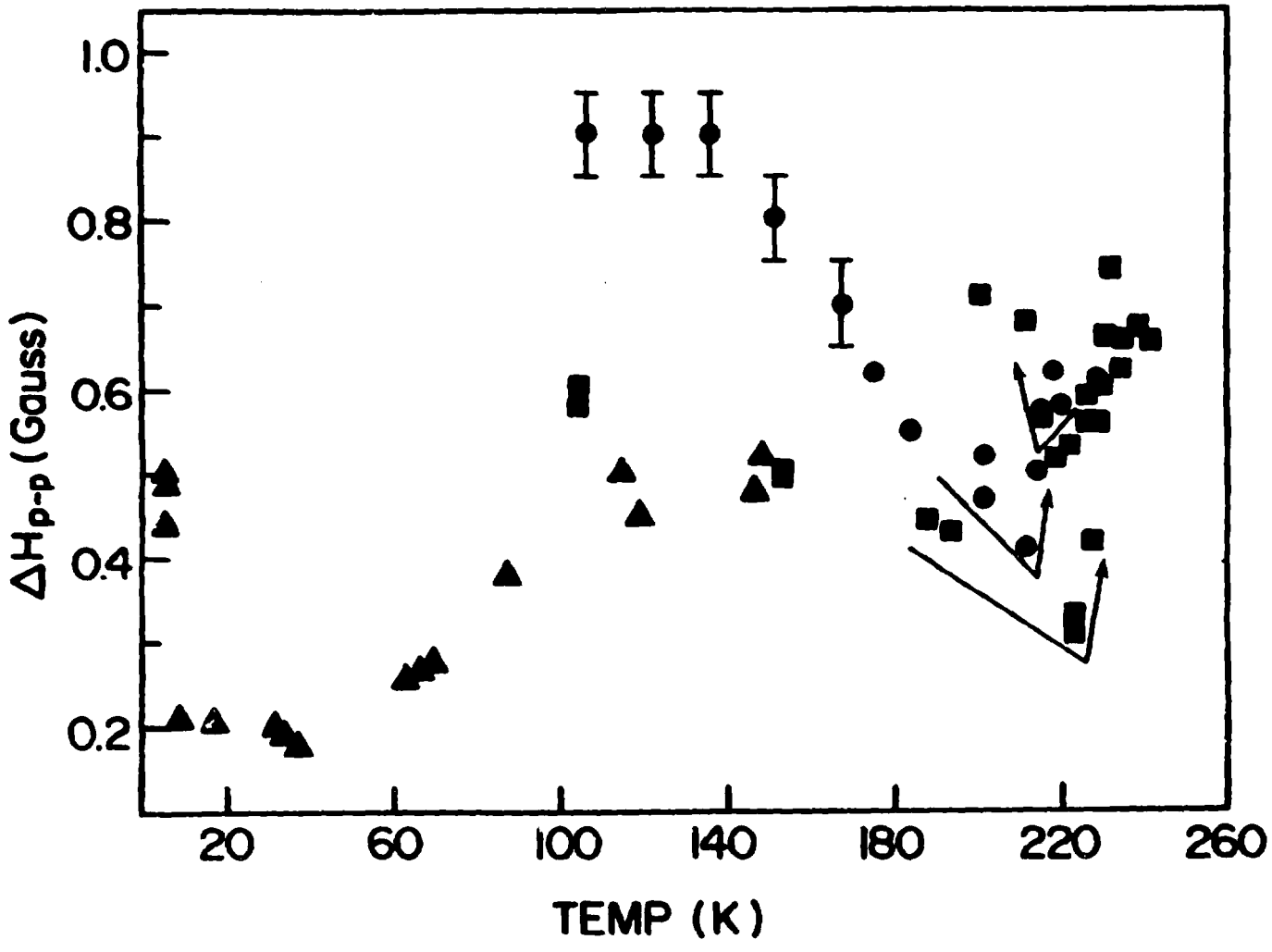

Figure 15. Linewidths from $Li^{+}C211 \cdot e^{-}$ (II) EPR spectra. The three different kinds of symbols represent the same three data collections as in Figure 14.

of sample spins was then calculated from the following equation (85):

$$N = \frac{2\, N_o g_o U^{\alpha_o \beta_o}}{g} \frac{(\text{Intensity})\ (\text{M.A.})_o\ (\text{R.G.})_o}{(\text{Intensity})_o (\text{M.A.})\ (\text{R.G.})}$$

where N is the number of spins, g is the g-value, $U^{\alpha_o \beta_o}$ is the integrated intensity of the ruby signal which varies with ruby crystal orientation in the E4 EPR cavity, M.A. is modulation amplitude and R.G. is receiver gain. The subscript "o" refers to the ruby standard. Figure 16 shows the results of this spin calibration for $Li^+C211 \cdot e^-$ (II). The absolute number of spins participating in the EPR signal is very low, but undergoes an order of magnitude increase at the transition temperature.

The EPR samples for $Li^+C211.e^-$ (III) and (IV) each contained approximately 1.5×10^{18} spins, a factor of three less than for sample II. Yet both of these samples were far too large for E4 AFC stability, hence the results will not be reported here. The effects noted by Catterall (70) which were discussed in Section II.C.2.b. were most pronounced for sample III in the range 30 - 160K where rapid signal crossover caused many apparent linewidths to be <0.10 G. One observation which was independent of these effects was the same signal change at ∿5K as noted for system II. From 3.9 to 4.8 and 6.2K the gain was increased by a factor of 500 to obtain a comparably sized signal and

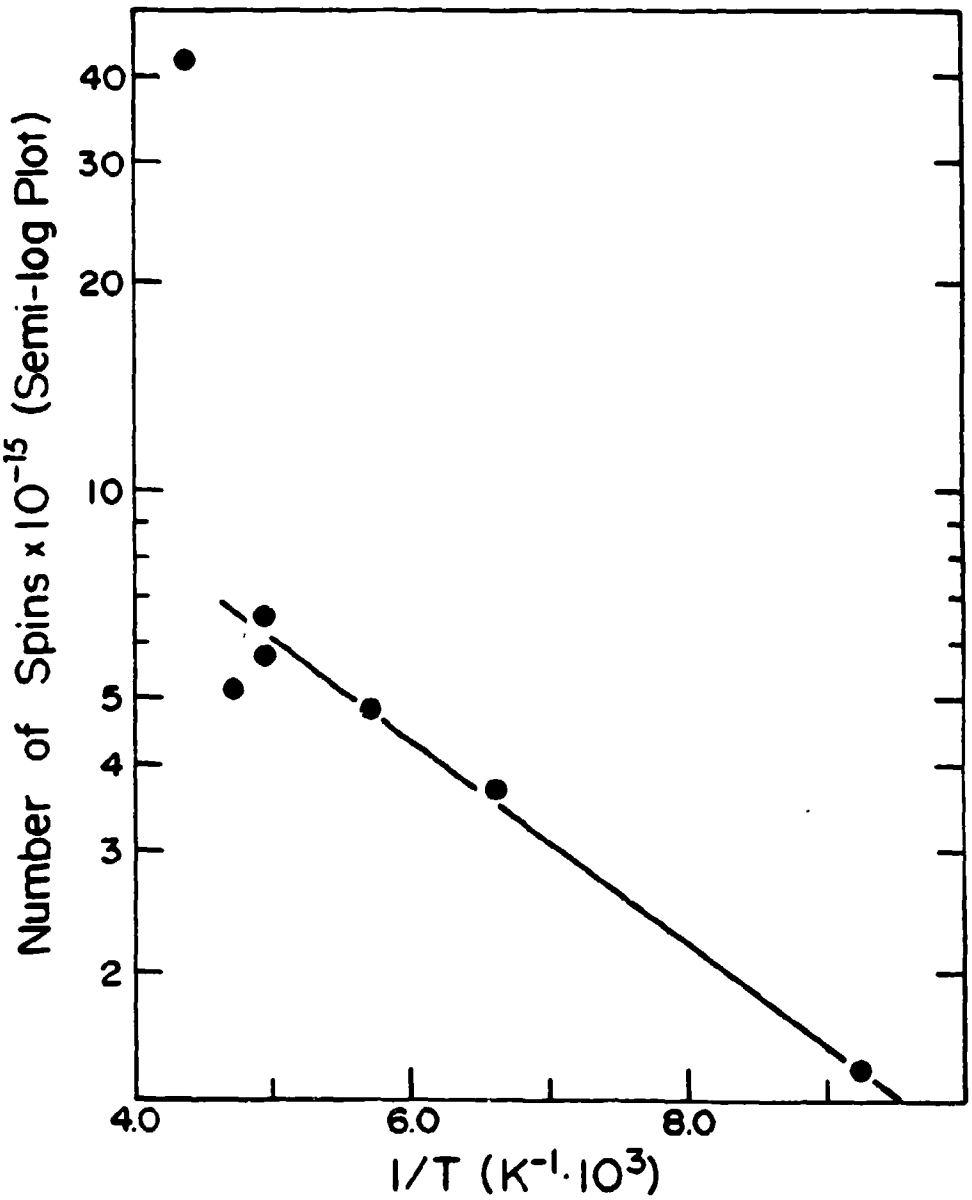

Figure 16. Semi-log plot of the number of unpaired spins from $Li^{+}C_{21}l \cdot e^{-}$ (II) EPR spectra. Data point in upper left corner represents 0.6% of the spins potentially present in the sample while the lower right data point represents .02% of the spins potentially present.

at 8.3K it was reduced back to near the 3.9K settings. Later both samples III and IV were reduced in size and data were collected in the liquid nitrogen temperature range only. Electronic g-values for both samples are included in Figure 20, and in Table 4. Because both samples were reduced in size by an unknown amount, no calibration of the number of spins was attempted.

Table 4. Results of EPR for $Li^{+}C211 \cdot e^{-}$ (III) and (IV).

	Sample III, R = 0.98		Sample IV, R = 0.99	
Temp (K)	115	233	118	233
A/B Ratio	1.21	1.23	1.08	1.29
ΔH_{p-p} (G)	0.37	0.31	0.28	0.24
g-value	2.00200	2.00229	2.00230	2.00229

EPR samples for systems V (R = 0.97), VI (R = 1.15), VII (R = 0.60) and VIII (R = 1.57) were prepared with $\sim 2 \times 10^{17}$ spins and were apparently just small enough to avoid signal distortion. All samples except VIII had multiple signals up to approximately 30K, as depicted in Figure 17. The asymmetry ratios A/B are presented in Figure 18, the linewidths in Figure 19 and the g-values in Figure 20. The percentages of unpaired spins in the samples studied with the liquid nitrogen cryostat are shown on a

Figure 17. EPR spectra of $Li^{+}C211 \cdot e^{-}$ (VI) with R = 1.15. The shift of the low field signals which is apparent from the lower to the upper spectrum continued until all signals appeared to have the same g-value at 65K. This merging of signals was generally complete in other samples by 30K.

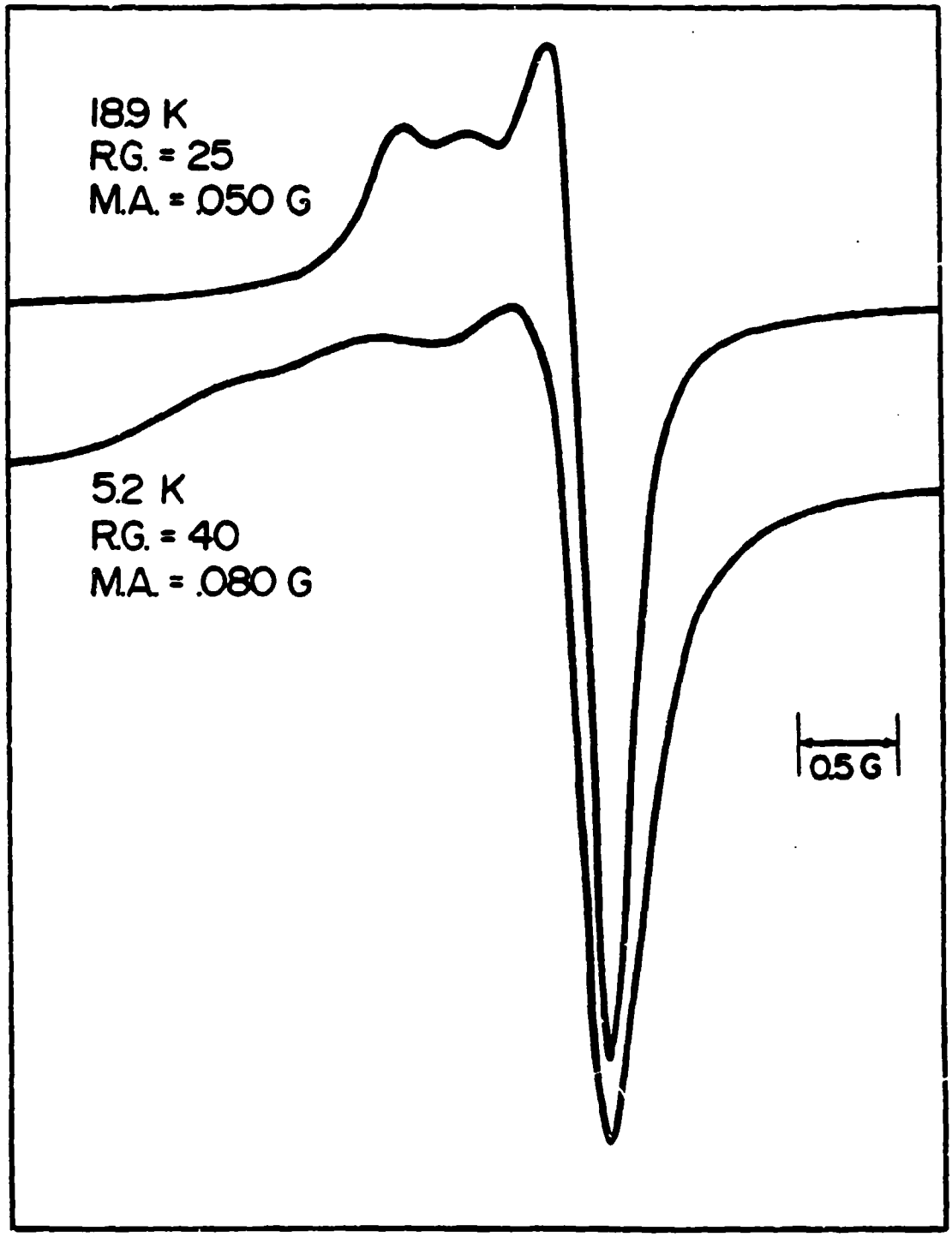

Figure 17.

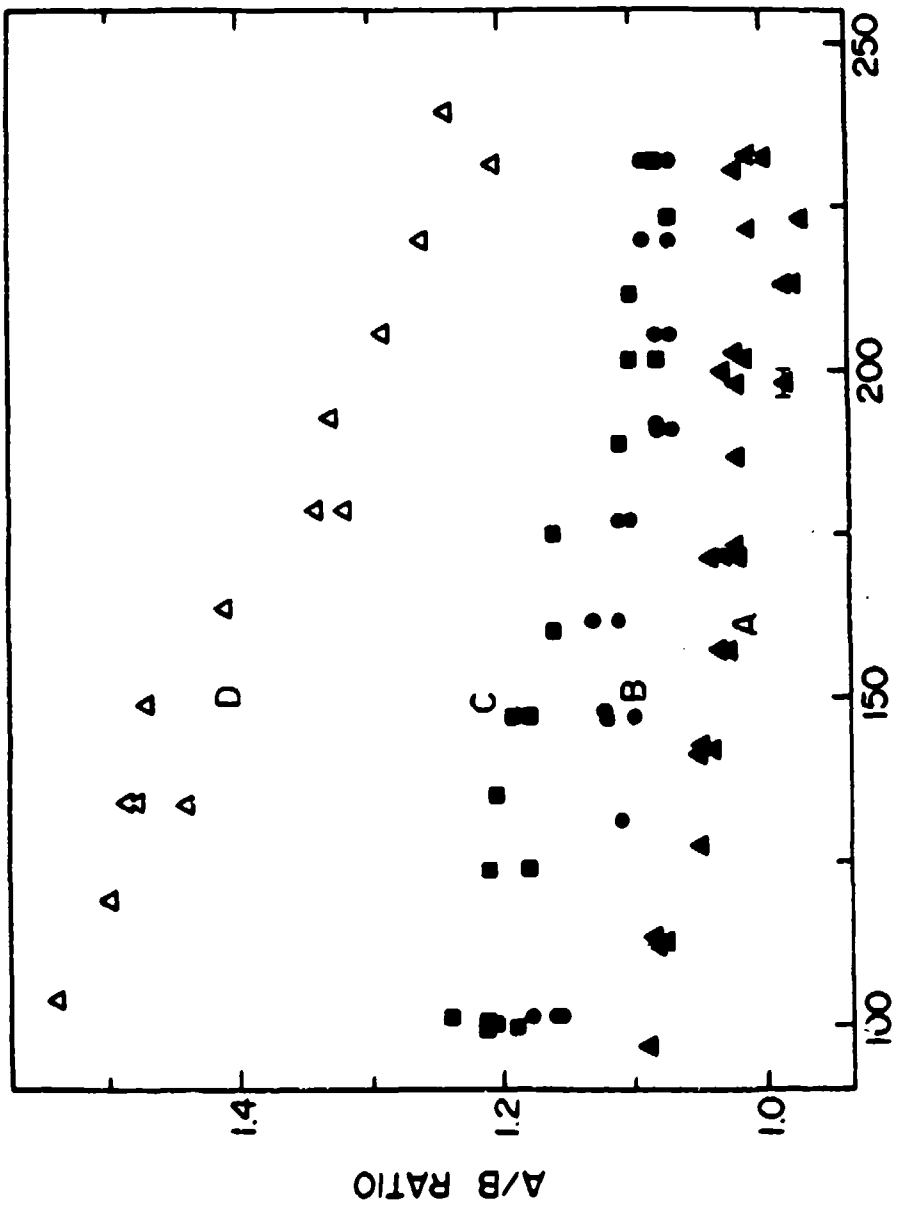

Figure 18. A/B ratios from $Li^{+}C211 \cdot e^{-}$ EPR spectra: A - VII with R = 0.60; B - VIII with R = 1.57; C - V with R = 0.97; D - VI with R = 1.15.

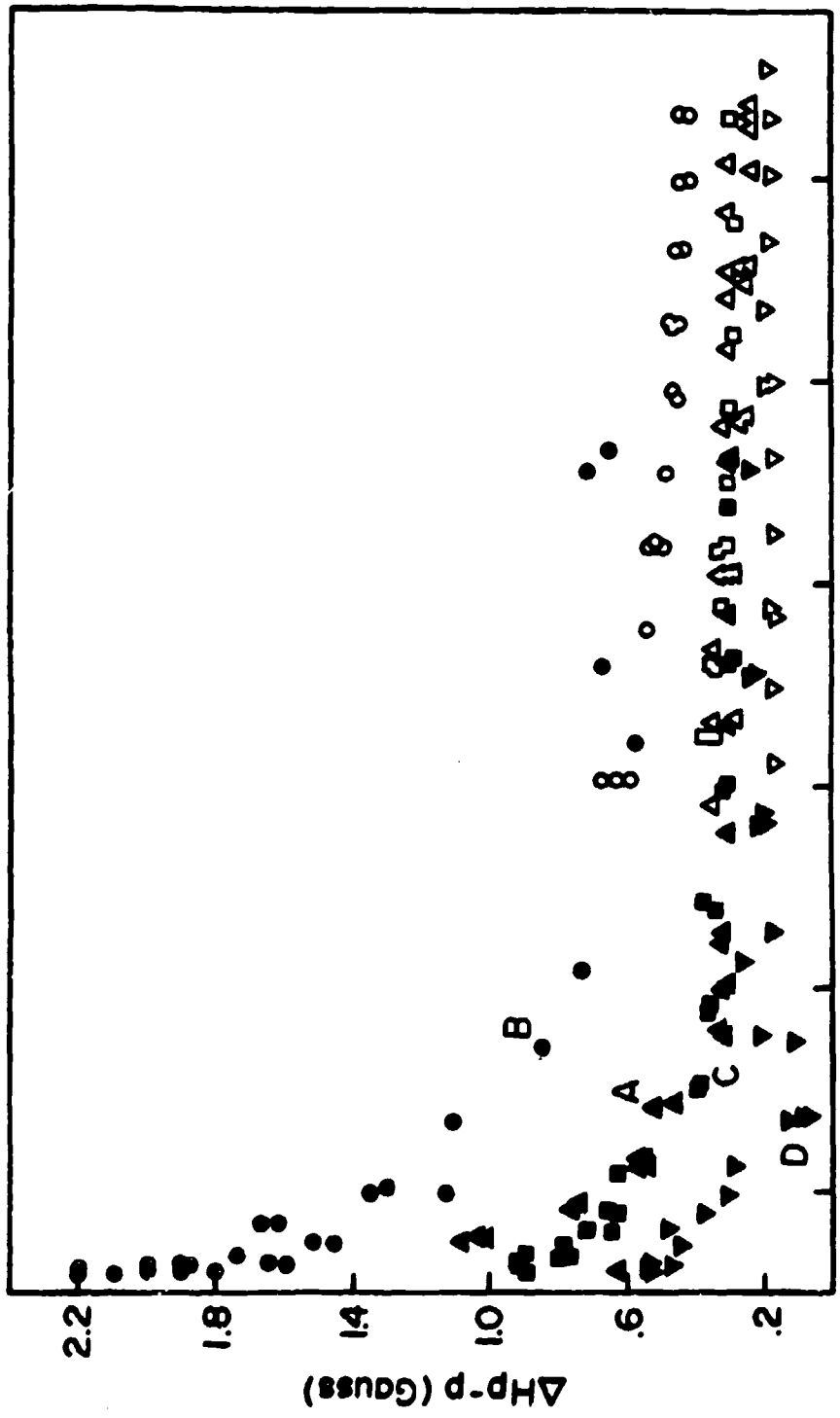

Figure 19. Linewidths from $Li^{+}C211 \cdot e^{-}$ EPR spectra: A - VII with R = 0.60; B - VIII with R = 1.57; C - V with R = 0.97; D - VI with R = 1.15. Solid symbols - data collected with the ℓ-He cryostat; open symbols - ℓ-N_2 cryostat.

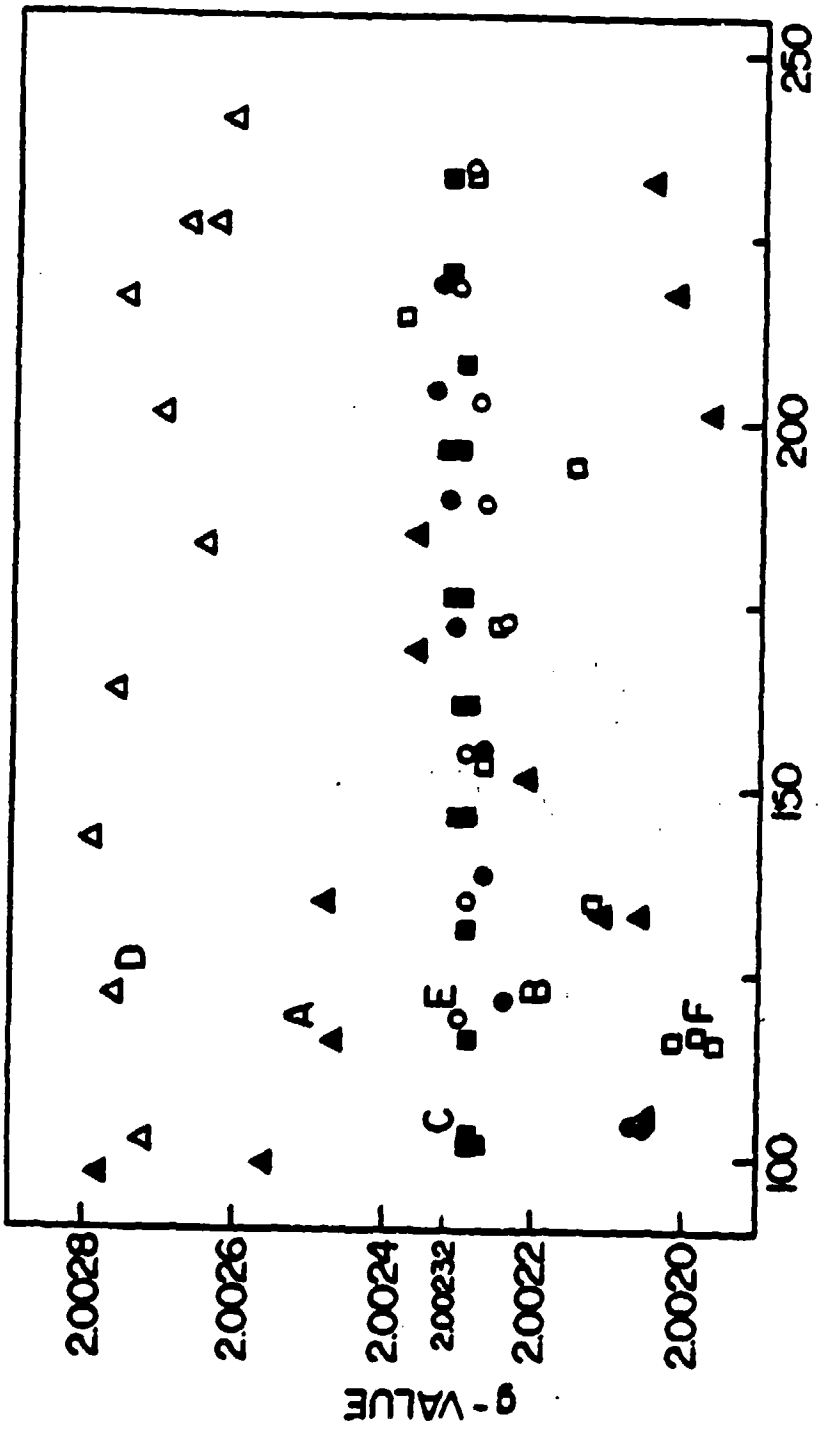

Figure 20. Electronic g-values from $Li^{+}C211 \cdot e^{-}$ EPR spectra: A - VII with R = 0.60; B - VIII with R = 1.57; C - V with R = 0.97; D - VI with R = 1.15; E - IV with R = 0.99; F - III with R = 0.98.

semi-log plot in Figure 21. Neither the ruby nor DPPH standards would fit into the liquid helium cryostat along with the sample, hence g-values and the calibrated number of unpaired spins are not shown below 95K. However, by direct comparison of spectrometer settings the percentages of unpaired spins were approximated down to 3.5K and these values are also included in Figure 21. Only sample V had a signal which could have been from free lithium metal. The approximately 7 Gauss wide signal appeared between 3 and 4K. Calculations from three different spectra placed the quantity of unpaired spins in this signal at 0.3 ± 0.1% of those potentially present.

EPR samples from the vapor pressure study $Li^{+}C211 \cdot e^{-}$ (IX) were evaluated in the nitrogen-cooled range only. Because the ruby standard would not fit into the cryostat with these sample tubes, no information is available for the numbers of spins contributing to the signals. The data for the EPR samples which were sealed off at -116/-65°C and at -91/-65°C are in Table 5. Each of these data values remained fairly constant or changed smoothly over the temperature range; no transitions were obvious. One item of considerable interest was the extremely high receiver gain settings required for Sample B. They were 25 - 50 times those for Sample A even though the sample sizes were comparable.

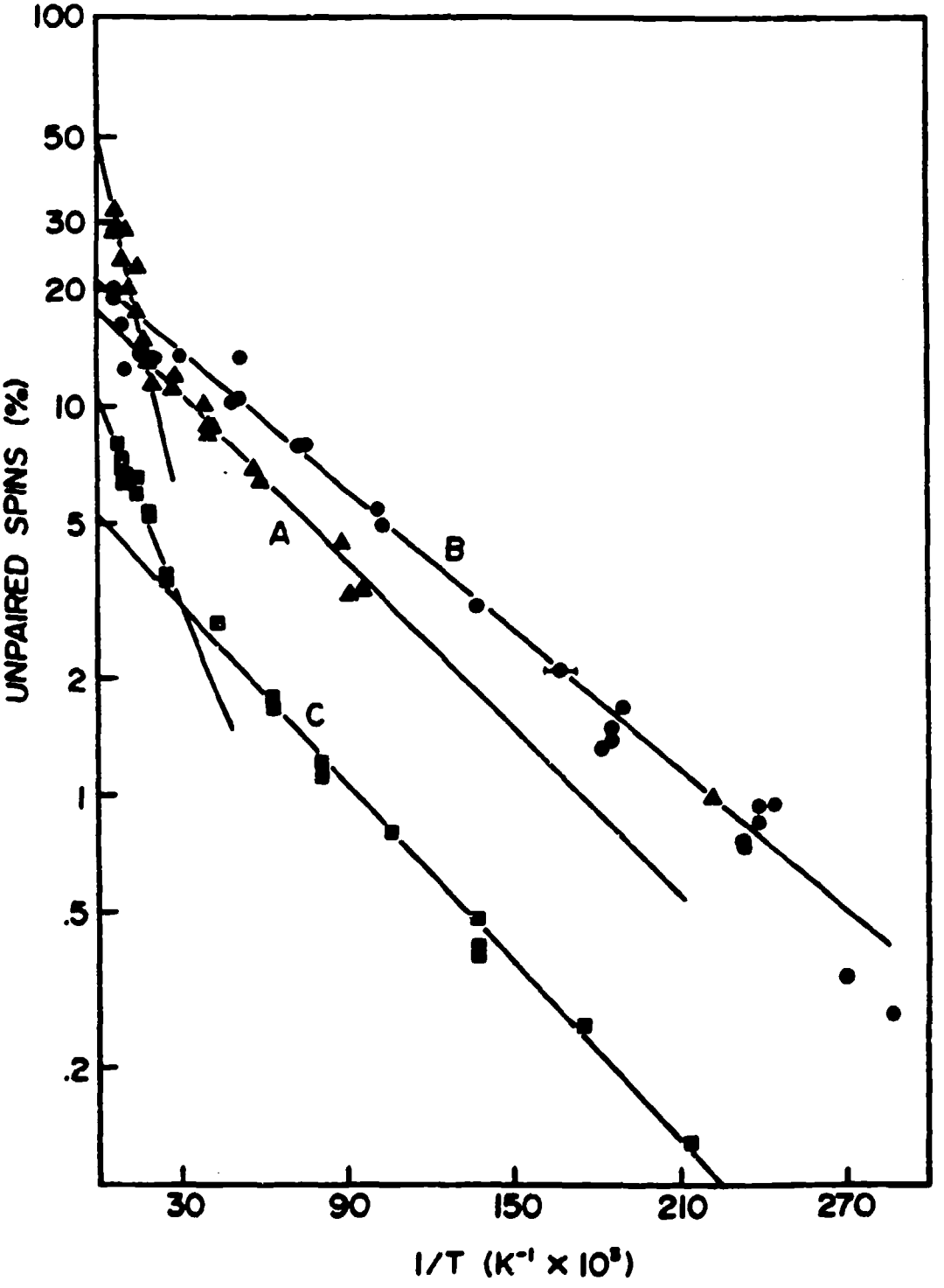

Figure 21. Semi-log plot of the percent of unpaired spins vs. reciprocal temperature from $Li^{+}C211 \cdot e^{-}$ EPR spectra: A - VII with R = 0.60; B - VIII with R = 1.57; C - V with R = 0.97.

Table 5. Results of EPR for $Li^{+}C211 \cdot e^{-}$ (IX), vapor pressure study.

	Sample A[a]		Sample B[b]	
Temp. (K)	118	243	118	243
A/B ratio	1.27	1.26	~1.1	1.11
ΔH_{p-p} (G)	0.32	0.24	0.55	0.22
g-value	2.0026	2.00264	2.0023	2.0022

[a]EPR sample sealed with sample at -65°C and bulk solution at -116°C.

[b]EPR sample at -65°C, bulk solution -91°C when sealed.

III.B.2. DPPH Calibration

DPPH, α,α'-diphenyl-β-picrylhydrazyl, is often used as a standard for g-value determinations. While its g-value is normally reported as 2.0037 ± .0002 (69), presumably any given DPPH sample could be calibrated to greater accuracy by using a standard whose g factor is accurately known. In this study the DPPH sample used for all lithium electride g-value studies was calibrated against the benzene radical anion. Benzene^{-} in a 2:1 solvent of THF:DME is reported to have a g-value of 2.002854 ± .000007 at -101°C with a splitting constant of 3.781 Gauss (86). The seven-peaked benzene^{-} signal showed a splitting of 3.80 Gauss in this study, and four determinations of the DPPH

g-value after repositioning the adjacent DPPH/benzene$^-$ sample tubes yielded a g-value of 2.00370 (3) at -102°C (the value in parentheses is the standard deviation of the last digit). The DPPH g-value at -73°C determined in the same way was 2.00351 (1). Segal, Kaplan and Fraenkel stated that their g-value for benzene$^-$ did not vary with temperature over the range from room temperature to -100°C, so presumably the variation observed here is due to DPPH. This DPPH sample was not calibrated at other temperatures, hence all electride g-values in this study are determined by comparison with DPPH as though it were at -102°C with a g-value of 2.00370.

III.B.3. Summary and Discussion

$Li^+C211 \cdot e^-$, regardless of R value, does not appear to contain any free lithium metal with the possible exception of a very minor amount in sample V. The unpaired electrons in the signals are all at or near the free electron g-value, 2.00232, indicating that there is virtually no spin-orbit coupling present. The A/B ratios in some cases (Figures 14 and 18) are less than expected. There is no theoretical basis for A/B < 1.0 (19,21) so systems II and VII, whose optical spectra show electrons in several trapping sites at 200 - 220K, may have interference from multiple electron-site signals which skew the EPR spectra. System II shows a dramatic jump in the A/B ratio near 225K which is

presumably associated with its transition to metallic character. Metallic samples thick compared to the microwave penetration depths normally show much higher A/B ratios. Only when the skin depth is comparable to the sample thickness will the ratio be low and this is probably the case for $Li^+C211 \cdot e^-$(II) in its metallic region.

The ΔH_{p-p} values of sample II increase with increasing temperature in the metallic regime (Figure 15) corresponding to a decrease in the spin-lattice relaxation time. This decrease is characteristic of delocalized electrons (24). All systems have signals which are quite narrow, but the widest lines are those of systems II and VIII. The former underwent a MNM transition and the latter has the highest R value (1.57) of those thoroughly studied by EPR. These two samples have the most efficient relaxation mechanisms.

There seems to be a significant difference in the number of unpaired spins in samples which appear metallic and in those which are non-metallic. $Li^+C211 \cdot e^-$ (II), by calibration with a ruby standard, was approximately 0.02% unpaired at 110K and 0.6% unpaired at 228K after the MNM transition. The optical spectra of $K^+C222 \cdot e^-$ show high metallic character and the EPR results by DaGue on a sample from the same solution indicated only 0.024% of the spins were unpaired at 157K (64). For metallic systems only the fraction of electrons (T/T_F), where T_F is the Fermi

temperature, would be in the conduction band and presumably unpaired. Table 6 contains a comparison of these systems.

One other result which indicates that metallic samples have few unpaired spins is the high receiver gain required for sample B of system IX. While nothing in Table 5 suggests it has peculiar behavior, the sample was approximately the same size as sample A, yet it required receiver gain settings 25 - 50 times those for sample A. This may indicate that spin pairing was occurring in the sample as it acquired NH_3 on its way to metallic character. The optical spectrum (curve B, Figure 10) appears to be in transition from a dry, standard spectrum to a damp, metallic one. It is probable that the EPR sample is indicating the same transition, hence the onset of spin pairing and an abnormally low EPR signal.

On the other hand, the fact that the non-metallic and/or near-metallic systems V - VIII have a considerable percentage of their spins unpaired is clear from Figure 21. There is a systematic alignment of spins in each system as the temperature is decreased and in several samples the rate of spin pairing changes in the region of 50K. The energy of this antiferromagnetic spin coupling can be readily calculated from the equation

$$N = N_{\infty} e^{-E_a/RT}$$

Table 6. Fermi temperatures of several systems.

System	Temp (K)	Fermi Temp (K)
$Li^+C211 \cdot e^-$ (II)	228	3.8×10^4
$Li^+C211 \cdot e^-$ (II)	110	5.5×10^5
$K^+C222 \cdot e^-$	157	6.5×10^5 (a)
$K^+C222 \cdot e^-$	---	5.6×10^3 (b)
$Li^+C211 \cdot e^-$ (VIII)	4	8.0×10^2
$Li^+C211 \cdot e^-$ (VIII)	225	1.1×10^3
Free Metals		
Li	78	5.5×10^4 (c)
K	78	2.5×10^4 (c)

[a]Reference 64.

[b]Reference 64, based upon estimated conduction electron density.

[c]Reference 42.

where N_∞ is the fraction of spins N unpaired at infinite temperature, R is the gas constant and E_a is the energy of coupling/decoupling. While system VI with R = 1.15 is not included in Figure 21 because its unsymmetric EPR lineshapes yielded very scattered data, it is still included below. The spin pairing energies for systems V - VIII are listed in Table 7.

Table 7. Spin pairing energies for $Li^+C211 \cdot e^-$ systems.

		Spin Pairing Energy (cal/mole)	
System	R	Low Temp	High Temp
V	0.97	35	74
VI	1.15	28	177
VII	0.60	32	117
VIII	1.57	26	26

Note that the energies are in calories: the spin pairing in these lithium electrides is very weak. The percentages of unpaired spins for System VIII appear to lie along a single straight line in Figure 21. Hence it only has one pairing energy in Table 7. This is also the system which showed the most homogeneous optical spectra (Section III.A.2). It is perhaps quite significant that the same systems exhibiting inhomogeneous, multi-peaked optical

spectra are the systems in Figure 21 and Table 7 which have two different spin pairing energies. It is conceivable that the two major electron trap sites indicated in the optical spectra are the same sites where spin pairing is occurring and that each site has its own pairing energy.

Sample VI with R = 1.15 showed EPR properties which did not seem to follow any pattern set by the systems with other mole ratios. Sample VI had the highest A/B ratio by far, the highest g-value, the narrowest spectra and the greatest number of unpaired spins of Systems V - VIII. It is not clear whether this EPR sample or the whole preparation might have been anomalous or whether the pattern which this sample fits is just obscured.

III.C. Magnetic Susceptibility

Magnetic susceptibility is the bulk response of a material when it is placed in a static magnetic field. All matter has a diamagnetic, or negative, contribution to its susceptibility associated with the orbital motion of its electrons. When the material is placed in a magnetic field, the electronic motion is altered such that the induced current creates a magnetic moment which opposes the applied field (87). For materials with no unpaired electrons, this diamagnetism may provide the major contribution to the susceptibility. For other systems with spin angular

momentum only or spin and orbital angular momentum, there is a positive (paramagnetic) contribution to the susceptibility which may or may not be larger than the diamagnetic contribution. If it is, the magnetic susceptibility is positive and the bulk material is labeled paramagnetic. There are a number of sources for this positive contribution to the susceptibility, several of which will be discussed here.

When an isotropic substance is placed in a magnetic field $\vec{H}$, the ratio of the magnetization $\vec{M}$, the magnetic moment per unit volume, to the magnetic field is defined as the magnetic susceptibility χ, or

$$\chi_v = M/H \tag{3}$$

in units of cm^3. The susceptibility is also commonly expressed as gram susceptibility χ_g (cm^3/g) and molar susceptibility χ_M (cm^3/mole). For a system with independent unpaired electrons, the molar susceptibility may be described by the Curie Law (42):

$$\frac{M}{H} = \chi_M = \frac{N(p\mu_B)^2}{3k_B T} = \frac{C}{T} \tag{4}$$

where N is Avogadro's number, μ_B is the Bohr magneton, k_B is the Boltzmann constant and p is the effective number of

Bohr magnetons defined by

$$p \equiv g[J(J + 1)]^{1/2} \tag{5}$$

where J is the total angular momentum quantum number. For a system with a negligible orbital angular momentum, p becomes equal to $g[S(S+1)]^{1/2}$ where S is the atomic spin quantum number. Then the Curie constant C becomes 0.37604 cm^3 K $mole^{-1}$ for a mole of free spins. If only a fraction n of the potentially available "free" spins is unpaired, then

$$\chi_M = \frac{0.37604n}{T} \tag{6}$$

and the units are as previously noted for molar susceptibility.

The molar susceptibility of free spins expressed by Equation 6 is modified when there is an internal interaction in the material tending to align the spins. Weiss postulated this exchange field and Heisenberg showed that it is a result of the quantum mechanical exchange interaction (87). The exchange energy of two electrons may be written as $-2J_{12}S_1 \cdot S_2$ where the exchange integral J_{12} is a direct result of the requirement that the electrons be indistinguishable (87). There is no direct coupling between the spins; the interaction is electrostatic and

is related to the overlap of the charge distributions. For a ferromagnetic system in which the magnetic moments tend to align parallel with one another, the exchange integral is positive, and for an antiferromagnetic system, $J < 0$.

In terms of Weiss' description, if the field due to interacting magnetic ion neighbors is designated $N_W M$, where N_W is a constant, then the Curie Law can be modified:

$$M = \frac{C}{T}(H + N_W M)$$

Then $M(T - CN_W) = CH$ and

$$M = \left(\frac{C}{T - CN_W}\right)H$$

The susceptibility χ must therefore be

$$\chi = \frac{C}{T - CN_W}$$

or in more familiar form

$$\chi = \frac{C}{T - \theta} \qquad (7)$$

where θ is the Weiss constant and is equal to CN_W. For $\theta = T_C > 0$, T_C is the Curie temperature of a ferromagnet above which the spontaneous magnetization (i.e., in the absence of an applied field) vanishes. For $\theta = T_N > 0$,

T_N is the Néel temperature above which the ordered antiparallel arrangement of dipoles disappears. Weiss also expressed the susceptibility above the Néel temperature as

$$\chi = \frac{C}{T + CN_w}$$

where $N_w = 1/2(N_{ii} + N_{AB})$ in a body-centered cubic lattice (87). If an atom on site A has nearest neighbors on sites B and next nearest neighbors on sites A, then $N_{AB} = N_{BA}$ is the molecular field constant for nearest neighbors and for next nearest neighbors $N_{AA} = N_{BB} = N_{ii}$ since the same types of atoms occupy the A sublattice and B sublattice sites. The interaction between nearest neighbors is antiferromagnetic, hence N_{AB} is positive and it is generally greater than N_{ii}. So,

$$\chi = \frac{C}{T + \theta} \qquad (8)$$

where $\theta = 1/2C(N_{AB} + N_{ii})$. Below the Néel temperature the theory predicts that the polycrystalline susceptibility χ_p can be expressed by

$$\chi_p = 1/3\chi_{||} + 2/3\chi_{\perp}$$

where $\chi_{||}$ and $\chi_{\perp}$ refer to susceptibilities parallel and

perpendicular to the z-axis or easy direction. At T = OK the parallel component vanishes and

$$\frac{\chi_p(\text{zero K})}{\chi_p\ (T_N)} = 2/3 \qquad (9)$$

For a metallic system with conduction electrons, Pauli explained the paramagnetism in terms of the Fermi-Dirac distribution of electron energies. The net magnetization of this conduction electron system is given by $N\mu^2 H/k_B T$, but only those electrons within approximately $k_B T$ of the Fermi energy are likely to change spin in the presence of an applied field (42). Only this fraction of the electrons T/T_F contributes to the susceptibility, hence

$$\chi_M = \frac{N\mu_B^2}{k_B\ T_F} \qquad (10)$$

which is the Pauli susceptibility after Landau's diamagnetic correction. If the electrides may be thought of as expanded (low electron density) metals, then they would presumably follow this temperature-independent Pauli susceptibility for conduction electrons.

III.C.1. Results

For both the magnetic susceptibility and EPR experiments, degenerate spin levels are split by an applied magnetic field. If it were possible to calculate the number of spins contributing to the EPR spin susceptibility, it might then be possible to estimate the bulk magnetic susceptibility for samples made from the same solutions. In this study, the number of unpaired spins in various samples was determined from spin susceptibilities by comparison with a ruby standard. The molar susceptibility was then calculated from Equation 6:

$$\chi_M = \frac{0.37604\ n}{T}$$

using the temperature-dependent fraction of unpaired spins in each sample as depicted in Figure 21. It should be noted that the fraction of unpaired spins was taken from the straight lines of Figure 21, not from actual data points. The spin susceptibility results for samples VII (sample A, R = 0.60), VIII (sample B, R = 1.57) and VI (sample D, R = 1.15) are shown in Figures 22, 23 and 24, respectively. In Figure 25 they are combined for comparison.

Results of the bulk static magnetic susceptibilities are displayed in Figure 26 for samples VII (R = 0.60), curve A; VIII (R = 1.57), curve B; and IV (R = 0.99),

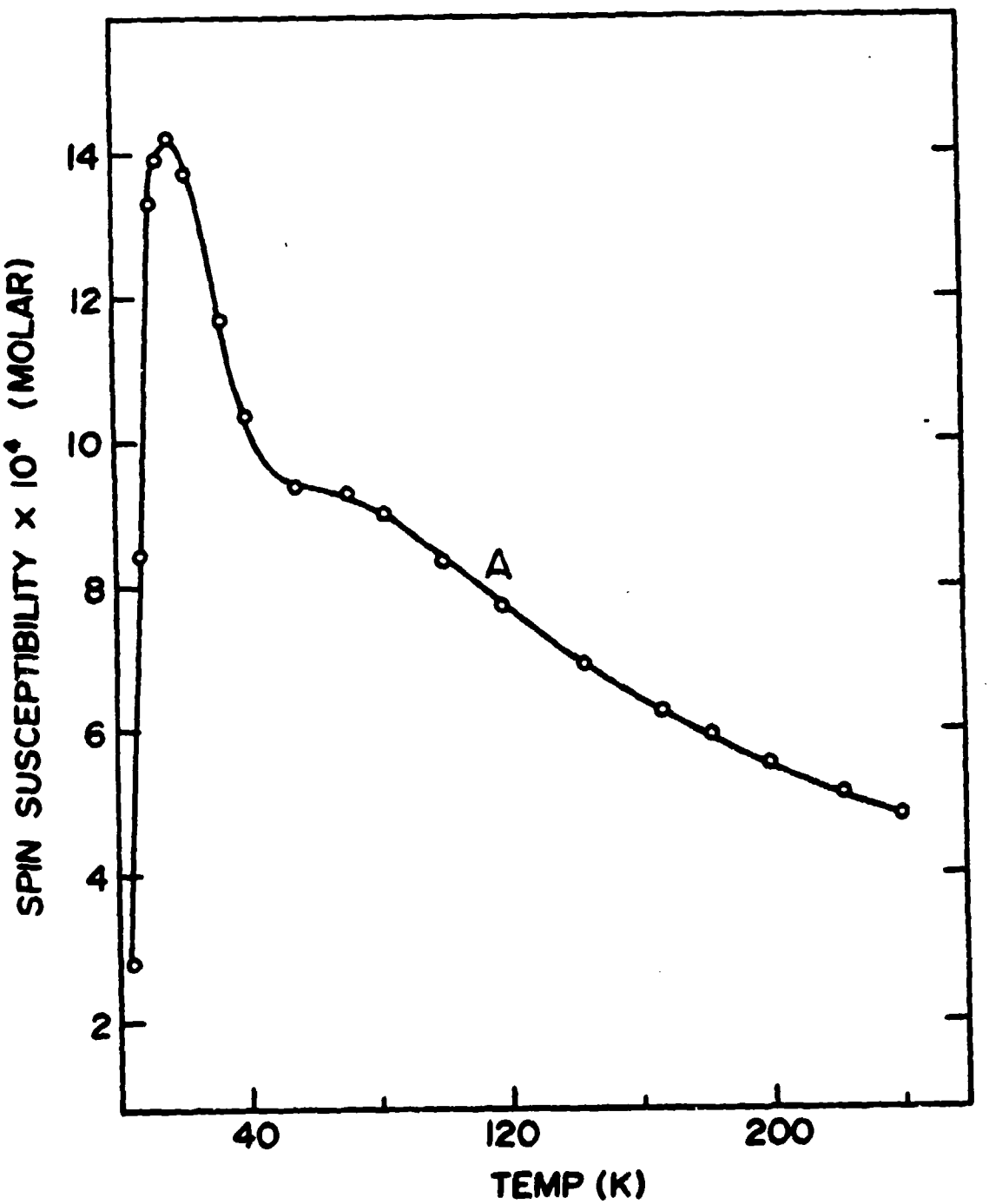

Figure 22. Molar spin susceptibility of $Li^{+}C211 \cdot e^{-}$ (VII): sample A with R = 0.60. The fraction of unpaired spins used to determine χ_M was from the straight lines of Figure 21, not from actual data points.

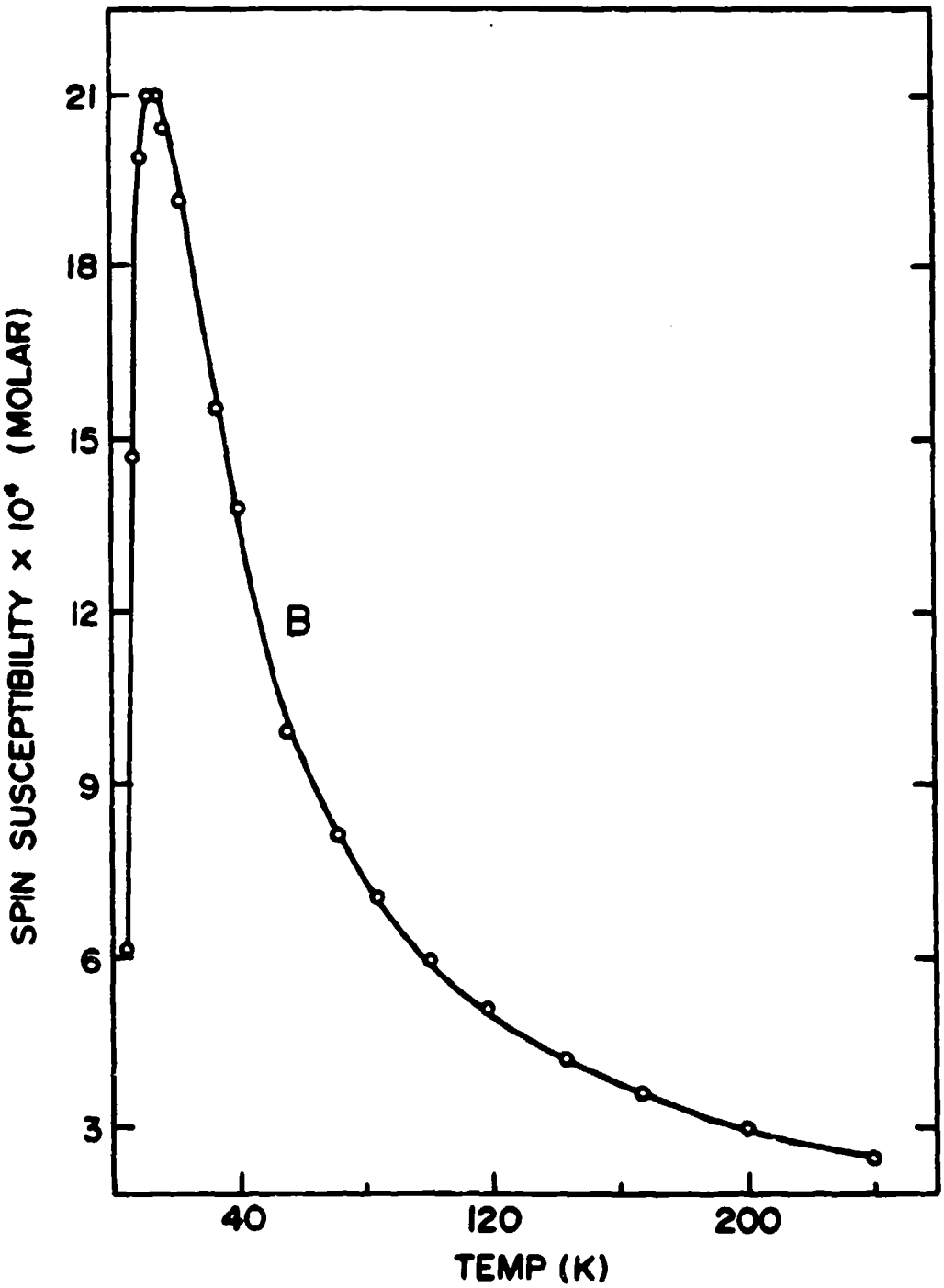

Figure 23. Molar spin susceptibility of $Li^{+}C211 \cdot e^{-}$ (VIII): sample B with R = 1.57. The fraction of unpaired spins used to determine χ_M was from the straight lines of Figure 21, not from actual data points.

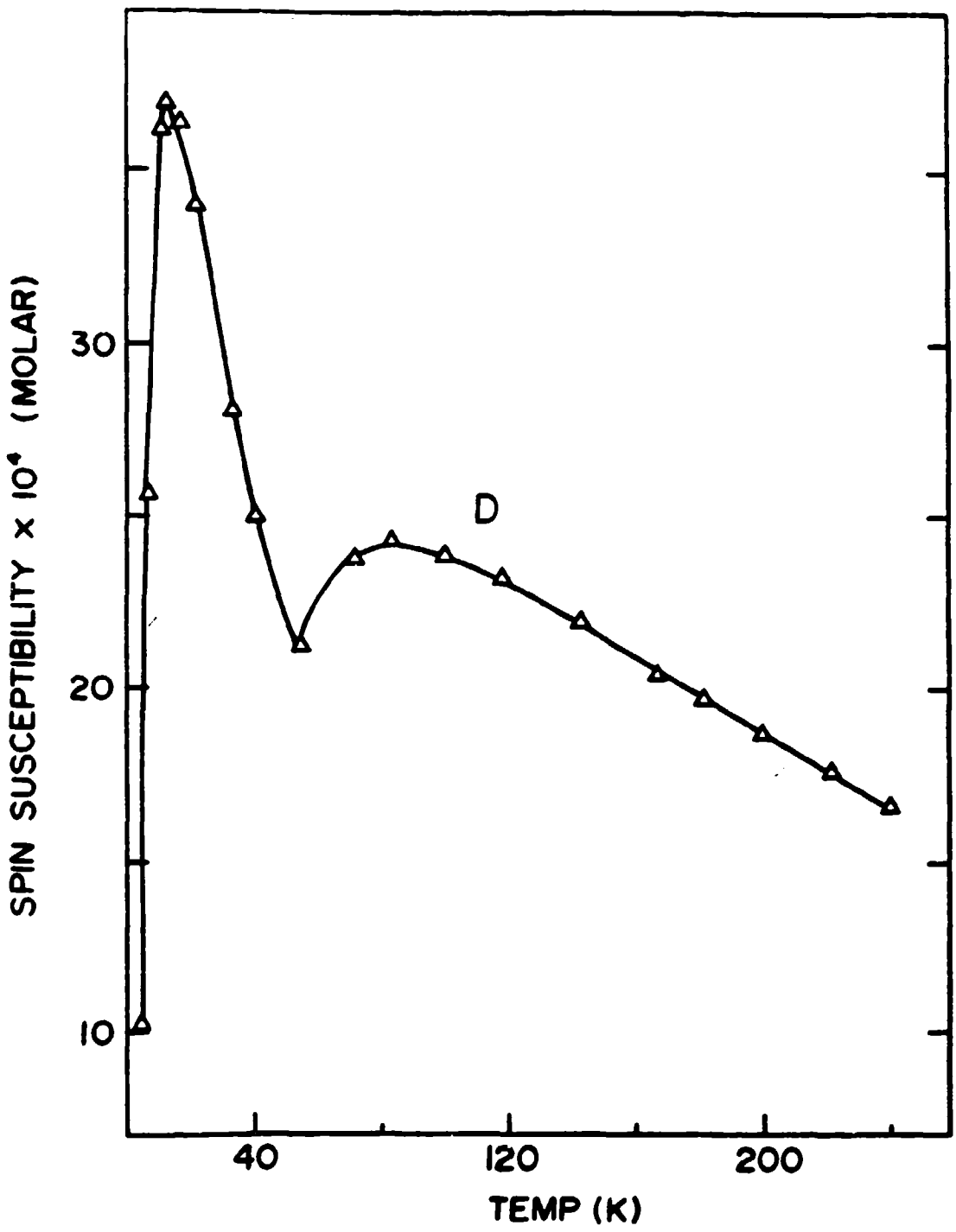

Figure 24. Molar spin susceptibility of $Li^{+}C211 \cdot e^{-}$ (VI): sample D with R = 1.15. The fraction of unpaired spins used to determine χ_M was from the straight lines of Figure 21, not from actual data points.

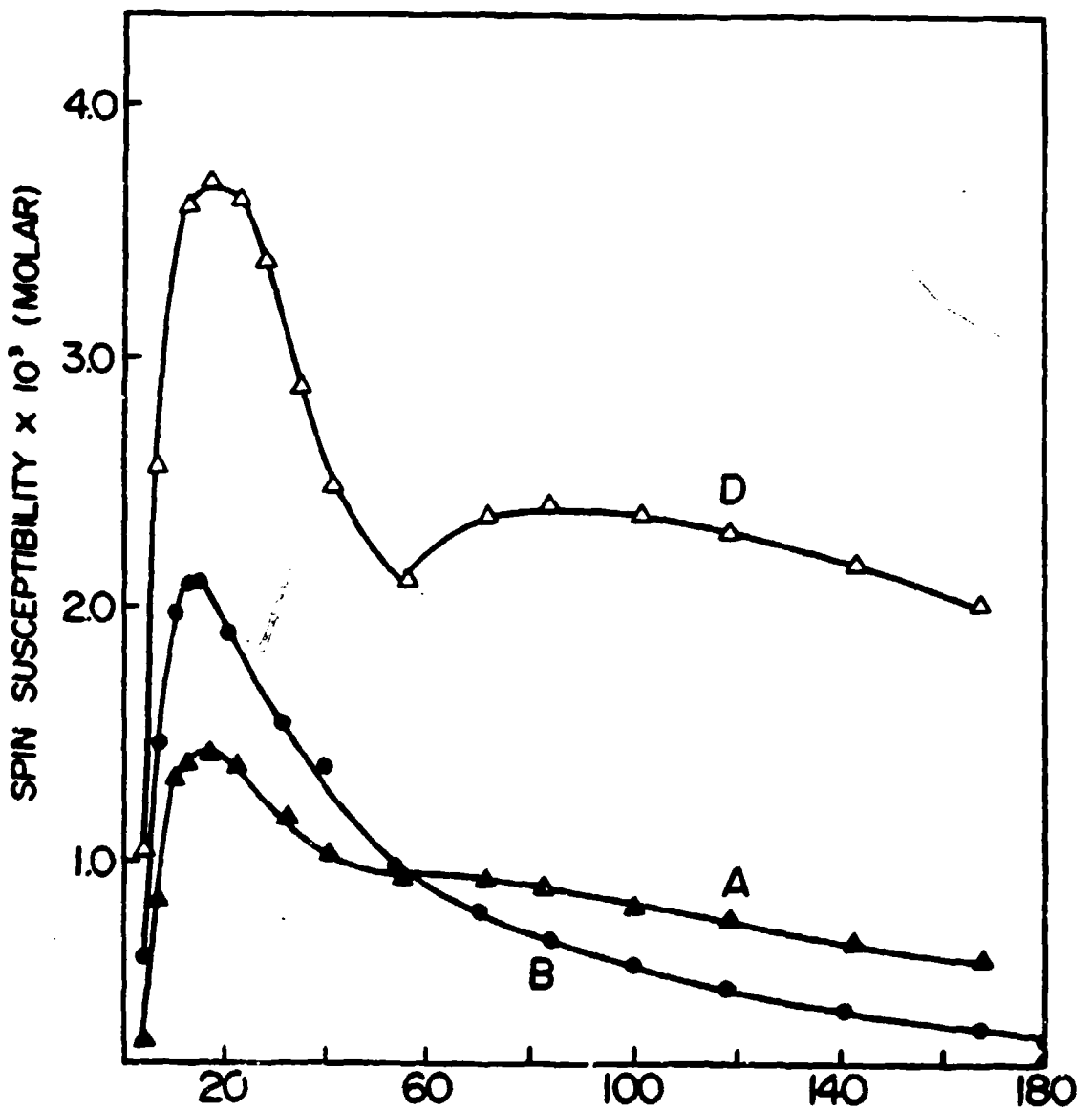

Figure 25. Molar spin susceptibilities for $Li^{+}C211 \cdot e^{-}$ from Figures 22, 23 and 24: A - VII with R = 0.60; B - VIII with R = 1.57; D - VI with R = 1.15. The fraction of unpaired spins used to determine χ_M was from the straight lines of Figure 21, not from actual data points.

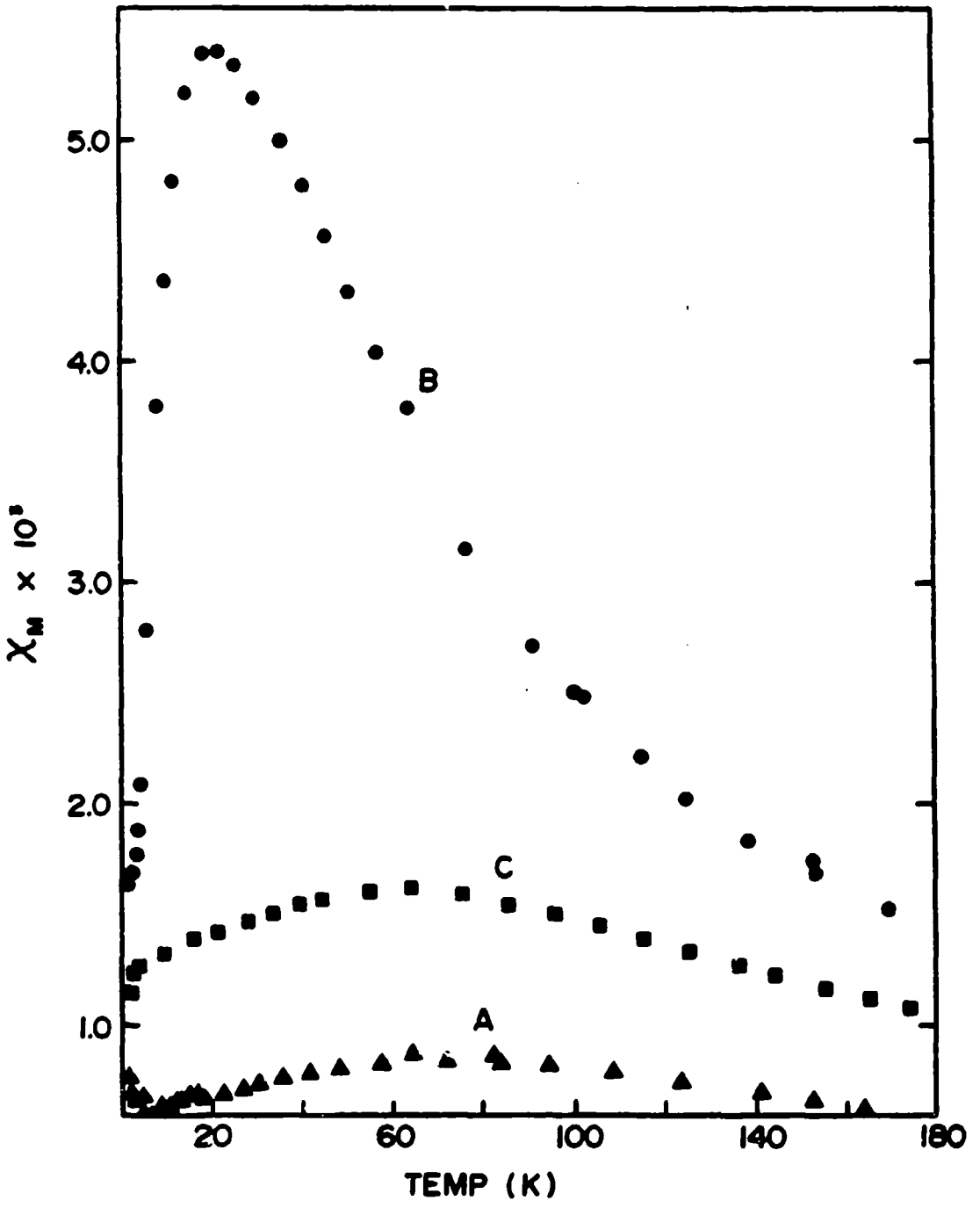

Figure 26. Molar static susceptibilities for $Li^+C211 \cdot e^-$: A - VII with R = 0.60; B - VIII with R = 1.57; C - IV with R = 0.99. Note: the mole ratio of sample C is approximately the same as for samples labeled C in Figures 18-21, but this curve C represents a different preparation.

curve C, for which no spin susceptibility is available. Sample VI did not yield any data. It probably decomposed while being inserted into the Faraday balance Dewar. The molar static susceptibilities were calculated by Ms. Angelica Stacy at Cornell University based upon the number of moles of lithium in the samples determined during post-analysis for samples VII and VIII (Section III.E.) and by an estimate from the solution stoichiometry and sample size for IV. The bucket correction for sample C was initially determined by reconstructing and rehanging the empty bucket (Section II.C.2.a.). This was judged unsatisfactory because of the apparent presence of field-dependent paramagnetic impurities on the empty bucket. Ms. Stacy then scaled bucket corrections based upon the combined sample/bucket mass from those for VII and VIII, and this method, though not exact, appears quite satisfactory.

Figure 27 displays the reciprocal molar susceptibilities for the systems of Figure 26. Each has a negative Weiss constant: VII (curve A): -130K; VIII (curve B): -11.8K; and IV (curve C): -102K. In addition the high temperature regions (> $\sim$80K) are fit by the Curie-Weiss Law rather well with approximately one unpaired electron per lithium: VII, $\sim$.94 unpaired electrons/Li; VIII, .70/Li; and IV, $\sim$.94/Li.

The susceptibilities of the samples observed in the SQUID susceptometer in the MSU Physics Department were

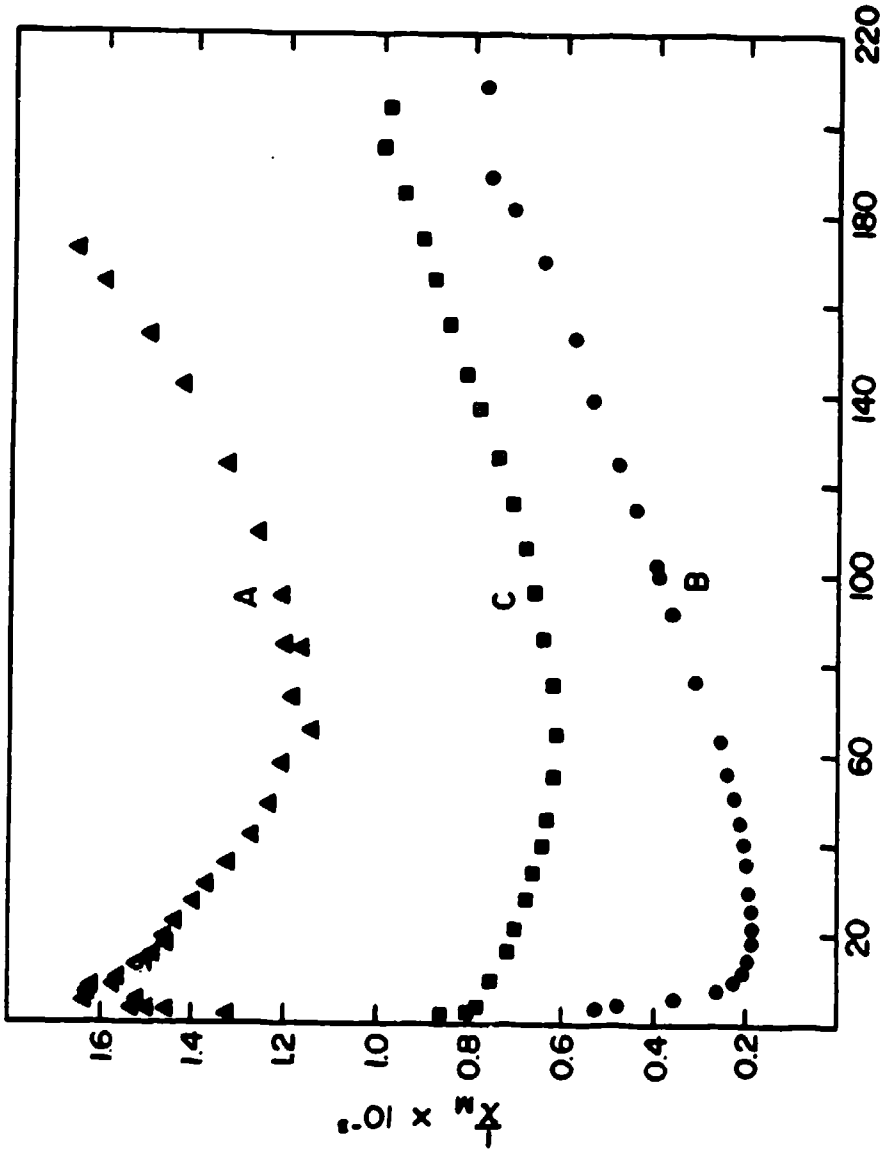

Figure 27. Reciprocal of the molar susceptibilities displayed in Figure 26. Figures 26 and 27 courtesy of A. Stacy, Cornell University.

inconclusive. Certainly there was no strong paramagnetism in any of the samples and some appeared diamagnetic at 4K. Larger samples would have been necessary for any definitive results with that system. However, after the success with magnetic susceptibility at Cornell University, no large sample preparations were attempted.

There have been several attempts to fit the experimental magnetic susceptibility results for systems VII and VIII to theoretical expressions. The generalized weighted non-linear least-squares KINFIT program (88) was used for the analysis. Equations based upon Fermi-Dirac and upon Bose-Einstein statistics involving singlet-triplet equilibria have not reproduced the experimental shapes well, even when two different types of electron-trapping sites (evident in optical spectra and spin susceptibility studies) were employed. To date the best reproduction of the experimental susceptibility shape has been with an equation by Wojciechowski (89). He derived expressions for the magnetic susceptibility of a metal-metal interaction in coordination compounds with a $d^n - d^n$ electronic configuration. His curves for $d^1 - d^1$, or $S_1 = 1/2$ and $S_2 = 1/2$ with an exchange integral $J < 0$, look similar to both Figure 23 and curve B of Figure 26. His expression is

$$\chi_M = \frac{Ng^2\mu_B^2}{2k_B T} \frac{4}{3 + EXP(-J/k_B T)}$$

where N is the number of pairs of interacting spins and the other symbols have their usual meaning. This expression did not fit the experimental susceptibility data for system VIII until two exchange integrals were employed, corresponding to two different electron trapping sites in the sample. The fractional populations η_1 and η_2, based upon total lithium content, and the exchange integrals J_1 and J_2 for sites 1 and 2 were the adjustable parameters, as well as a Curie term C to account for the paramagnetic signal evident in the EPR spectra below approximately 6K. Table 8 lists the computer-fit values of these parameters.

Table 8. Values for the parameters in the fit of the sample VIII static susceptibility results with the Wojciechowski equation for interacting spin 1/2 systems.

Parameter	Value ± Standard Deviation
η_1 (%)	17.2 ± 1.1
J_1 (cal)	33.5 ± 1.2
η_2 (%)	46.3 ± 1.1
J_2 (cal)	107. ± 3.3
C (%)	0.20 ± 0.01

Populations η_1 and η_2 were not constrained by making their sum equal 100%, nor were η_1, η_2 and C forced to equal 100%.

The KINFIT program determined the populations necessary to fit the experimental data.

Wojciechowski's equation did not fit the data for sample VII where two sites were evident in the optical spectra and in the spin susceptibility. Using the same five parameters as for system VIII, the fit was poor. Even then, the population $\eta_1 + \eta_2$ was 84.8%. The search for theoretical expressions of antiferromagnetically interacting spin systems continues. The general theory of Oguchi (90) as extended by Ohya-Nishiguchi (91) holds some promise. Basically they include longer range interactions than that of spin i and spin j with exchange integral J: the exchange integral J' is for spin i with all nearest neighbors excluding j and also for spin j with all nearest neighbors excluding i. Ohya-Nishiguchi defines a parameter κ: $\kappa = z|J'|/|J|$ in which z is the number of nearest neighbors and κ indicates the relative strength of the long-range molecular field. Theoretical susceptibility curves $0.0 < \kappa < 1.5$ show a broad maximum and indistinct Néel temperature (there is no Néel temperature for $\kappa < 1$) similar to the curves of Figures 22 and 24 and the lower two curves of Figure 26. This similarity raises the possibility that these experimental data may eventually be fit with the Ohya-Nishiguchi expression or a similar one which incorporates multiple nearest-neighbor interactions. Without a crystal structure or prior knowledge of the number of types of

sites available for the electron, it is difficult to apply any theoretical analysis.

III.C.2. Summary and Discussion

The spin pairing phenomena detected by EPR were also evident in the static magnetic susceptibility studies. Table 9 contains the values of maximum susceptibility for the spin and static susceptibility samples and the temperature at which each maximum occurred. None of the susceptibility curves has a sharp transition point (Néel temperature) at which antiferromagnetic alignment occurs, although sample VIII is close to that appearance, and none of the curves show $\chi(0)/\chi(T_N) \approx 2/3$, as expected for a polycrystalline antiferromagnetic powder. The static susceptibility maxima are broad as might be expected where spin pairing is occurring gradually instead of at a specific transition temperature. The static susceptibility curves, then, are the result of the interplay of two factors: the susceptibility of the spins present is enhanced as the temperature decreases ($\chi \propto 1/T$), but there are progressively fewer free or unpaired spins to contribute to the susceptibility. There is definitely an antiferromagnetic interaction, but not in the Néel sense.

The similarity of the general temperature dependence of spin and static susceptibilities for sample VII and for sample VIII is reassuring. To be sure, the results are not

Table 9. Summary of $Li^{+}C_{24}^{-}\cdot e^{-}$ spin and static susceptibility data.

Sample	R	Maximum χ_M (esu/mole x 10^3)	Temperature (K) of Maximum
Spin Susceptibilities			
VI	1.15	3.71	13
		2.44	~85
VII	0.60	1.42	17
		0.93	~70
VIII	1.57	2.11	13
Static Susceptibilities			
IV	0.99	1.63	64
VII	0.60	~0.89	~70
VIII	1.57	5.42	21

identical, nor are they expected to be. Since EPR probes the local environment while susceptibility studies the bulk property, and since the EPR samples were essentially thin films while the susceptibility samples were bulk powders with approximately twenty times the mass of the EPR samples, differences are expected and it is gratifying that the results are so close. Optical spectra and spin susceptibility indicated that system VIII with R = 1.57 had primarily one type of electron site in which spin pairing occurred. However static magnetic susceptibility indicated

two sites. It is interesting that EPR spin pairing showed an interaction energy of 26 cal/mole while Wojciechowski's equation for antiferromagnetic interaction yielded an energy of 33.5 cal/mole at low temperatures. On the other hand both the optical spectra and the spin susceptibility results for system VII with R = 0.60 showed at least two sites for electron localization. However the static magnetic susceptibility showed only one broad maximum at ~70K for sample VII. EPR spin pairing indicated an interaction energy of 117 cal/mole while the (poor) fit with Wojciechowski's equation yielded an approximate interaction energy of 237 cal/mole. It is likely that more than one site is involved in both cases.

The presence or absence of the various spin pairing sites cannot be explicitly explained. Rather the differences are not unexpected for samples of different sizes, different shapes, with possibly different grain boundary effects and probed with different experimental techniques.

The spin and static susceptibilities of samples IV, VII and VIII show that the temperature of maximum susceptibility decreases with increasing lithium to cryptand ratio and the susceptibility at the maximum increases. The spin susceptibility for VI with R = 1.15 indicates that it might be an exception to both of these trends, though there is no obvious reason why this is so. From spin susceptibility and the Wojciechowski equation fit, the

higher the sample lithium content, the weaker the interaction energy, again with the exception of system VI. System VI with R = 1.15 showed unexplained behavior as noted in Section III.B. and no explanation is evident after the spin susceptibility determination.

III.D. Conductivity

The conductivity of several lithium electride samples was investigated, some by microwave conductivity and one by D.C. conductivity.

One of the first indications of the metallic character of $Li^{+}C211 \cdot e^{-}$ was the microwave conductivity of sample I. At -50°C it possessed a conductivity between that of zinc and insulators. Later liquid nitrogen providing the cooling boiled away, causing the sample to warm. The oversight was discovered and the sample was rechilled, but not before the microwave power absorption at -15°C increased to that of zinc or slightly higher. The sample did not appear to decompose and later the -50°C relative conductivity was repeated.

Sample II showed the MNM transition evident in optical and EPR studies. At -45°C the conductivity increased significantly, showing microwave power absorption equal to or greater than that of an equal volume of palladium powder, as shown in Figure 28. This rapid change in conductivity was repeated many times both as the sample temperature was

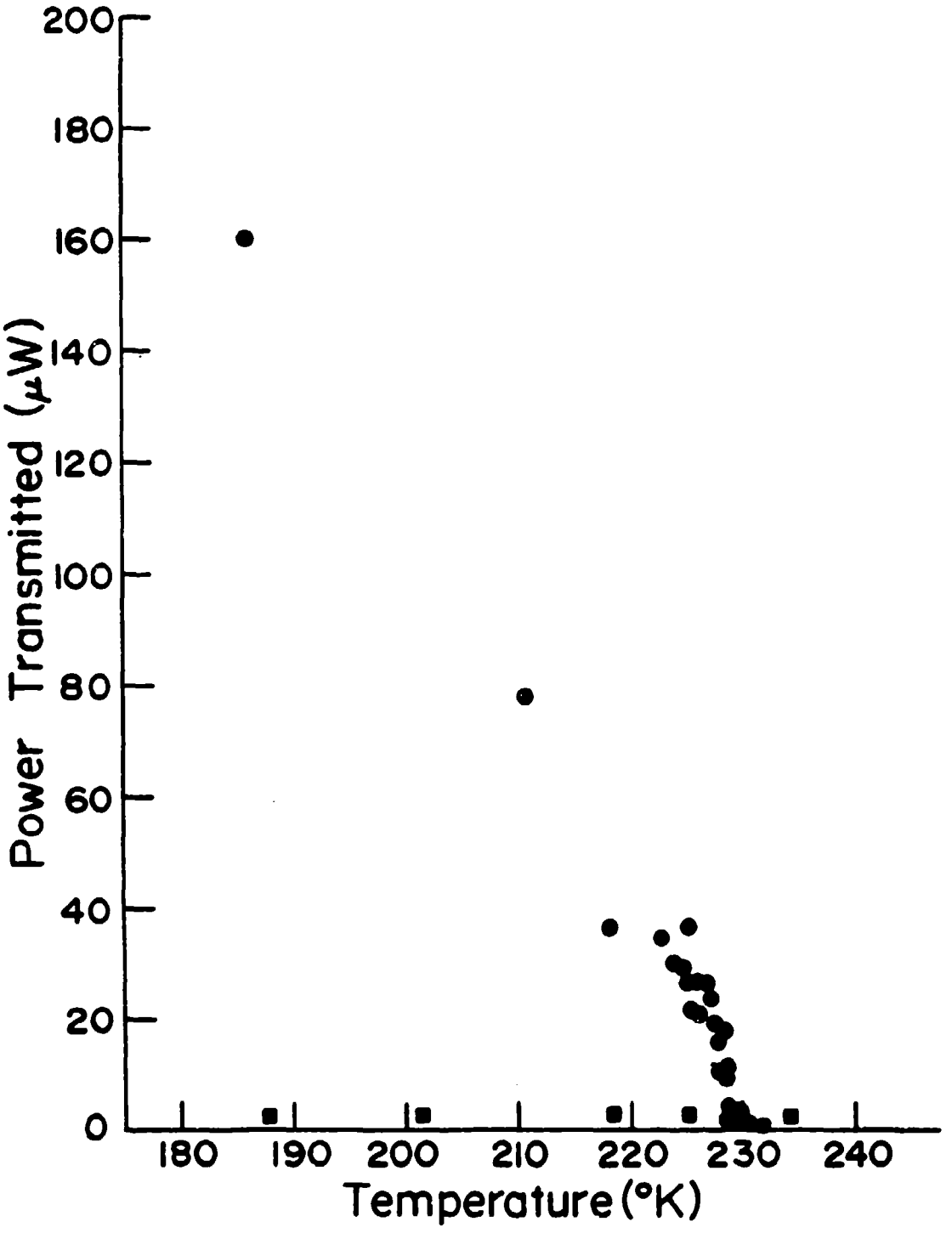

Figure 28. Microwave power transmitted by equal volume samples of $Li^{+}C211 \cdot e^{-}$ (II) (circles) and palladium (squares) in a TE_{103} cavity.

raised and lowered. There was a slight hysteresis in the transition, but in general the change was very reproducible in that sample.

It is possible to calculate the conductivity, or at least the limits of conductivity, for the $Li^+C211 \cdot e^-$ (II) EPR sample from its response in the E4 spectrometer microwave cavity. Penetration of a radio-frequency field into a metal is limited by the material's skin depth, δ (19). Classically the skin depth is

$$\delta = (c^2/2\pi\sigma\omega)^{1/2} \qquad (11)$$

where σ is the conductivity and ω is the angular frequency of the r-f radiation. Limits can be placed on the $Li^+C211 \cdot e^-$ conductivity by comparing it with the response of a well characterized metal such as silver. Then Equation 11 becomes

$$\frac{\delta_1}{\delta_2} = \left(\frac{\sigma_2\omega_2}{\sigma_1\omega_1}\right)^{1/2}$$

If the skin depth of silver is taken at the same frequency as that in the EPR cavity ($\sim$9.2 GHz), then

$$\sigma_2 = \sigma_1\left(\frac{\delta_1}{\delta_2}\right)^2 \qquad (12)$$

At 9.2 GHz, the skin depth of silver is .7μ (83) and at

295K the conductivity is 6.2×10^5 $(\text{ohm-cm})^{-1}$ (42). In the metallic region, the A/B ratio for $Li^+C211 \cdot e^-$ is $\sim$1.5 which yields $\sim$1.25 for the ratio a/δ in Webb's theory for the EPR spectra of conduction electrons where a is the spherical particle radius (21). The limits on the conductivity then arise from the estimates for a. At the lower limit, a may be $\sim 1\mu$ as observed under a microscope or at the other extreme, the whole sample may act as one large conducting particle. In that case $a = 945\mu$ for the EPR sample. With $945\mu \geq a \geq 1\mu$, then $756\mu \geq \delta \geq .8\mu$. Therefore

$$\sigma \geq (6.2 \times 10^5)\left(\frac{.7}{756}\right)^2 (\text{ohm-cm})^{-1}$$

so

$$\sigma \geq 0.5\ (\text{ohm-cm})^{-1}$$

and

$$\sigma \leq 5. \times 10^5\ (\text{ohm-cm})^{-1}$$

assuming the conductivity of silver is essentially unchanged at 228K. EPR samples are normally thin films on the tubing walls. This appeared to be true for sample II also. With the assumption that the sample was spread out uniformly on the EPR tube walls and using the measured tube I.D. and the sample mass and height in the tube, the sample thickness was approximately 76μ. With these

assumptions the lower limit of the conductivity becomes $8. \times 10^{1}$ $(ohm\text{-}cm)^{-1}$.

$Li^{+}C211 \cdot e^{-}$ sample III was definitely an insulator in the region -68° to -44°C according to its microwave conductivity. System X was also non-metallic as determined from the D.C. conductivity of a packed powder sample. The current at various temperatures was read and converted to resistance. Figure 29 is a plot of log R against reciprocal temperature. An HP-65 calculator fit of the right-hand line yields $\log R = -5.34 + 2.47 \times 10^{+3}$ (1/T), giving a band gap of 0.99 eV. From $\sigma = \frac{IL}{VA}$ or $(\frac{1}{R})\frac{L}{A}$ where L is the length of the conductivity sample and A is the area of the electrode, $\sigma = 5.1 \times 10^{-5}$ $(ohm\text{-}cm)^{-1}$ at -45°C for sample X. For 298K, $\sigma = 1.8 \times 10^{-3}$ $(ohm\text{-}cm)^{-1}$ and at infinite temperature $\sigma_o = 3.6 \times 10^{+5}$ $(ohm\text{-}cm)^{-1}$. The band gap for the other straight line is 1.28 eV.

The high temperature segment of Figure 29 (> -32°C) shows an increasing resistance with increasing temperature. That could be because the sample underwent a MNM transition at -33°C or because it began decomposing there. When the sample was removed from the conductivity apparatus at -10°C, it still appeared to be blue, though that would not rule out the presence of sufficient decomposition to raise the resistance less than an order of magnitude.

In summary, $Li^{+}C211 \cdot e^{-}$ samples I and II showed metallic character by conductivity, though II was metallic only

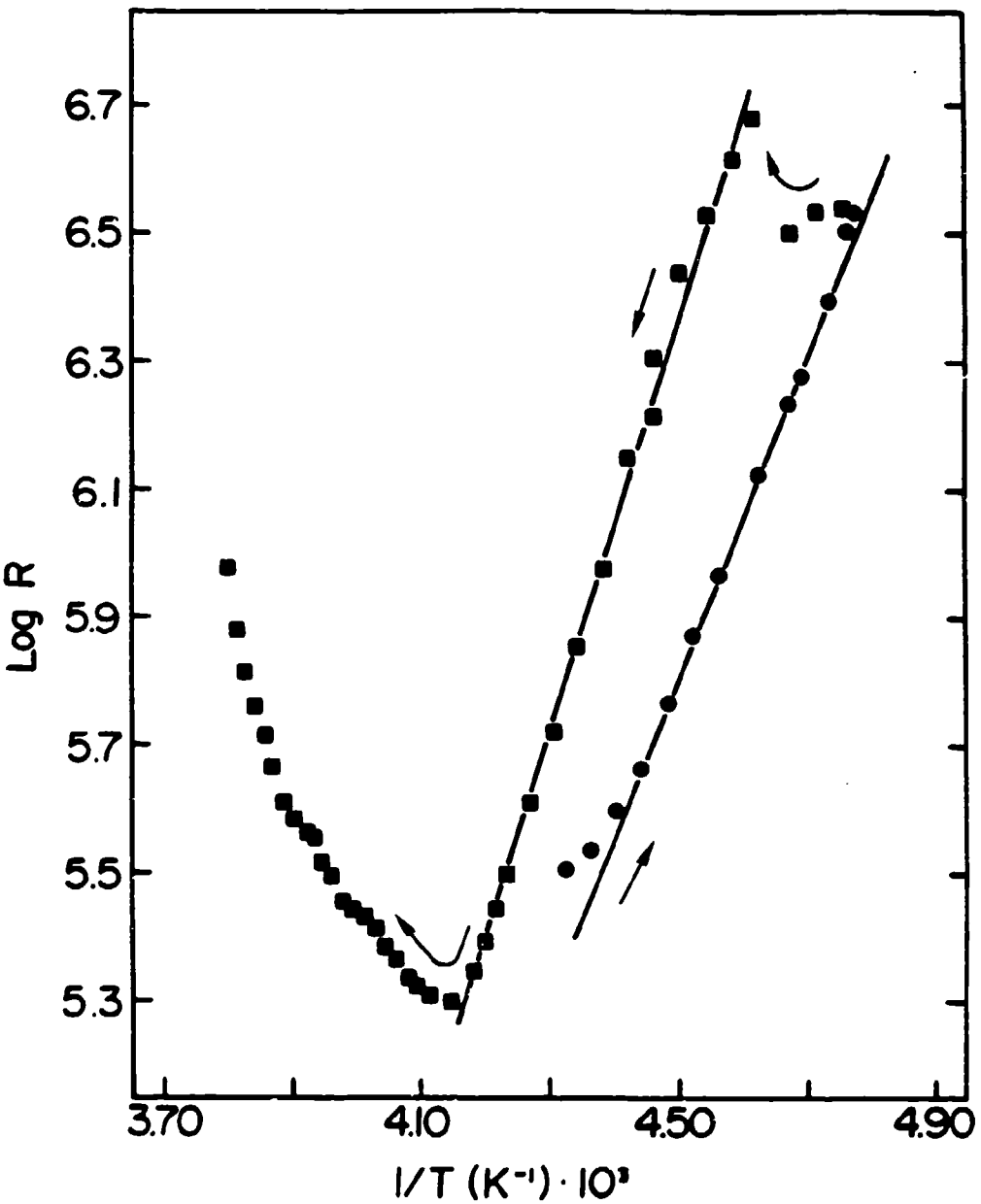

Figure 29. Temperature-dependent resistance of $Li^{+}C211 \cdot e^{-}$ (X) with R = 0.96. The region on the left above -33°C with $\partial R/\partial T > 0$ may either indicate the sample has decomposed slightly or has undergone a MNM transition.

after a transition at -45°C. The conductivity limits at -45°C of EPR sample II, $8 \times 10^{1} \leq \sigma \leq 5 \times 10^{5}$ $(\text{ohm-cm})^{-1}$, places it between a near-metal and an excellent metallic conductor. Sample III was an insulator by microwave conductivity and sample X was a low band-gap (0.99 eV) semiconductor by D.C. conductivity.. As previously described, there is no obvious reason why the character of these $R \approx 1$ samples should have varied so widely. However, the conductivity measurements correlate well with the optical spectra. High conductivity occurs with samples whose optical spectra indicate plasma character.

III.E. Sample Analyses

A series of tests was performed on the decomposed magnetic susceptibility samples VII and VIII to precisely determine the amount of material present in each. Then the same tests plus an additional one were conducted on (presumably) undecomposed magnetic susceptibility samples VII and VIII used in the MSU Physics Department. This additional analysis shows the amount of reducing power still present in samples handled similarly to the susceptibility samples VII and VIII.

When samples VII and VIII were removed from the Faraday balance at Cornell University, each appeared white. But after three weeks of room temperature storage, the material seemed to be a yellow-brown viscous liquid with a reddish

tint, as though it were primarily impure cryptand. Table 10 lists the results for these samples.

Table 10. Results of the analyses of magnetic susceptibility samples VII and VIII.

	VII	VIII
Moles Li from flame emission	5.25×10^{-6}	4.93×10^{-6}
Moles C211 from titration	9.85×10^{-6}	3.11×10^{-6}
Total sample mass (mg)	2.84	0.93
Estimated sample mass (mg)	3.4	1.1
Error in mass estimate	+ 20%	+ 18%
Mole ratio Li:C211, R	0.53	1.59
Estimated R	0.60	1.57

After the flame emission, each solution was dried and then the samples were dissolved in D_2O and t-butanol. Proton NMR graciously accomplished by B. Van Eck was not of sufficient quality for an accurate integration because of very low cryptand concentrations. However qualitatively both spectra showed that the C211 was substantially intact. Signals that could have been from decomposed cryptand were very minor. This indicates that thermal decomposition

in the absence of any external oxidizing agent may occur with very little rupture of the cryptand. Table 11 lists the results for samples handled similarly to those of Table 10, but which were not intentionally decomposed before the hydrogen evolution was performed.

Table 11. Results of the analyses of MSU magnetic susceptibility samples VII and VIII.

	VII	VIII
Moles Li from H_2 evolution	7.9×10^{-6}	4.3×10^{-6}
Moles Li from flame emission	5.03×10^{-6}	7.29×10^{-6}
Moles C211 from titration	8.55×10^{-6}	5.05×10^{-6}
Total sample mass (mg)	2.50	1.51
Estimated sample mass (mg)	2.9	1.8
Error in mass estimate	+ 16%	+ 19%
Mole ratio Li:C211, R	0.58	1.44
Estimated R	0.60	1.57

Tables 10 and 11 show some interesting results. In Table 11 the number of moles of reducing species, presumably electrons equal in quantity to the moles of Li, varied considerably. The measurement of the amount of H_2 evolved contained the greatest error of all the results. The gas was collected in a 10.00 ml volume, creating only a pressure of several torr because the samples were so small.

This H_2 pressure was the difference between two large numbers, yielding a large percentage error. It should be noted that the sample sizes were an order of magnitude smaller than those usually analyzed in this laboratory. The results are not inconsistent with the assumption that both samples were substantially undecomposed before the analyses were begun. The inference is, then, that the magnetic susceptibility samples at Cornell University were substantially undecomposed during the measurements. Therefore most of the electrons potentially present were participating in the spin-pairing process in those samples. The estimated sample masses appear to be systematically ~18% high. The reason is unknown but the effect is not substantial. If the same error existed in the EPR sample sizes, then the actual number of unpaired spins for the samples described by Figure 21 would be increased 2 - 5% at high temperatures. Finally, the estimated sample mole ratios are close to those from the analyses. It is not surprising that three of the four actual ratios are a bit lower than the estimates. If decomposed, uncomplexed C211 were present in the sample, it would still gain protons during the titration and be included in the moles of C211. But if the Li had been contaminated prior to the preparation or if the reducing power had decreased during the sample lifetime and if either situation had created NH_3- or H_2O-insoluble products, the Li flame emission result would have

been low. Hence the R value would be low. The conclusion, then, is that the Li was nearly free of contamination.

III.F. $Li^+C211 \cdot e^-$ Summary and Conclusions

Some of the results for lithium electride systems from ammonia are briefly summarized in Table 12. One of the major thrusts of this study was to determine the consistency of results from samples prepared from the same solution but analyzed by different methods. This correspondence is quite good as typified by the internal consistency of samples VII and VIII. Also, the consistency between different preparations with the same mole ratio seems good, as in the optical spectra of III, IV and V. So, in the future, individual preparations for EPR and magnetic susceptibility can be made to optimize the sample size with an assurance that the results will be fairly representative for a given mole ratio.

The second major objective of this study was to characterize $Li^+C211 \cdot e^-$ and the results are quite interesting. The material apparently consists of large cryptated cations of about 8Å diameter and interstitial electrons when $R \leq 1$. At higher values of R both Li^+ and e^- are in the interstices, but they do not form lithium metal. The system has a low electron density near that required for a metal-nonmetal transition. The metallic region is approached when the mole fraction of lithium is raised to

Table 12. Summary of the data for $Li^{+}C211 \cdot e^{-}$ systems.

System # & R Value	Optical Spectra	EPR Spectra	Magnetic Susceptibility	Other Data; Comments
I 0.93	metallic	only at -150°C; A/B ∿1.0 ΔH_{p-p} = .37G	----------	Microwave conduct. between M & NM; Metallic when warmed
II 0.95	MNM transition at -45°C	MNM transition at -45°C low % unpaired spins	----------	Microwave conduct. MNM transition at -44°C
III 0.98	Standard multi-bump spectra; warmer-more plasma-like	sample too large	no data; decomposed at Cornell	----------
IV 0.99		Sample too large	hi temp site only; susc. max 64K	----------
V 0.97		Standard for R ∿ 1	destroyed in prep.	----------
VI 1.15		highest % of spins unpaired; highest A/B ratio and g-value; narrowest spectra	no data; decomposed in Faraday balance	this mole ratio warrants further investigation based upon EPR results

Table 12. Continued.

System # & R Value	Optical Spectra	EPR Spectra	Magnetic Susceptibility	Other Data; Comments
VII 0.60	standard multi-bump	much like R ∿ 1 spectra	hi temp site only susc max ∿70K	consistently like systems with R ∿ 1
VIII 1.57	homogeneous; warm, ann. - plasma edge	most homogeneous spectra at low temps; one site	low temp site predominates susc. with max ∿20K	significantly different than R ∿ 1 systems
IX 0.97	----------	-91°/-65°C } fairly -116°/-65°C } standard	-----	vapor pressure study: IX & X
X 0.96	-78°/-65°C plasma edge -91°/-65° transition; all others - low IR absorbance	----------	-----	packed powder conduct. 0.99 eV band gap $\sigma_{298K} = 2 \times 10^{-3}$ $(ohm\text{-}cm)^{-1}$

$\sim$1.5 and the system is metallic at R = 2. One system at R = 1 was also metallic and another existed so near to the metallic state that warming the samples (optical, EPR and microwave) above -45°C caused the MNM transition. It is still unclear what caused these two systems to be metallic while so many others with the same mole ratio were not. In the nonmetallic systems the large inter-electron distances result in weak electron-electron interactions which lead to spin pairing as the temperature is lowered. In the high temperature region there is approximately one unpaired electron per lithium atom, indicating that essentially all of the electrons in the sample are participating in this spin-pairing process. This is perhaps the most encouraging aspect of this study since it proves that the properties attributed to electrides are not just those of a minor constituent.

CHAPTER IV

OPTICAL SPECTRA OF OTHER SYSTEMS

Many systems other than Li/C211 were studied, though none as thoroughly as this metal/complexer combination. Optical transmission spectroscopy of thin films was the method for study, chosen because of its relative ease and because of its apparent ability to accurately depict, albeit qualitatively, the nature of the solution or solid being investigated. As noted in this chapter and in the previous one, the initial indications of transmission spectroscopy were corroborated by any other method used.

Thin film optical transmission spectroscopy as used in this study was not without its problems, however. The splashing, rapid solvent evaporation method of film formation produced heterogeneous films of probably varying thicknesses, geometries and degrees of coverage of the optical beam path. As detailed in the Appendix, peak positions should be unchanged by these effects, but amplitudes are decreased and peak widths are broadened, the extent of which is dependent upon the film's deviation from uniform thickness over the optical beam area on both cell walls. Particularly in K/C222 systems, but in other

systems from ammonia as well, apparently solvent-free dry films showed changes with time, and required up to forty minutes to reach stable time-independent values. In several cases excessive light scattering from isopropanol on the outside of the optical cell was noted, especially when the sample cavity was -60°C and lower. Also, it was possible that differential rates of precipitation changed the stoichiometry between the initial portions of the film and the regions from which final bulk solvent evaporation occurred. To guard against such artifacts, only reproducible spectra are reported. Throughout this chapter when the mole ratio is given as R = 1, the system is slightly cryptand rich with R $\leq$ 1.0.

IV.A. Spectra in the Absence of Complexer

IV.A.1. Na and K with Ammonia

Before obtaining spectra of alkali metals in the presence of complexing agents, it seemed worthwhile to ascertain the effect of alkali metals alone and then in the presence of a non-complexing diluent. To determine if the alkali metals might be responsible for the observed absorption spectra of concentrated metal-ammonia solutions (MAS), sodium and potassium films were prepared by evaporating the MAS to dryness on the optical cell walls. When the bulk solution in the apparatus sidearm was frozen, the MAS film

in the optical cell lost its characteristic blue color in 2 - 3 seconds, resulting in an inhomogeneous "film" which appeared to contain lusterless gray-white flecks of metal. Spectra of each metal were virtually flat without any absorption bands. There was a pronounced absorption, however, when these dry metal "films" were damp with ammonia as shown in Figure 30 for sodium (spectrum A) and potassium (spectrum B). The bulk solution temperature was within 10°C of the film temperature before the absorption was noticeable and within 3 - 5°C before the absorption was significant. This indicates that sodium and potassium have low ammonia affinities compared to lithium and that $Na(NH_3)_x$ and $K(NH_3)_x$ compounds are not readily formed, if they are at all.

The two spectra in Figure 30 are the first transmission spectra of concentrated MAS. The general shape is quite similar to reflectance spectra of sodium in ammonia in Figure 1 by Beckman and Pitzer (7). They found an extremely sharp drop in reflectance (a plasma edge) at approximately 7700 cm^{-1} (1300 nm) for solutions between 15.4 and 7.0 mole percent metal (MPM). In addition the general shape is similar to that calculated from reflectance spectra of 14 MPM (Li) solutions in ammonia by Thompson (92). Figure 30 spectra have a more gentle descent which occurs at shorter wavelengths than in either reflectance study. This more gradual slope could be the result of film

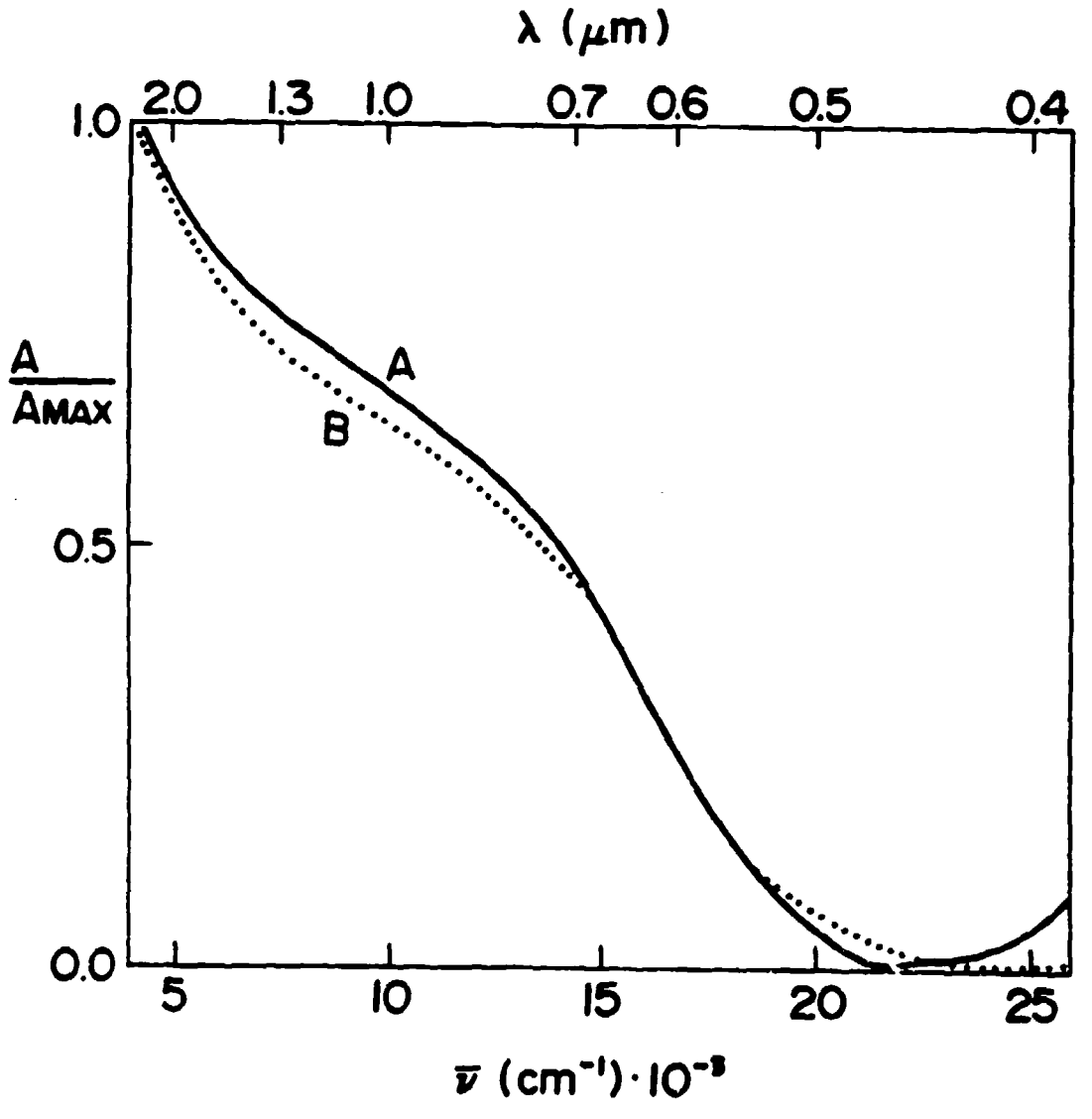

Figure 30. Spectra of metal films which are damp with ammonia (concentrated M-NH_3 solutions): A - Na; B - K.

inhomogeneity in this study. The continued rise into the infrared, also noted by Beckman and Pitzer, contrasts sharply with the localized absorption peaks attributed to trapped electrons in later spectra. The spectra in Figure 30 for concentrated MAS were reproducible and will be considered typical of conduction electron plasma absorption.

IV.A.2. Na/DABCO Films from Ammonia

Optical films of sodium and the non-complexing bicyclic diamine DABCO, $N(CH_2CH_2)_3N$, were also studied. Ammonia was evaporated from a film of approximately R = 2 (ratio of moles metal to moles complexer, or in this case diluent) and no absorption bands were evident. Even a wet film of this system had little character. Presumably the diluent dispersed the metal sufficiently to affect the plasma absorption, though the general shape was as depicted in Figure 30. It is apparent, then, that neither the presence of an alkali metal nor a bicyclic diamine with an alkali metal can account for dry film absorption bands.

IV.B. Films from Ammonia

IV.B.1. Na/C222 Systems

An ammonia solution containing sodium and C222 in the ratio R = 1 gives the dry film spectrum A in Figure 31 at -49°C. The predominant peak at 8500 cm^{-1} (1175 nm) is a locally trapped electron (e_t^-) band while the other peak at 16,100 cm^{-1} (620 nm) is due to Na^-. A dry film re-formed by removing NH_3 from a wet film yielded broader peaks which were slightly red shifted compared to those of spectrum A. Two different dry films initially showed a small, separate e_t^- peak at 5000 cm^{-1} (2000 nm) which decayed within fifteen minutes. As it did so, both e_t^- and Na^- peaks increased in amplitude by approximately 40%, reflecting a probable re-distribution of electrons from low energy traps into deeper, more stable traps.

That both e_t^- and Na^- peaks exist in these spectra is somewhat surprising for an R = 1 system and is indicative of incomplete complexation of Na^+ by C222. The solution was prepared with a nominal 11% excess of C222 over the amount of Na, thus increasing the probability that this equilibrium was shifted to the right:

$$Na^\circ + C222 \rightleftarrows Na^+C222 + e^-_{solv}$$

However there were still uncomplexed sodium cations present

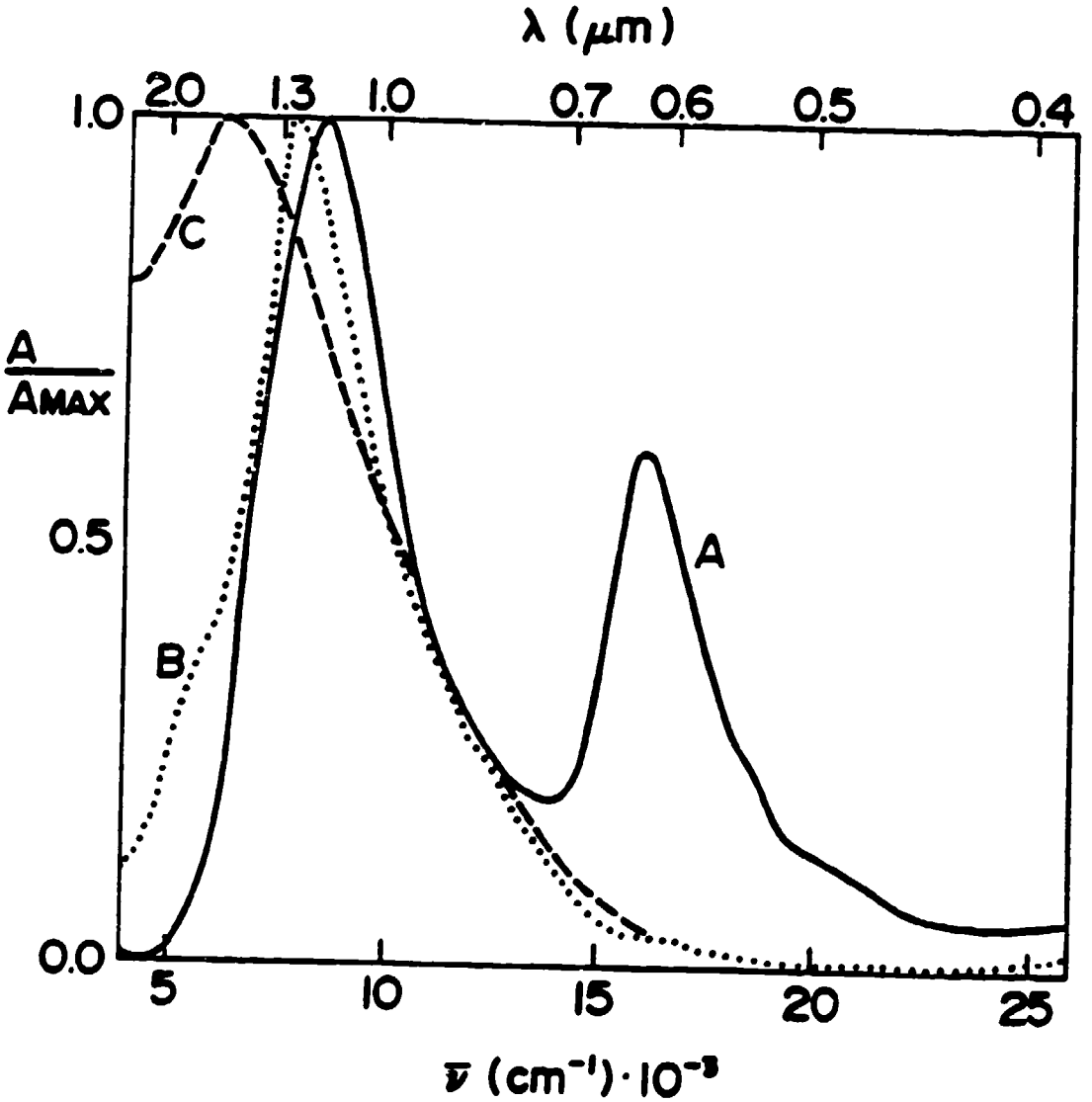

Figure 31. Spectra of Na/C222 films with R = 1 from ammonia: A - dry; B - damp; C - wet.

in solution which acted as electron scavengers during flash solvent evaporation, yielding the Na^- absorption peak. Possibly the sodium cations may have become uncomplexed during the 10 - 15 second solvent evaporation process, but this seems unlikely in light of thermodynamic evidence from NMR on alkali metal decomplexation rates in numerous solvents (93). For example extrapolation of aqueous solution data to -45°C yields a complexation half-life for Na^+ into C222 of 6×10^{-5} sec and a decomplexation half-life of 27 sec when using an equilibrium constant obtained from a solution of 5% water in methanol (52). Although the current study is in ammonia, complexation should still be favored over decomplexation by a wide margin.

Spectral behavior during decomposition supports the sodium scavenger idea. As the solution aged, decomposition most likely destroyed some of the cryptand, thereby releasing more Na^+. The ratio of absorbances $A_{Na^-}/A_{e^-_t}$ increased steadily from 0.6 to 2.0 during this time, as expected for a system in which metal concentration was increasing relative to cryptand.

Damp and wet films for Na/C222 with R = 1 are depicted as spectra B and C respectively in Figure 31. The damp spectrum has a single localized electron peak at 7800 cm^{-1} (1280 nm) with a slight low energy shoulder, while the wet film shows an electron peak at 6200 cm^{-1} (1615 nm) with very high absorbance extending into the infrared. These

films which contain ammonia will be discussed collectively with those of Na C222 for R = 3 and 4 later in this section.

Solutions containing Na/C222 with R = 2 have been reported elsewhere (61) and will only be described here in comparison with solutions of different R values. To ascertain the effect of amounts of Na in excess of R = 2, experiments were conducted with R = 3 and R = 4. The dry film spectra are depicted as curves A in Figures 32 and 33 for R = 3 and 4, respectively. Both curves have a typical peak attributable to Na^- which is almost identical to that found in methylamine (58) and in NH_3 (61) with R = 2: a major peak at 15,400 cm^{-1} (650 nm) with a pronounced high energy shoulder and a small low energy shoulder and a distinct small peak at 25,000 cm^{-1} (400 nm). A surprising feature of the R = 3 and 4 spectra is the continued existence of e_t^- peaks. Perhaps sodium cations and monomers are not as effective at trapping electrons as first thought. Even though there are nominally twice as many sodium atoms present outside the cryptand in the R = 3 films as there are electrons, there still must be non-anionic traps which are more stable for the electrons. As a result the initial dry R = 3 films have a substantial e_t^- peak at 8100 cm^{-1} (1235 nm) and a small peak at 5500 cm^{-1} (1820 nm). With more sodium present in the R = 4 films, however, the relative intensity of e_t^- peaks is decreased, as the excess sodium perhaps traps more of the available electrons.

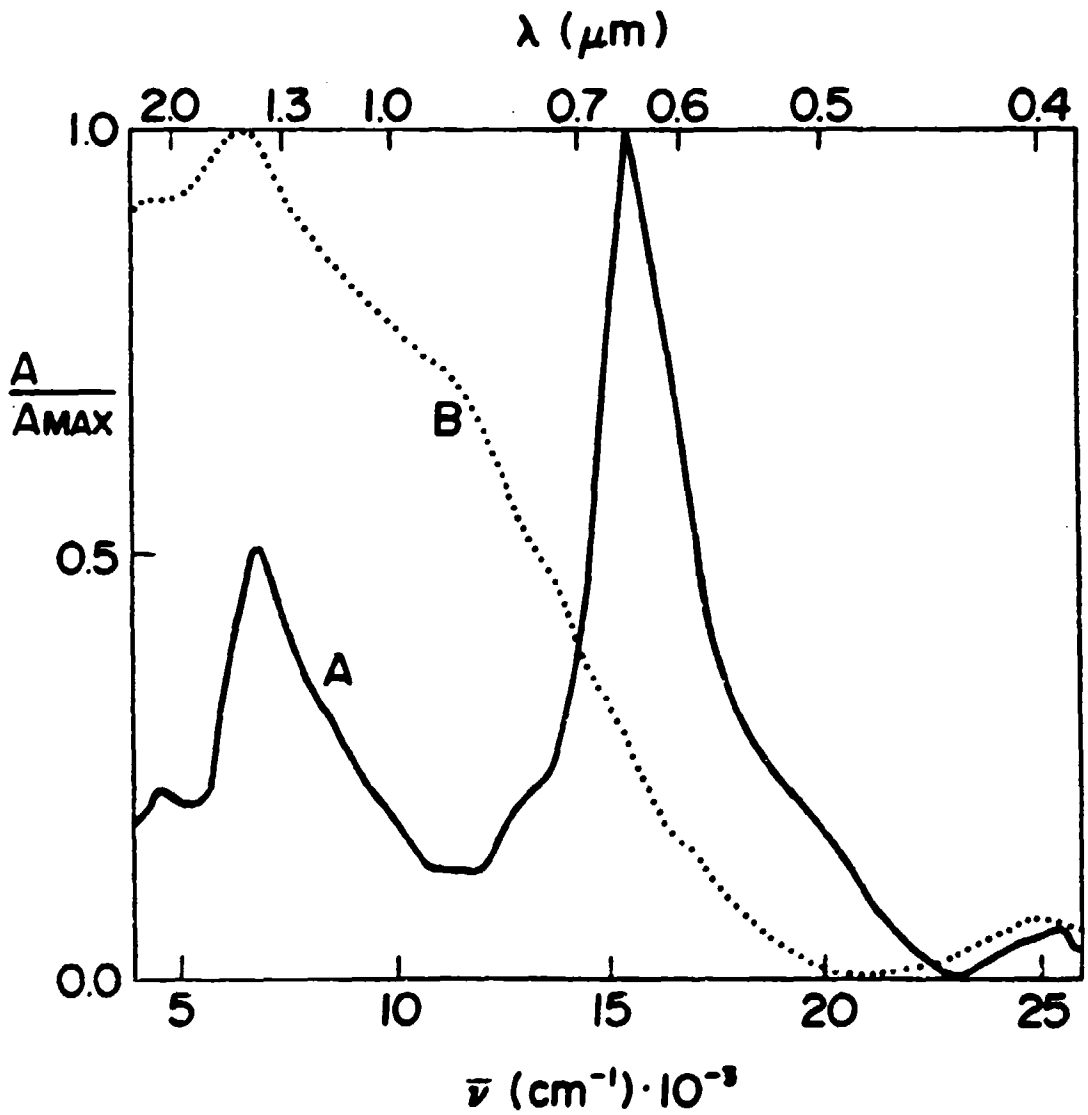

Figure 32. Spectra of Na/C222 films with R = 3 from ammonia: A - dry; B - wet.

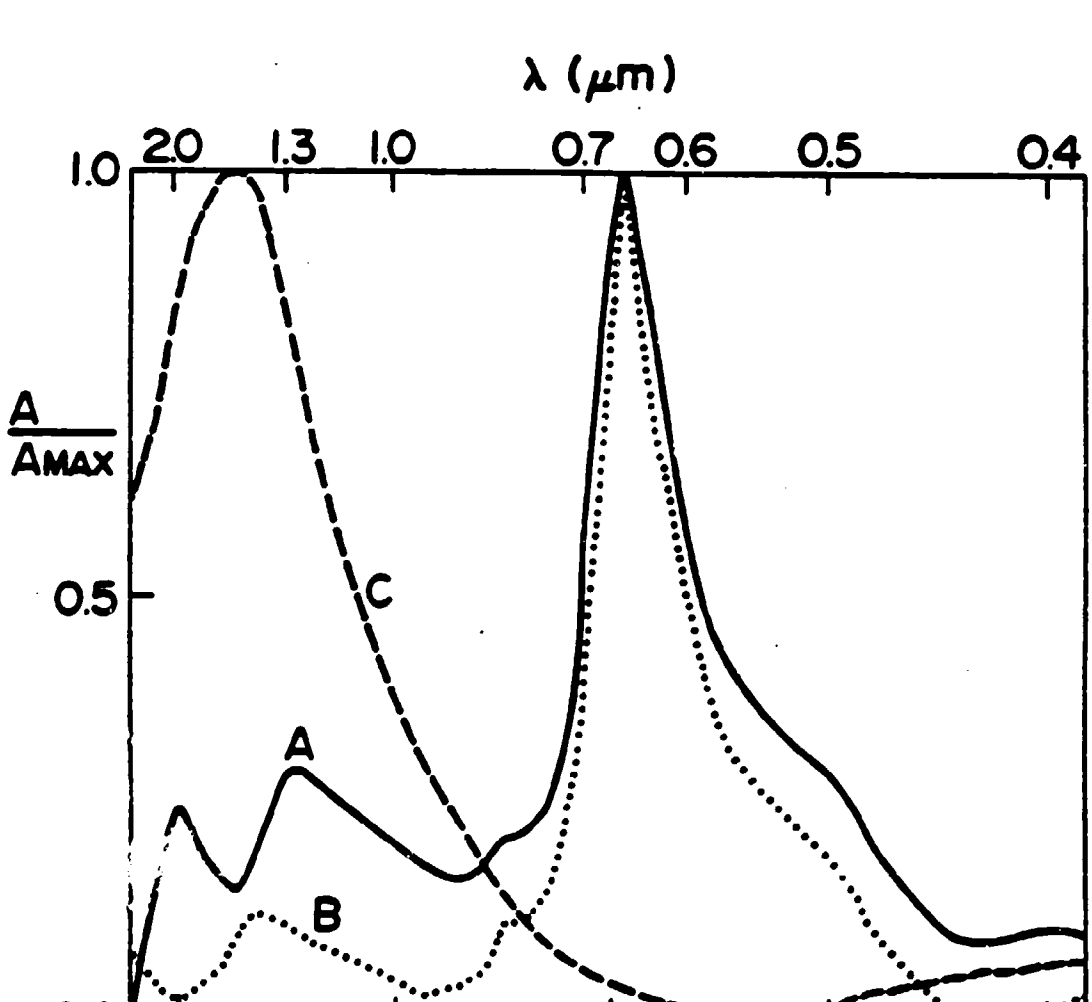

Figure 33. Spectra of Na/C222 films with R = 4 from ammonia: A - dry (fresh); B - dry (annealed); C - wet.

In the R = 4 initial dry films, the e_t^- peaks are at 7800 cm^{-1} (1280 nm) and 5100 cm^{-1} (1960 nm).

In both R = 3 and 4 films there are reproducible, significant changes with time. A typical annealed R = 4 spectrum is shown in Figure 33 as curve B. In this case the Na^- peak is slightly narrower but otherwise unchanged and the high energy e_t^- peak has shifted to 6800 cm^{-1} (1470 nm). The low energy e_t^- peak is at approximately 3850 cm^{-1} (2600 nm) though it is somewhat obscured by instrumental peaks at that location (not depicted). The R = 3 annealed films, while not pictured in Figure 32, show similar movement of the e_t^- peaks: 6900 cm^{-1} (1450 nm) with a shoulder at 4500 cm^{-1} (2220 nm). These peak positions for both R = 3 and 4 films represent the extremes of observed e_t^- peak movement. Virtually all positions between these extremes were observed while the Na^- peak position and absolute magnitude were constant. The excess sodium perhaps provides an inhomogeneous environment in the dry films such that multiple electron trapping sites exist which are of nearly the same energy. Electron movement between these sites is quite easy, though the cause of such travel is unknown. Temperature changes of the film had no apparent effect on the direction or rate of peak movement, nor did photolysis. It should be noted, however, that the Beckman DK-2A tungsten lamp was the photolytic light source and that it took 30 - 60 sec to reset the DK-2A

from the particular bleaching wavelength and scan the region of interest.

Spectra of films of all three R values are similar when the films contain ammonia. As the temperature of the bulk solution in the sidearm is raised increasing the NH_3 vapor pressure, the immediate consequence is the disappearance of the Na^- peak followed by a significant, broad increase in the infrared absorption. A film of R = 3 which contains nearly enough NH_3 to wash off the optical cell walls (wet) is shown as spectrum B in Figure 32. Wet films for R = 1 and 4 (spectra C in Figures 31 and 33) appear to have considerable plasma absorption. While the absorptions do not continue to rise into the infrared as in wet metal films (Figure 30), they are characteristic of wet alkali metal/complexing agent films and will hereafter be referred to as having plasma character. These spectra are quite similar to those of Na in NH_3 between 5.6 and 2.5 MPM by Beckman and Pitzer in Figure 1 (7). From the plasma edge of higher MPM spectra, the reflectance between 5000 and 10,000 cm^{-1} (2000 to 1000 nm) drops significantly in the lower energy region until a peak is formed, although there is still considerable reflectance on the infrared side compared to the higher energy side. Possibly the conduction electrons now have a shorter mean free path due to the presence of excess NH_3 and are no longer in the conduction band. This change is gradual, though, on the macroscopic scale as

depicted in Figure 1. It may be that the height of the infrared absorbance of wet spectra at 4000 cm^{-1} in Figures 31 and 33 depicts a similar decrease in the conduction character due to the increased presence of NH_3 in the film's structure.

IV.B.2. Na/C221 System

Because C221 is the optimum cryptand for complexation of sodium, rather than C222 (Figure 3), a solution of Na/C221 in NH_3 with R = 2 was prepared to determine the effect cryptand cavity size might have. Spectrum A (Figure 34) indicates that the effect may be very significant. Absent are the high and low energy shoulders on the Na^- peak as well as the small peak at 25,000 cm^{-1} (400 nm). Additionally, there is absolutely no indication of any peak attributable to e_t^- in any of the solvent-free Na/C221 spectra. No annealing effects were noted, no peaks shifted position with film temperature changes or with time and no other peaks were observed from 220 - 3200 nm. The lack of these phenomena indicate that no other traps compete favorably with sodium cations for electrons when solvent is removed from the films. The dry film structure may be fairly homogeneous, implying that the Na^+ encryptation by C221 is substantially complete. The Na^- peak at 14,400 cm^{-1} (695 nm) is quite broad and is red shifted by 1000 cm^{-1} or more from the similar peak in Na/C222 spectra. This broadness may

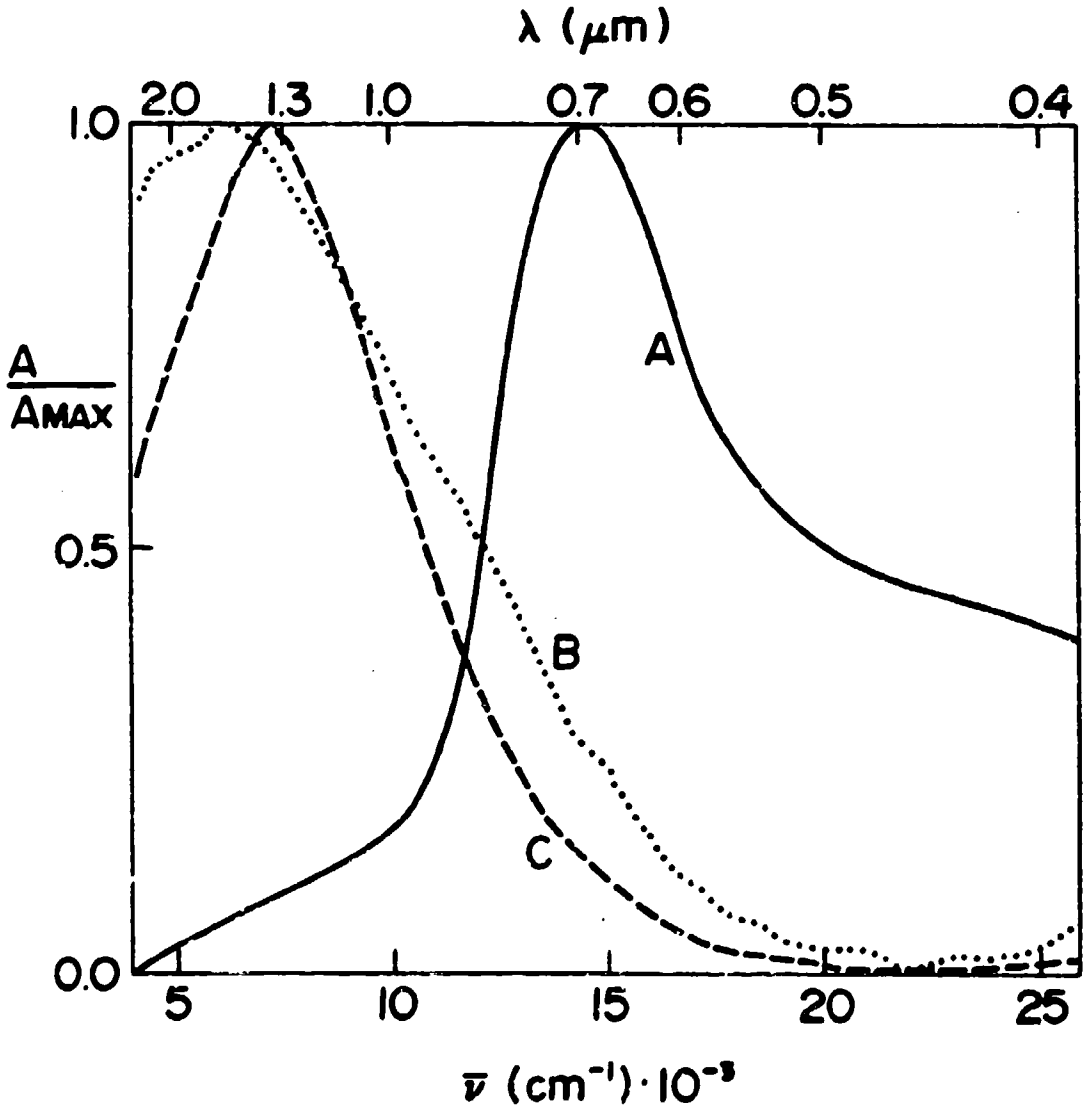

Figure 34. Spectra of Na/C221 films with R = 2 from ammonia: A - dry; B - damp; C - wet.

be due to the unsymmetrical nature of C221, resulting in a range of similar but not identical locations for the sodium anions.

Spectra of Na/C221 films with R = 2 which contain ammonia are shown as spectra B and C of Figure 34. They are typical films damp and wet with NH_3. All three spectra have an underlying rising absorbance which may have been caused by light scattering from the sample cell but which were more likely the result of poor spectrometer adjustment. This rise is an artifact and should be disregarded though it is evident only in spectrum A.

IV.B.3. K/C222 and K/C2N22 Systems

A previous study in NH_3 showed that K/C222 with R = 1 annealed from a predominant K^- peak at 11,200 cm^{-1} (890 nm) to strong plasma character (61). This experiment was repeated to verify the plasma character: the annealed film does indeed show nearly identical plasma character (Figure 35, spectrum B), but the fresh dry film is significantly different than that previously reported. The major feature of the fresh dry film (spectrum A) is a localized electron peak at 6500 cm^{-1} (1540 nm) with only a very slight shoulder at 10,500 cm^{-1} (950 nm) which is probably due to K^-. The difference is most certainly caused by the mole ratios of K and C222 in the two studies. Though both nominally had a ratio of R = 1, the prior study actually

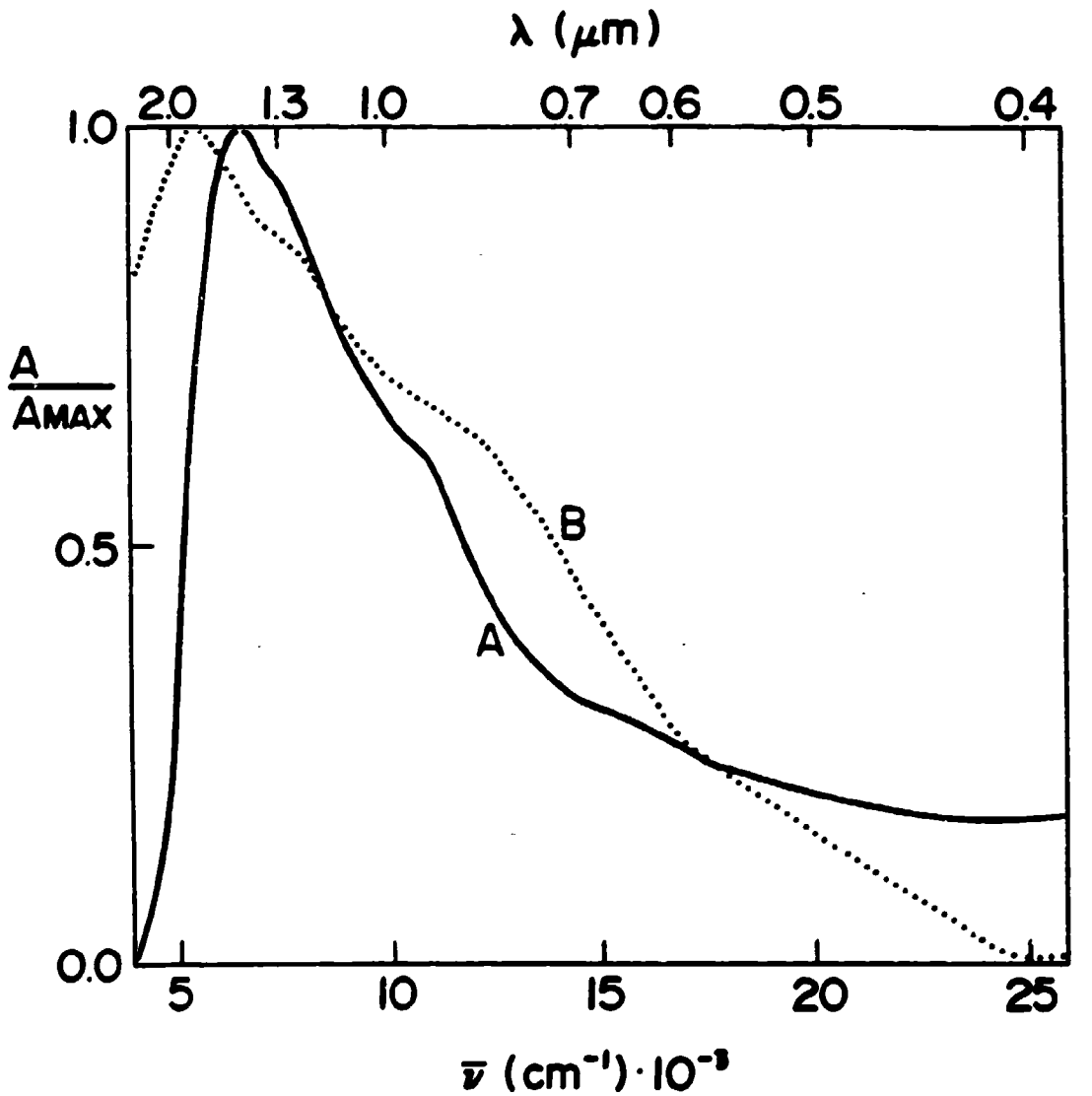

Figure 35. Spectra of solvent-free films of K/C222 with R = 0.95 from ammonia: A - fresh; B - annealed.

had R = 1.05 (94) while the current ratio is R = 0.95. Thus it is understandable that the previous fresh dry spectrum would show a larger peak due to K^-. It is interesting, however, that both systems anneal to yield spectra which are virtually indistinguishable despite the mole ratio difference.

The study of K/C222 in NH_3 with R = 1 was repeated at R = 0.94. The spectra of Figure 36, though presented on an absolute absorbance scale, are virtually identical to those of the R = 0.95 system. Figure 36 depicts the changes occurring in a film at -49°C over an 80 minute period after subtraction of the quartz cell background from all spectra. The same film, dampened with NH_3 vapor, changed immediately back to a localized electron system (spectrum D, Figure 37), followed by the appearance of typical plasma character in spectra E and F.

A limited study of potassium electride was undertaken to confirm by other means the possible metallic character indicated by dry annealed thin films. A $K^+C222 \cdot e^-$ microwave sample at -71° and -50°C appeared to be strongly conducting. Another microwave sample, from the same solution as the films whose spectra are shown in Figure 35, was an insulator at -80°C. Unfortunately the tube was broken before the temperature could be raised to ∿-45°C where annealing may have occurred. Details of the response of an EPR sample from this same solution are reported by

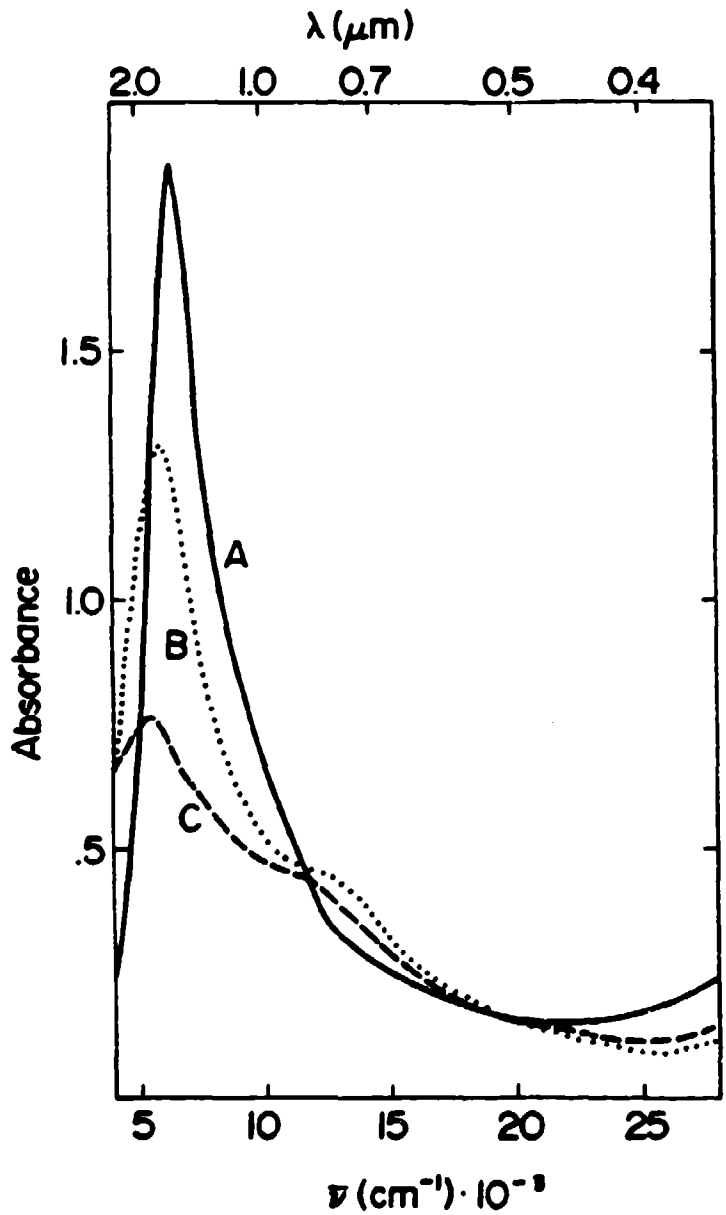

Figure 36. Unnormalized spectra of a K/C222 solvent-free film with R = 0.94 from ammonia. Spectra were recorded at the following times after solvent removal: A - 2 min (fresh); B - 28 min (intermediate); C - 81 min (annealed).

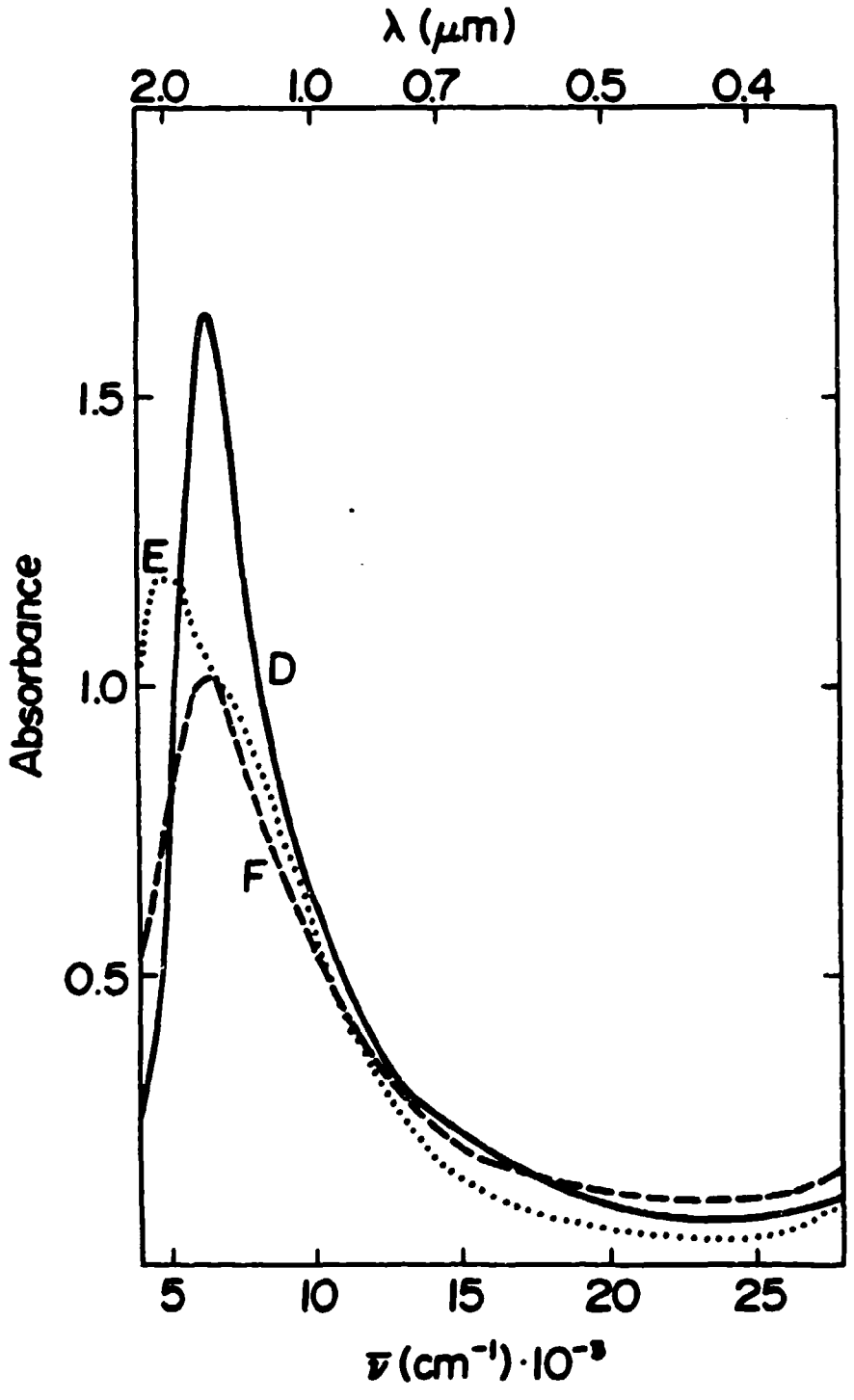

Figure 37. Unnormalized spectra of the same K/C222 film from which the spectra of Figure 36 were obtained: D - damp; E - intermediate; F - wet.

DaGue (64). The sample did not appear to be metallic but an unusually low percentage of electron spins seemed to be unpaired. An EPR sample from the same solution as the film whose spectra are in Figures 36 and 37 was too large for the E4 AFC. Since it nominally contained fewer spins than the previous $K^+C222 \cdot e^-$ sample, this may indicate its conductivity was somewhat higher. The data collected to date on $K^+C222 \cdot e^-$ systems concerning their metallic character are inconclusive.

Professor J. M. Lehn gave the Dye research group a quantity of C2N22, the tetraza analog of C222 in which both oxygens of one strand are replaced by nitrogens, depicted in Figure 2. Curve A of Figure 38 shows the spectrum of an ammonia-free fresh film of K/C2N22 in which R = 0.91. At -39°C a broad peak due to e_t^- is centered at 6600 cm^{-1} (1515 nm). Considerable potassium must be uncomplexed to give the additional peak at 11,700 cm^{-1} (855 nm) which is due to K^-. Over a 70 minute period the fresh film annealed, yielding spectrum B at -35°C where the K^- presence is even more pronounced. Peak positions are nearly unchanged at 11,800 cm^{-1} (845 nm) for K^- and 6300 cm^{-1} (1590 nm) for e_t^-. The change in relative peak magnitudes apparently occurred independently of numerous temperature cycles between -30° and -60°C during the 70 minutes. Because the tetraza C2N22 gave a mixed alkalide/electride spectrum rather than a pure electride absorption when there was excess cryptand, its properties in ammonia were not investigated further.

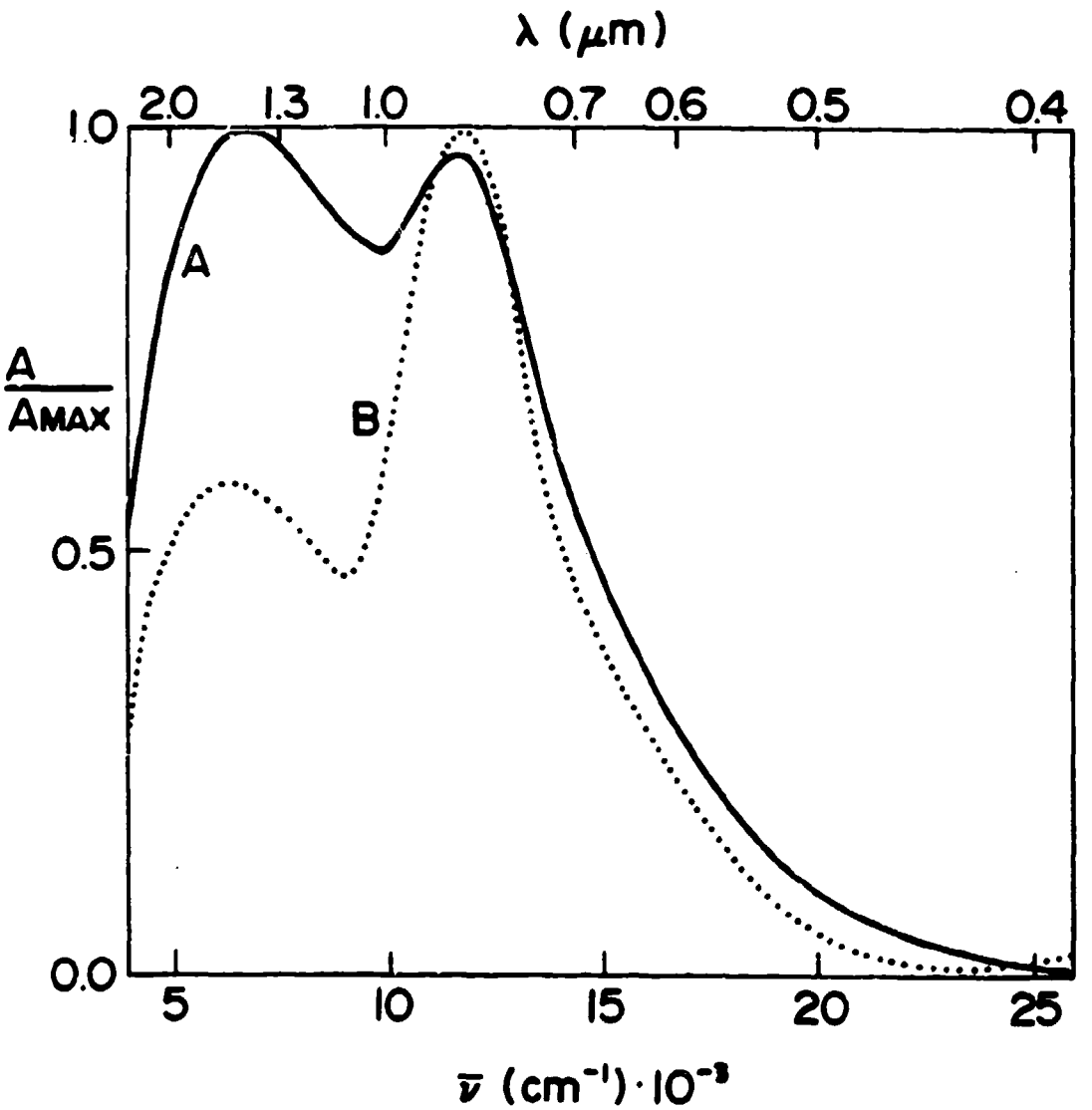

Figure 38. Spectra of a solvent-free film of K/C2N22 with R = 0.91 from ammonia: A - fresh; B - annealed, 70 min after spectrum A.

IV.B.4. Rb/C222 System

Curve A of Figure 39 is the initial spectrum of a dry Rb/C222 film with R = 1. The major feature is an e_t^- peak at 6750 cm^{-1} (1485 nm) while the Rb^- absorption is just a shoulder at 12,050 cm^{-1} (830 nm). Over a period of 40 min, the spectral shape gradually changed to that shown by curve B in Figure 39. With the optical cell maintained at -50° ± 2°C and the bulk solution in the sidearm at liquid nitrogen temperature, the magnitude of the e_t^- peak decreased by 25% and the peak shifted to 5600 cm^{-1} (1785 nm), a red shift of 1100 cm^{-1}. Meanwhile, the absolute absorbance of the Rb^- peak remained nearly constant. This appears to be another C222 system in which complexation of the alkali metal cation is not quite complete. Spectrum C of Figure 39 is that of a semi-wet film which shows a significant, broad infrared absorption that appears to result from the superposition of solvated electron bands with a plasma absorption.

IV.B.5. Cs/C322 Systems

This is the first report of the use of 3,2,2-cryptand as the alkali metal complexing agent in optical spectra. The previously reported dry film spectrum of Cs/C222 with R = 2 had four peaks of nearly the same amplitude: one attributable to e_t^- and three in the region of Cs^- (61).

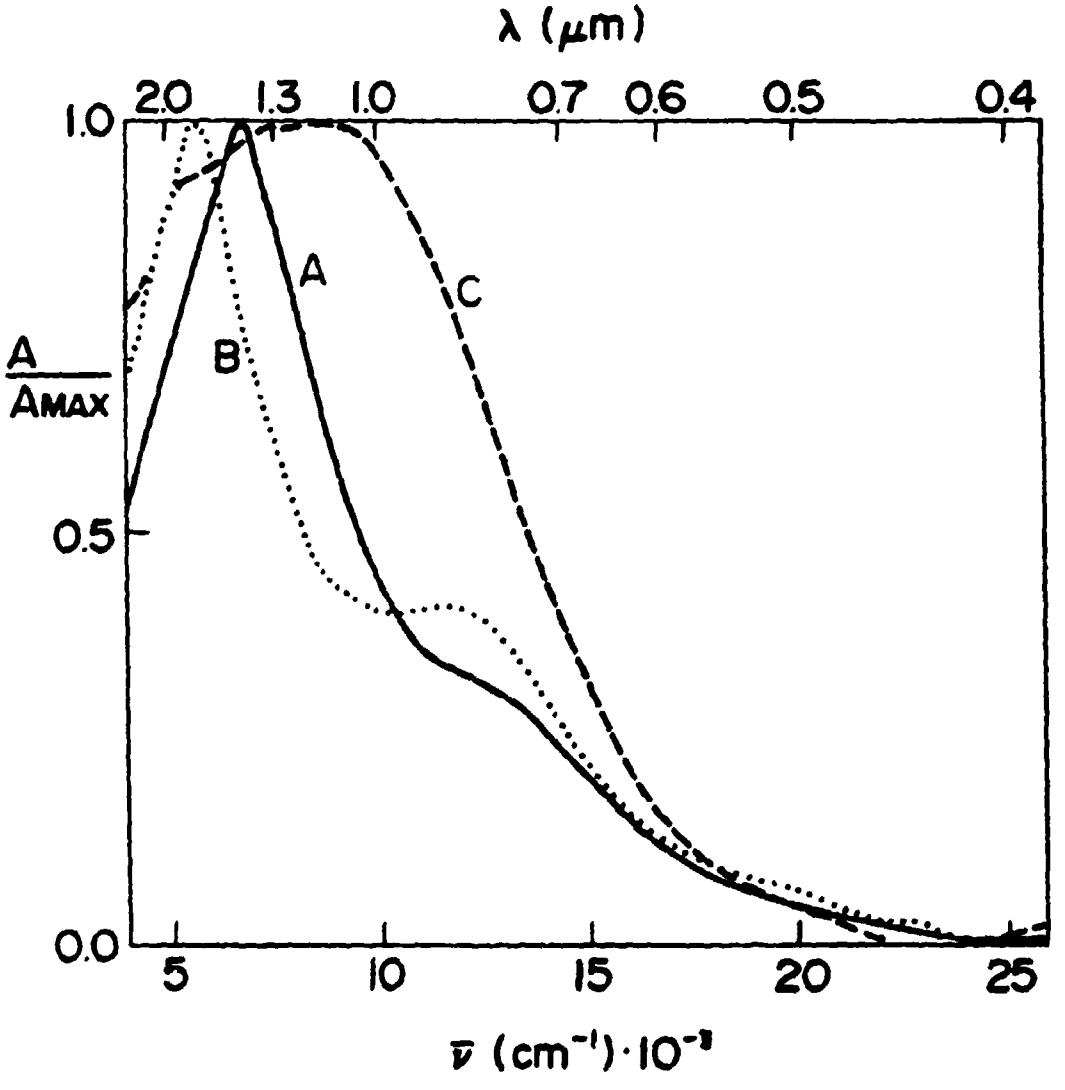

Figure 39. Spectra of Rb/3222 films with R = 1 from ammonia: A - dry (fresh); B - dry (annealed), 40 minutes after spectrum A; C - semi-wet.

NMR studies have shown that C222 forms both inclusive and exclusive complexes with Cs^+ in solution (81,95), so the films from NH_3 may have had a variety of sites for e_t^- and Cs^-. On the other hand NMR has shown that complexes of Cs^+ with C322 are only inclusive (96). The C322 cavity size is more compatible with the Cs^+ 3.3Å radius (Figure 3). An experiment was conducted to determine if Cs/C322 films from NH_3 with R = 2 might be more homogeneous than corresponding C222 films.

The improvement appears to be only marginal. Curve A of Figure 40 shows a very broad peak in a fresh dry film. The major peak at 7800 cm^{-1} (1280 nm) and the shoulder at 6500 cm^{-1} (1540 nm) are probably due to e_t^- species while the shoulders at 9800 cm^{-1} (1020 nm) and 13,000 cm^{-1} (770 nm) are thought to be caused by Cs^- species. An interesting change occurred in this spectrum when it annealed: a single e_t^- peak became predominant and shifted to 6200 cm^{-1} (1615 nm) while a Cs^- peak at 10,000 cm^{-1} (1000 nm) and a shoulder at 12,500 cm^{-1} (800 nm) maintained their positions but became more pronounced (spectrum B, Figure 40). This irreversible change only occurred after a warm film was chilled to approximately -57°C and rewarmed slightly. Because the phenomenon was repeated in three films over a one week period, it is not regarded as an artifact though the change was sluggish in the final film when decomposition was more likely.

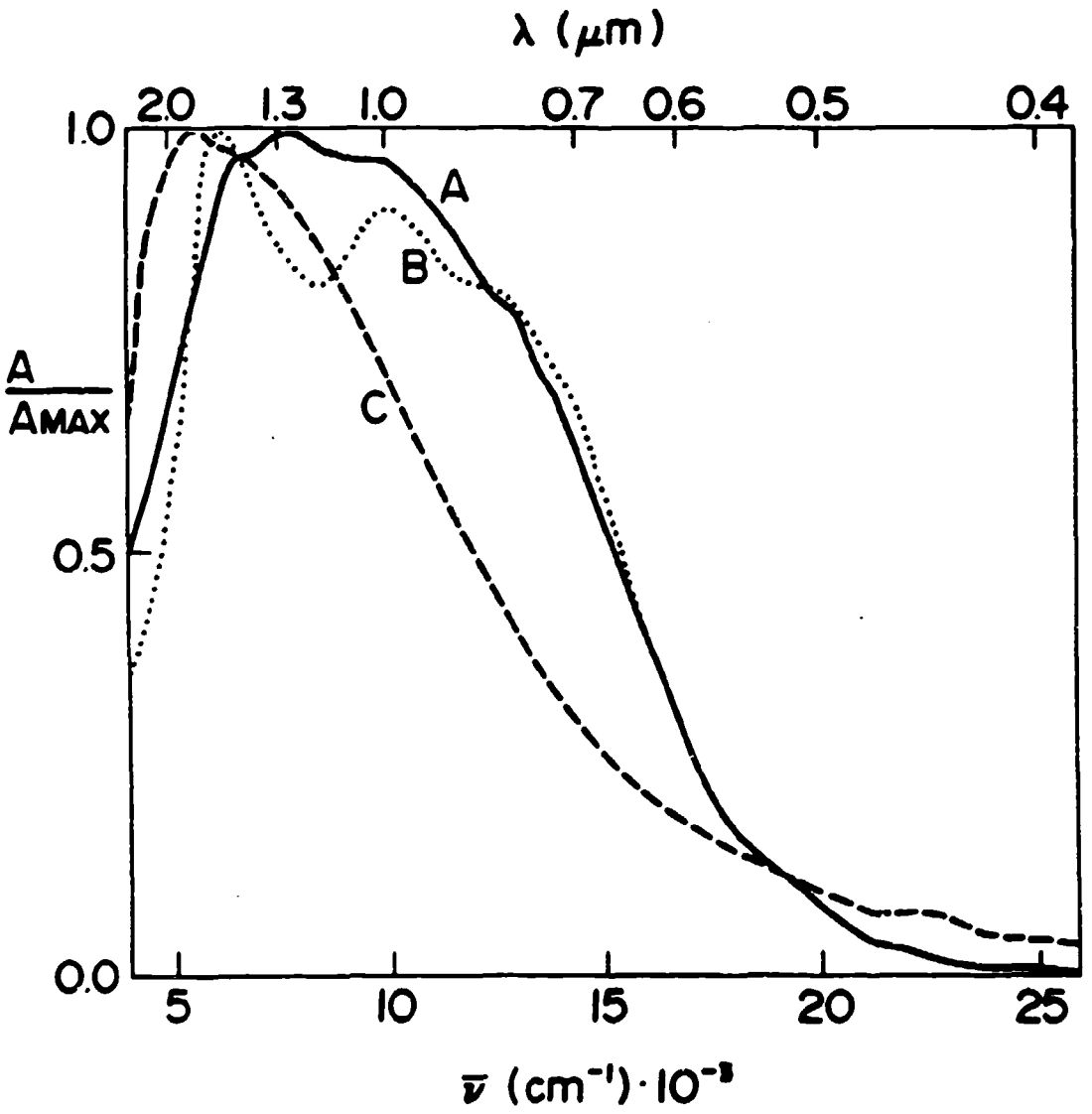

Figure 40. Spectra of Cs/C322 solvent-free films from ammonia: A - R = 2 dry (fresh) film at -48°C; B - same film, dry (annealed) at -48°C after cycling temperature to -58°C; C - R = 1 dry film at -45°C.

Regardless of the interesting annealing, the spectrum is not as homogeneous as might be expected if the Cs^+ complex of C322 were entirely inclusive. The e_t^- and low energy Cs^- annealed peak positions are nearly unchanged from those found for the Cs/C222 system (Figure 41, spectrum B). The two lowest energy Cs^- peaks in Cs/C222 spectra may have collapsed into a single peak in Cs/C322 spectra (spectrum A, Figure 41) located midway between their Cs/C222 positions. If so, then that represents the only move toward homogeneity that is evident in the Cs/C322 system in NH_3 with R = 2. The effect that the unsymmetrical 3,2,2-cryptand may have on the homogeneity of the solid state film structure is undetermined. Damp and wet spectra of these films show typical plasma character.

By contrast, curve C of Figure 40 depicts the slightly asymmetric but smooth spectrum of a dry Cs/C322 film with R = 1. No annealing was noted and no Cs^- shoulder or peak is visible. The peak broadness indicates that the e_t^- environment in the solid film is probably not particularly homogeneous, while the lack of Cs^- structure indicates that Cs^+ complexation in C322 is fairly complete.

IV.C. Films from Methylamine

Spectra of films from methylamine (MA) often lack shoulders and extra peaks found in the spectra of films from ammonia with comparable stoichiometry (61). Bands in

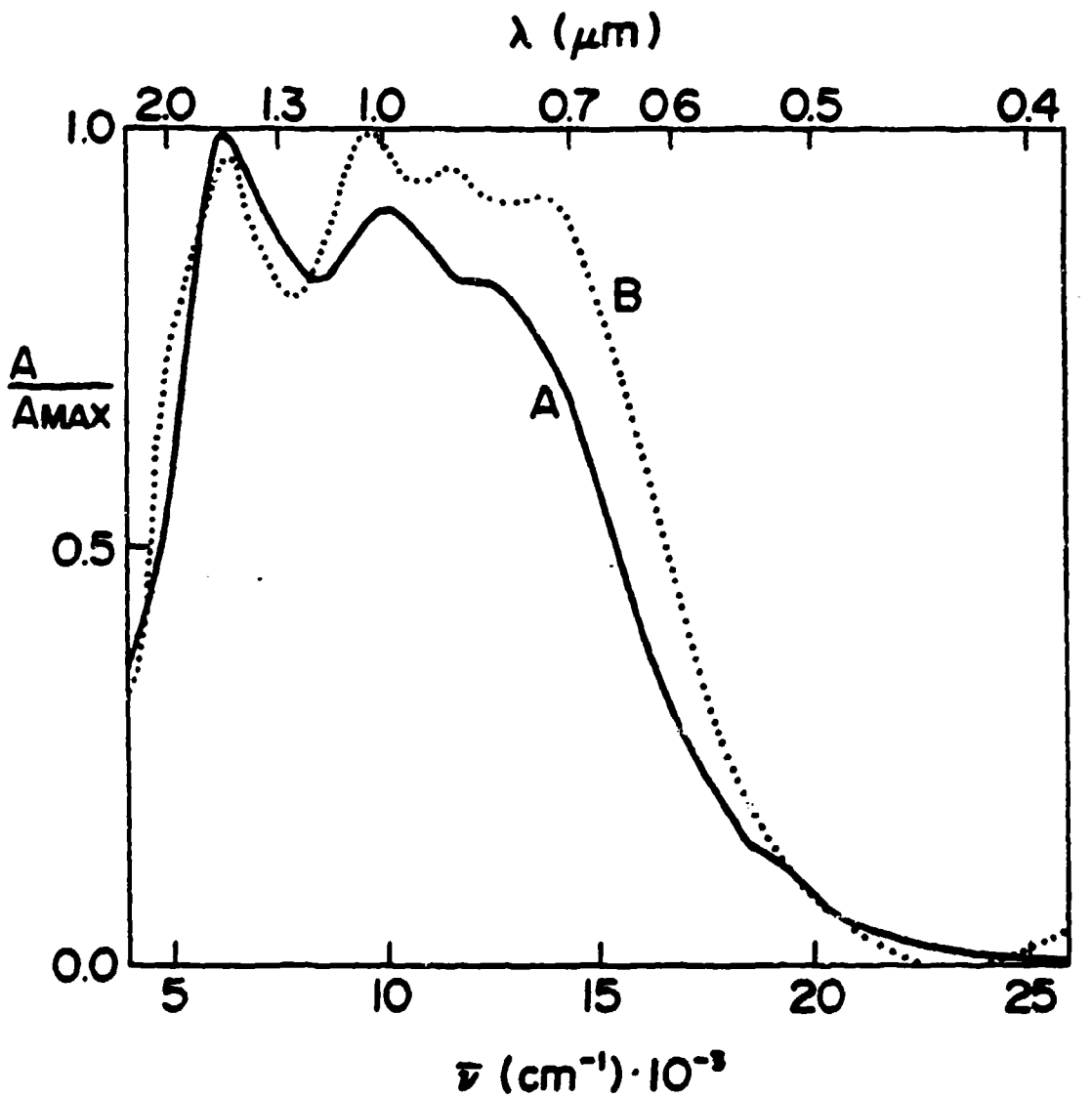

Figure 41. Spectra of solvent-free Cs/cryptand films with R = 2 from ammonia: A - with C322; B - with C222, from Reference 61.

solids from MA are the same ones present in solution while solids from NH_3 exhibit bands not seen in the solutions (64). In an attempt to produce more homogeneous films, then, several systems were prepared with MA as the solvent.

IV.C.1. K/C2N22 System

Two attempts were made to study K/C2N22 with R = 1 from methylamine solutions. However, in both cases the only peak observed was at 15,500 cm^{-1} (645 nm). A simple flame test on the decomposed second solution confirmed the presence of a large quantity of sodium. A quantitative flame emission study of the "potassium" sample taken immediately adjacent to the metal sample used in the second cryptate solution showed a sodium contamination of approximately 20%. A check of potassium sample tubing of various sizes showed that the smaller the tubing, the greater the sodium contamination. The conclusion is that there was significant exchange of the sodium from the borosilicate glass with the alkali metal (97). The more the metal was distilled (into smaller tubing), the greater was the contamination.

Despite the presence of Na^- instead of K^- or e_t^- in the spectra, several observations should be noted. The spectra usually contained only one species at a time: e_t^- in the early films and then the contaminant, Na^-. With the exception of one film, no spectra showed any

annealing. Both of these items would indicate that solids from MA are less complicated and more homogeneous than the multipeak, annealing films of K/C2N22 from NH_3. Films containing MA showed only the same Na^- peak as when dry and they continued to show it until they washed from the optical cell walls. This is consistent with the observation that solids from MA exhibit the same bands as the solutions from which they are formed.

IV.C.2. Cs/C322/Na System

Conservative thermodynamic estimates indicate that many alkalides and electrides should be stable in the crystalline state (54). For the reaction

$$C(s) + M_x(s) + M_y(s) \rightarrow M_x^+CM_y^-(s)$$

$\Delta G°$ for $Cs^+C322 \cdot Cs^-$ is +30 kJ/mole. From a similar calculation for $Na^+C222 \cdot Na^-$, $\Delta G°$ = +28 kJ/mole although the latter compound has been crystallized and its structure determined by single-crystal x-ray diffraction studies (6). So $Cs^+C322 \cdot Cs^-$ might actually be stable. However, sodide salts tend to be the most stable alkalides. For example $\Delta G°$ for $Li^+C211 \cdot Li^-$ = +2 kJ/mole while $\Delta G°$ for $Li^+C211 \cdot Na^-$ = -19 kJ/mole. So by comparison the cesium sodide should be more stable than the corresponding ceside, and a methylamine solution of the stoichiometry $Cs^+C322 \cdot Na^-$ was

produced. Curve A of Figure 42 shows the optical spectrum of a fresh dry film which includes a fairly broad peak for Na^- at 13,800 cm^{-1} (725 nm) and the hint of a shoulder at approximately 19,000 cm^{-1} (525 nm). Once the film was warmed above ~-33°C, it converted irreversibly to a more homogeneous film whose typical spectrum is depicted by curve B in Figure 42. This is the first indication of a definite peak protruding from the asymmetric, high energy side of the Na^- peak. With only minor shifts but no shape changes, this spectrum remained constant from -71°C to -0.7°C, indicating that it should be stable to even higher temperatures.

The most promising aspect of a $Cs^+C322 \cdot Na^-$ MA solution is its bronze color by reflectance. The viscous solution appeared ready to crystallize. After changing the solvent to diethylether, B. Van Eck forced deep red dendritic crystals from the solution in the original optical apparatus. He is taking steps to produce a single crystal of sufficient quality for x-ray structural determination and if he is successful, the origin of the high energy shoulder/peak on the Na^- peak may become evident.

IV.C.3. Li/C211/Na System

After the success of the $Cs^+C322 \cdot Na^-$ system, the thermodynamically favorable $Li^+C211 \cdot Na^-$ system was attempted. The viscous, bronze-colored solution gave the initial dry

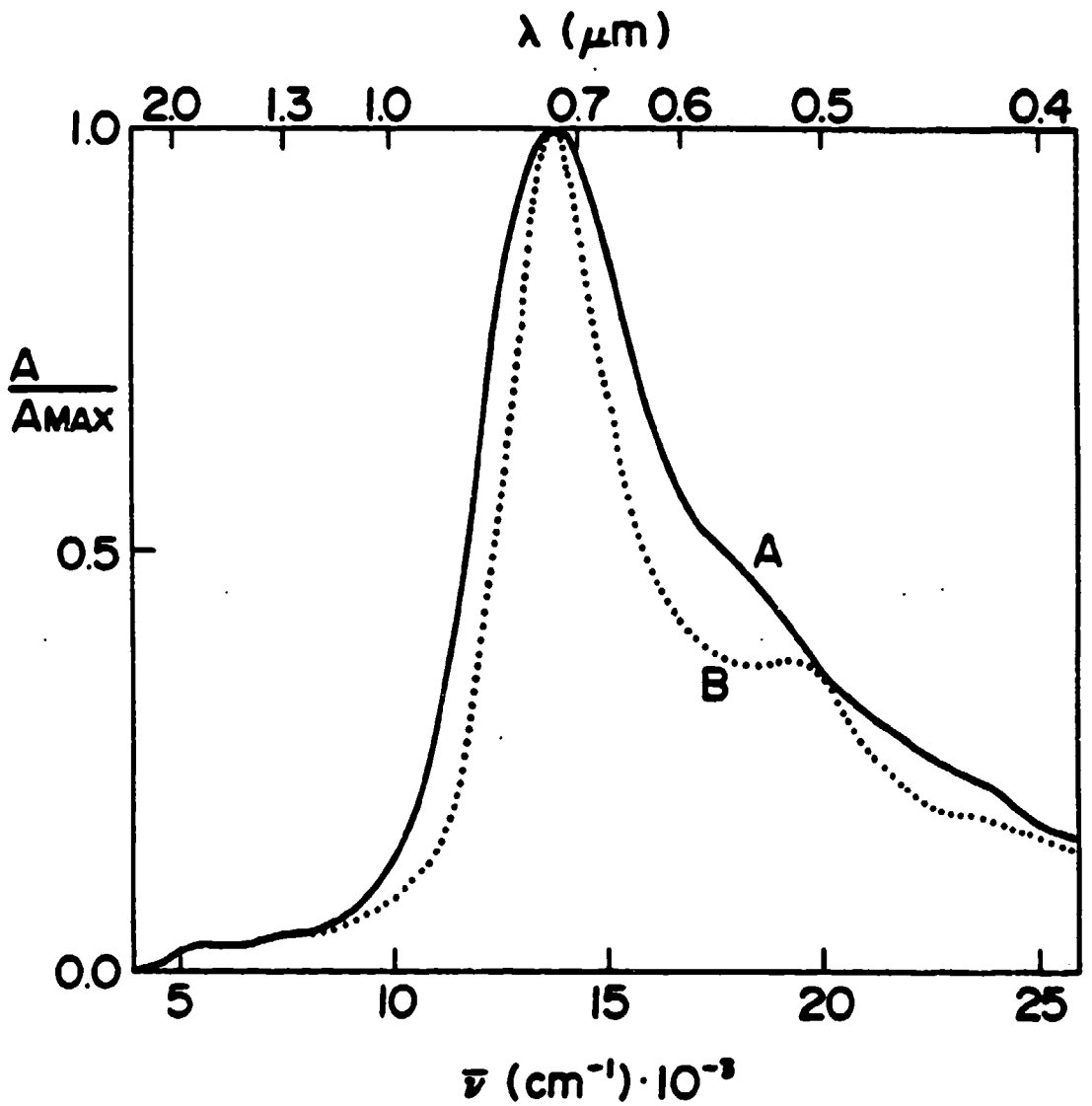

Figure 42. Spectra of solvent-free equimolar Cs/C322/Na films from methylamine: A - fresh film at -30°C; B - annealed film at -0.7°C.

film spectrum B in Figure 43 with a Na^- peak at 13,200 cm^{-1} (760 nm) and high energy shoulders at 15,000 cm^{-1} (665 nm) and 21,000 cm^{-1} (475 nm). Moderate temperature changes did not make this film anneal, but a subsequent film yielded the spectrum depicted by Curve A in which the Na^- peak at 13,900 cm^{-1} (720 nm) is accompanied by one high energy peak at 18,800 cm^{-1} (530 nm). This spectrum retained the same character, though it varied in amplitude, from -74° to -10°C. Dr. Long Dinh Le was able to precipitate crystals from this solution. He is attempting to produce more of these silver-colored rectangular crystals for x-ray structural determination.

IV.D. Optical Spectra Summary

Thin film optical transmission spectra are dependent upon the nature of the complexing agent, the metal, the ratio, R, of metal to complexer and the solvent used to make the film, as well as the solvent content of the film in the case of ammonia. Table 13 summarizes the peak positions for systems other than Li/C211. Four general classes of compounds previously reported (61) are evident in this study: (1) alkalides $M_x^+C \cdot M_y^-$ in which the anion is an alkali metal; (2) electrides $M^+C \cdot e^-$ in which the "anion" is a localized, trapped electron; (3) expanded metals $M^+C \cdot e^-$ in which the electron is in the conduction band; and (4) a combination in which localized electrons

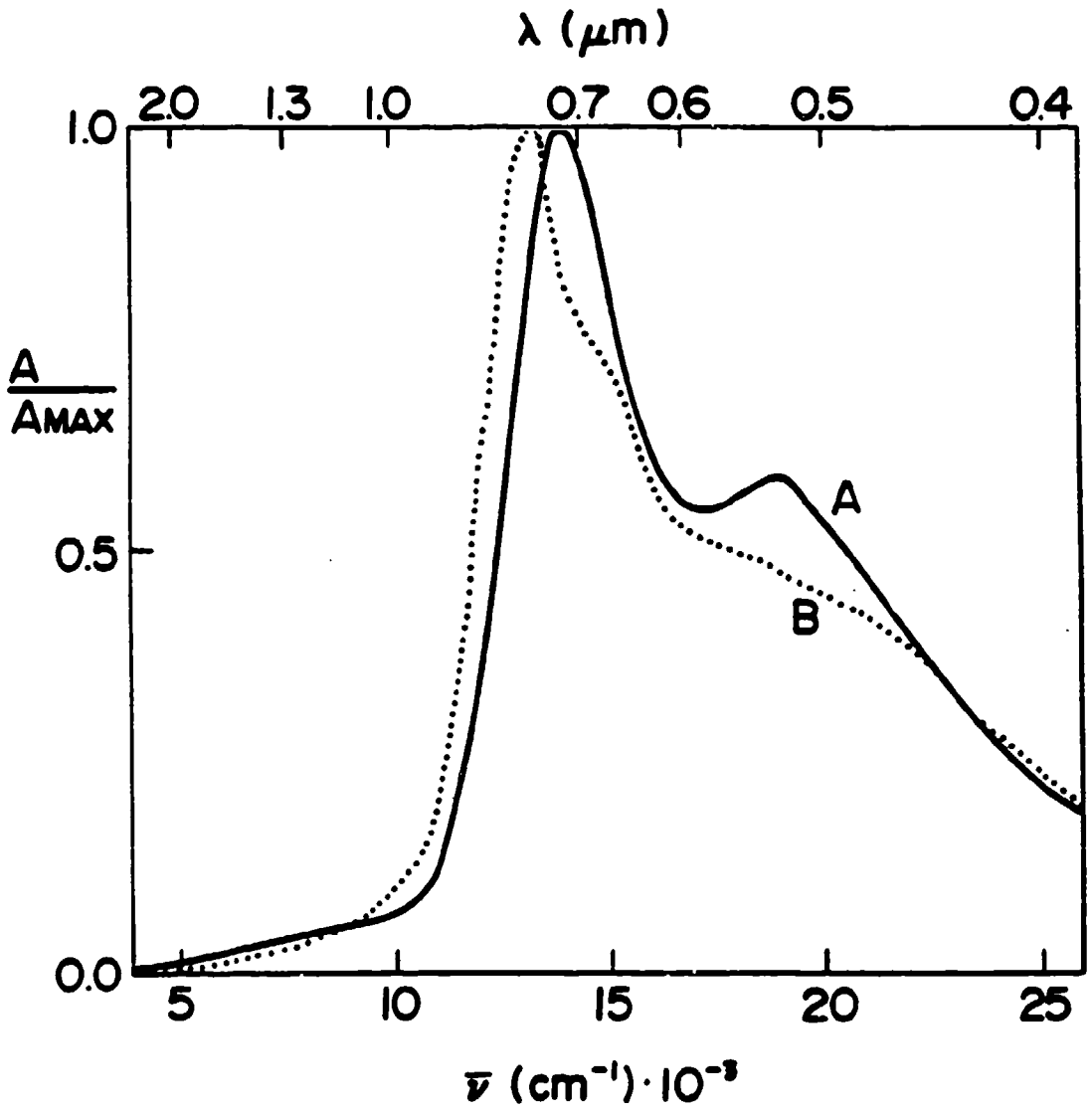

Figure 43. Spectra of solvent-free equimolar Li/C211/Na films from methylamine: B - initial film; A - subsequent film which annealed and then remained unchanged from -74° to -10°C.

Table 13. Summary of optical spectra peak positions; systems other than Li/C211.

M	Solvent	Ligand	R[a]	Film Condition[b]	Peak Positions[c] (cm^{-1}) M^-	e_t^-	Others
Na	NH_3	none	-	wet	------	----	plasma edge
		DABCO	3	wet	------	----	plasma edge
		C221	2	dry	14,400	----	----------
				damp	------	6000	plasma character
				wet	------	7200	plasma character
		C222	1	dry	16,100	8500(m)	----------
				damp	------	7800	----------
				wet	------	6200	plasma character
				redried	15,800	7800(m)	----------
			3	dry(fr)	15,500(m)	8100	5500(sh), 25,500(sp)
				dry(ann)	15,500(m)	6900	4500(sh), 25,000(sp)
				semi-wet	------	6700	11,500(s), 25,500(sp)
			4	dry(fr)	15,400(m)	7800(sp)	5100(sp)
				dry(ann)	15,400(m)	6800(sp)	~3850(sp)
				wet	------	6300	plasma character
K	NH_3	none	-	wet	------	----	plasma edge
		C222	1	dry(fr)	10,500(s)	6500(m)	----------
				dry(ann)	12,000(s)	5400(m)	plasma character
				damp	------	6500	----------
				wet	------	6000	plasma character

Table 13. Continued.

M	Solvent	Ligand	R[a]	Film Condition[b]	Peak Positions[c] (cm^{-1})		
					M^-	e_t^-	Others
K	NH_3	C2N22	1	dry(fr)	11,700	6600(m)	----------
				dry(ann)	11,800(m)	6300	----------
Rb	NH_3	C222	1	dry(fr)	12,050(s)	6750	----------
				dry(ann)	11,800(sp)	5600	----------
				semi-wet	------	~8350	plasma character
Cs	NH_3	C322	1	dry	------	~5500	----------
				wet	------	~7000	----------
			2	dry(fr)	9800(s)	7800(m)	6500(s), 13,000(s)
				dry(ann)	10,000	6200(m)	12,500(s)
Li and Na	CH_3NH_2	C211	1:1	dry(fr)	13,200	----	15,000(s), 21,000(s)
				dry(ann)	13,900	----	18,800(sp)
Cs and Na	CH_3NH_2	C322	1:1	dry(fr)	13,800	----	~19,000(s)
				dry(ann)			
				-71°C	14,000	----	18,500(sp)
				-0.7°C	13,750	----	19,250(sp)

[a] R = ratio of moles of metal to one mole of complexer; 1:1 indicates one mole of each metal. Ratios listed as 1 are slightly less than one, normally 0.95-0.98.

[b] fr = fresh, ann = annealed. [c] m = major peak, s = shoulder, sp = small peak.

and alkalides exist in the same film. This combination most commonly exists in films from ammonia. Perhaps the solvation ability of ammonia is so pronounced that metal cation complexation by the cryptands is significantly reduced, as postulated for Li/C211 in Chapter III. When the solvent is removed by flash evaporation, the cations are trapped outside the cryptands. Spectra of these films are complex and the peaks are broadened reflecting multiple environments for the e_t^- and M^- species. These complex spectra often have time-dependent behavior as an equilibrium is established among the variety of available traps.

The nature of films containing solvent is dependent upon the solvent used. Films damp with methylamine do not change appreciably; the species in solution appear to be the same species present in dry films. Films damp with ammonia, however, show distinct changes. There is no specific evidence that the centrosymmetric alkali anion in the dry film exists in a damp or wet film. The M^- peak disappears rapidly as the film acquires ammonia and is replaced by a series of solvated electron peaks. As a concentrated MAS is formed most films assume plasma character, followed by a decrease in plasma absorption as the film becomes more dilute just before washing from the optical cell walls. This sequence is fairly consistent among the systems studied, however film response to the initial ammonia vapor (initial damp spectrum) varies.

Some dry films showing high plasma absorption immediately become localized before joining the sequence above. Others which show localized electron character when dry immediately assume plasma character when ammonia vapor is first introduced. This variety of responses in initially dampened films is currently without explanation.

CHAPTER V

AMMONIA ANALYSES

The presence of ammonia in liquid alkali metal solutions (7,11) or in solid alkali metal compounds (18) has a substantial impact on solution or solid properties. Alkali metal/cryptand systems have not been as thoroughly studied, yet there can be little doubt that ammonia, depending upon the relative amount present, can drastically alter some of the properties of these systems. This study is an attempt to determine the approximate relative amounts of cryptand and ammonia present. Properties of alkali metal/cryptand systems with variable amounts of ammonia were discussed briefly in Section III.A.2.

The indophenol blue formation test for the presence of ammonia (Section II.D.4.) was chosen because of its ease compared to spectrophotometric (quantitative) methods. Yet the test was still semi-quantitative because sample colors were compared with standards of known NH_4^+ concentration. In most instances after an aliquot of the original solution was removed for testing, the remaining original solution was diluted and retested. The results for each sample in Table 14 are normally the average for two or three tests.

Table 14. Summary of NH_3 content of samples.

Sample	Size (Moles C211)	Pumping Static or Dynamic (min)	Results C211 : NH_3	Comments
AT-1	8×10^{-6}	static 3m	1 : 4	Poor NH_3 tests; several adjacent samples were not dry when ℓ-N_2 placed on reservoir to begin static pumping.
AT-2	4×10^{-6}	static 5m	1 : 5	
AT-3	3×10^{-6}	static 11m	1 : 5	
AT-4	4×10^{-6}	static 61m	1 : 2	Vacuum in apparatus poor because of decomposition during seal offs; drying process probably slower than during high vacuum.
AT-5	6×10^{-6}	static 68m	1 : 3	
AT-6	5×10^{-6}	static 77 m	2 : 1	
AT-7	4×10^{-5}	static 135m	40 : 1	
III	4×10^{-6}	static 20m	10 : 1	Sample was optical film; very thin.

Table 14. Continued.

Sample	Size (Moles C211)	Pumping Static or Dynamic (min)	Results C211 : NH_3	Comments
EC-1	--------	dynamic 70m	>200 : 1*	Empty cells to check adsorption of NH_3; ratio computed as though 4×10^{-6} moles C211 in cell.
EC-2	--------	static 55m	20 : 1	
VIIa	9×10^{-6}	dynamic >25m	6 : 1	MSU magnetic susc. samples; both samples were bulk rather than films.
VIII	5×10^{-6}	dynamic >45m	5 : 1	
IX-1	3×10^{-7}	static 65m	>10 : 1*	Vapor pressure study; IX-1 at -65°C and reservoir at -116°C; IX-2 at -65°C with reservoir at -91°C; evacuated to 3×10^{-5} torr after each seal off.
IX-2	2×10^{-7}	static 65m	1.8 : 1	
II	1×10^{-5}	static 30m	7 : 1	EPR sample.

Table 14. Continued.

Sample	Size (Moles C211)	Pumping Static or Dynamic (min)	Results C211 : NH_3	Comments
VIIb	2×10^{-5}	dynamic 30m	110 : 1	Sample sidearm reservoir.
$Na^+C222 \cdot Na^-$	unknown	prob. static	>500 : 1	Methylamine analysis by PMR from Ref. 64; powders prepared under conditions similar to those of film formation.
$K^+C222 \cdot e^-$	unknown	prob. static	12.5 : 1	

*Quantity of NH_3 was less than the limit of detection.

Precision with these dilution steps was generally ±50%.

Ammonia tests 1 - 6 were specifically to determine the effect of static pumping time. A large apparatus was built with seven 8 mm O.D. tubes on the sample sidearm. $Li^+C211 \cdot e^-$ solution was poured into the tubes and evaporated to near dryness. The bulk solution in a reservoir was frozen with liquid nitrogen and the NH_3 was supposedly drawn from the samples to this trap while the apparatus was under static vacuum. Two problems were evident: first, samples adjacent to AT 1 - 3 were wet with NH_3 when ℓ-N_2 was placed on the reservoir, thus invalidating the results; and secondly, there was cryptate residue in the vicinity of the AT-2 sample seal-off. When this region was heated the cryptate decomposed and raised the pressure certainly higher than 10^{-2} torr, though the actual pressure was not measured. Thus the removal of NH_3 from the remaining samples was probably much slower than in a higher vacuum. However, samples AT 4 - 6 still show a progression of less NH_3 as static pumping time increases.

Sample shape also has an apparent effect on NH_3 retention. As expected, a thin optical film was more ammonia-free than either of two magnetic susceptibility samples in which the $Li^+C211 \cdot e^-$ powder was in a lump, even though the susceptibility samples were dynamically pumped to $\sim 10^{-5}$ torr.

Predictably dynamic vacuum pumping decreases the NH_3 content more effectively than static pumping. The empty

cell (EC) tests show this clearly, as do samples II and VIIb.

It is interesting to note the apparently similar dryness of the $Li^+C211 \cdot e^-$ (III) and the $K^+C222 \cdot e^-$ samples. The methylamine content of the potassium electride sample was determined by proton magnetic resonance (64) and was much more quantitative than the NH_3 analysis. Both samples were pumped statically, and although the two solvents have different vapor pressures at a given temperature, the result may indicate that alkali metal electrides have roughly similar solvent affinities.

The results in Table 14 show that sample solvent content decreases with increased drying time and that dynamic pumping is more effective at solvent removal than is static pumping. Regardless of conditions, thin samples lose their solvent more readily. Most importantly the tests indicate that $Li^+C211 \cdot e^-$ samples are substantially free of solvent. It is apparent that the MNM transition observed in the $Li^+C211 \cdot e^-$ (II) system was not solely due to the presence of some NH_3, although the precise effect has not been determined.

CHAPTER VI

SUMMARY AND SUGGESTIONS FOR FUTURE STUDIES

VI.A. Summary

The system $Li^+C211 \cdot e^-$ lies very nearly at the metal-nonmetal transition. This transition can be accomplished by changing the mole fraction of lithium: clearly the preparations with lithium to cryptand mole ratios of 0.60 and 2 lie on opposite sides of the transition. It appears that the system gradually changes to metallic character between $R \sim 1.5$ and 2. Accomplishing the MNM transition with the change of mole fraction of lithium indicates that the $Li^+C211 \cdot e^-$ MNM transition may be described by the Mott-Hubbard model. As the electron density increases, the increased screening allows the electrons to overcome the Coulombic potential and become itinerant. On the other hand sample II with $R = 0.95$ completed the transition rapidly as its temperature was raised or lowered through -45°C. Also, sample I with $R = 0.93$ showed only metallic character while three others with the same approximate mole ratio were predominantly nonmetallic. It is possible that disorder in these microcrystalline samples plays a role in

their approach to the MNM transition. If so, then perhaps the Anderson model provides a better description for the MNM transition in $Li^+C211 \cdot e^-$ or it may be that the system is best represented by a combination of Mott-Hubbard and Anderson models. A great deal of additional study must be accomplished on $Li^+C211 \cdot e^-$ before a conclusion may be drawn. In samples which are nonmetallic a significant percentage of the potentially available spins are unpaired at 245K. As the temperature is lowered, pairing occurs with very weak interaction energies until almost all spins are paired at liquid helium temperatures.

Many systems other than $Li^+C211 \cdot e^-$ were studied by optical transmission spectroscopy of solvent-free thin films. In some cases preparations with mole ratios slightly less than one show both electride and alkalide absorption peaks. This is particularly true when the films are made from ammonia solutions and it probably indicates that cation complexation by the cryptands is significantly reduced in ammonia. The mixed alkalides, $Li^+C211 \cdot Na^-$ and $Cs^+C322 \cdot Na^-$, showed very strong Na^- absorptions and the films were stable to nearly 0°C.

VI.B. Suggestions for Future Studies

The study of the $Li^+C211 \cdot e^-$ system should be continued in order to further characterize it and to determine, if possible, the factor(s) other than the mole ratio of

lithium influencing the MNM transition. Sample VI with R = 1.15 showed EPR results which did not seem to fit the pattern of the results from samples with other mole ratios. The slightly-metal-rich region should be investigated more thoroughly. A study could be accomplished by NMR to determine the rate of complexation of the lithium cation by C211. In either ammonia or methylamine the complexation at -45° or -50°C should be slow enough to observe a progressively smaller signal for the free cation and an increasingly larger signal for the complexed cation as equilibrium is approached. The result would give valuable kinetics and thermodynamic data. Finally, the study of $Li^+C211 \cdot e^-$ would be invaluably enhanced by the production of single crystals. This is not a trivial task because of the high chemical potential of the electrons. It may be necessary to include in the crystal structure some species upon which the electrons can localize so they will not destroy the cryptand. Perhaps then this difficult problem will become more tractable.

Optical spectra of systems other than $Li^+C211 \cdot e^-$ point towards some interesting possibilities. Most of the electrides appear to contain localized electrons. However $K^+C222 \cdot e^-$ seems to be metallic, depending upon annealing conditions. This may be another system which is near the MNM transition and it should be explored more thoroughly, possibly with samples from methylamine. The mixed alkalides,

$Li^+C211 \cdot Na^-$ and $Cs^+C322 \cdot Na^-$, are quite stable in their bronze-colored methylamine solutions. Both systems should be good candidates for producing single crystals.

APPENDIX

APPENDIX

EFFECT OF OPTICAL FILM NON-UNIFORMITY

A study was conducted to determine the effect on spectral band shape of films of variable thickness and of films partially covering the beam cross section as it passes through the optical cell. Professor J. L. Dye derived the spectral effect of non-uniform film thickness and Mr. Jim Anderson provided much of the computational effort.

Suppose there is a circular light beam of radius r_o with total intensity $I_o(\lambda)$ and local intensity $i_o(\lambda)$:

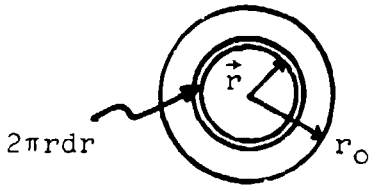

Then $I_c(\lambda) = i_o(\lambda) \cdot S$ where S is the beam cross section and

$$I_o(\lambda) = \int_o^{r_o} i_o(\lambda) 2\pi r dr = i_o \pi r_o^2 \qquad \text{(A-1)}$$

Let $I(\lambda)$ be the total light intensity passing through the sample, such that

$$I(\lambda) = \int_o^{r_o} i(\vec{r},\lambda) 2\pi r dr \qquad \text{(A-2)}$$

Bouguer-Lambert or Beer's Law states that, for a sample of uniform thickness x and a light beam of uniform cross section,

$$I = I_o e^{-\alpha x}$$

where $\alpha \equiv$ absorptivity $(cm^{-1}) = 2.303 \cdot \varepsilon(\lambda) \cdot c$ where $\varepsilon(\lambda)$ is the molar extinction coefficient and c is the molar concentration. Then

$$2.303 \log \frac{I_o(\lambda)}{I(\lambda)} = A = \alpha x$$

However, for a non-uniform thickness, $x(\vec{r})$,

$$i(\lambda) = i_o(\lambda) e^{-\alpha(\lambda) x(\vec{r})} \qquad \text{(A-3)}$$

and

$$I(\lambda) = 2\pi i_o(\lambda) \int_o^{r_o} r e^{-\alpha(\lambda) x(\vec{r})} d\vec{r} \qquad \text{(A-4)}$$

For simplicity, assume initially that the non-uniform film fills the light beam cross section and $x(r) = a + b(r/r_o)$

Using this model, Equation A-4 becomes

$$I(\lambda) = 2\pi i_o(\lambda)\int_o^{r_o} re^{-\alpha(\lambda)[a+(r/r_o)b]}d\vec{r}$$

After performing the integration with a table of integrals and using Equation A-1 for $I_o(\lambda)$:

$$\frac{I(\lambda)}{I_o(\lambda)} = 2e^{-\alpha(\lambda)\cdot a}\left[\frac{1 - e^{-\alpha(\lambda)b}(1 + \alpha(\lambda)b)}{(\alpha(\lambda)b)^2}\right] \qquad (A-5)$$

If the film were of uniform thickness $\langle\ell\rangle$ then $\frac{I(\lambda)}{I_o(\lambda)} = e^{-\alpha\langle\ell\rangle}$ and $\alpha\langle\ell\rangle = 2.303\log\frac{I_o}{I}$. Call $\log\frac{I_o}{I}$ the nominal absorbance A_{nom}. Therefore

$$2.303A_{nom} = \alpha\langle\ell\rangle \qquad (A-6)$$

But the film is not of uniform thickness and the "area weighted" or average film thickness $\langle\ell\rangle$ is calculated by

$$\langle\ell\rangle = \frac{\int_o^{r_o} dr x(r) 2\pi r dr}{\int_o^{r_o} dr 2\pi r dr} = \frac{2}{r_o^2}\int_o^{r_o} r\,x(r)dr \qquad (A-7)$$

For the model chosen, $x(r) = a + b(r/r_o)$, so

$$\langle \ell \rangle = \frac{2}{r_o^2} \int_o^{r_o} r \left[a + b\left(\frac{r}{r_o}\right)\right] dr$$

$$\langle \ell \rangle = \frac{2a}{r_o^2} \int_o^{r_o} r dr + \frac{2b}{r_o^3} \int_o^{r_o} r^2 dr$$

$$\langle \ell \rangle = \frac{2a}{r_o^2}\left(\frac{r_o^2}{2}\right) + \frac{2b}{r_o^3}\left(\frac{r_o^3}{3}\right) = a + \frac{2}{3}b \qquad \text{(A-8)}$$

The relationship of a to b can assume any value. If $b = -\frac{a}{2}$ is arbitrarily chosen, then Equation A-6 becomes

$$2.303A_{nom} = \alpha\left(a + \frac{2}{3}b\right) = \alpha a\left(\frac{2}{3}\right)$$

Then

$$\alpha a = \frac{3}{2}(2.303)A_{nom} \qquad \text{(A-9)}$$

and

$$\alpha b = -\frac{3}{4}(2.303)A_{nom} \qquad \text{(A-10)}$$

These values can now be used in Equation A-5 to compute $\frac{I}{I_o}$. But first make this specific case more general by allowing the film to cover a variable portion of the optical beam cross section. If

$$T = \text{(area of beam covered)/(total beam area)} = \left(\frac{r}{r_o}\right)^2$$

then

$$I(\lambda) = TI(\lambda)_{spot} + (1-T)I_o(\lambda) \qquad \text{(A-11)}$$

Thus Equation A-5 becomes

$$\frac{I(\lambda)}{I_o(\lambda)} = T2e^{-\alpha(\lambda)\cdot a}\left[\frac{1 - e^{-\alpha(\lambda)b}(1 + \alpha(\lambda)b)}{(\alpha(\lambda)b)^2}\right] + (1-T) \qquad \text{(A-12)}$$

Now, apply the following conditions:

$$\left(\frac{r}{r_o}\right)^2 = T = 1.00$$

$$A_{nom} = 1.50$$

as well as the previously selected b = -a/2. This calculation is for a film which covers the whole beam cross section. If the film were of uniform thickness, the nominal absorbance would be 1.5. However the film is conical:

Using Equations A-9 and A-10, αa = 5.18 and αb = -2.59. Therefore, Equation A-12 is

$$(I/I_o)_{max} = (1.00)(2)e^{-5.18}\left[\frac{1 - e^{2.59}(1 - 2.59)}{(2.59)^2}\right] - (1 - 1.00)$$

$$(I/I_o)_{max} = .0329 \text{ and } (I_o/I)_{max} = 26.9$$

$$A_{max} = \log(I_o/I)_{max} = 1.43$$

but $A_{nom} = 1.50$, so for this very specific case, the nominal absorbance is decreased 4.7% due to the non-uniform film thickness.

The results of a series of such calculations are tabulated in Tables A-1 through A-5 for various geometries and displayed in Figures A-1 and A-2 for the first two geometries.

Table A-1. Film shape effect: A_{max} for $b = -a/2$

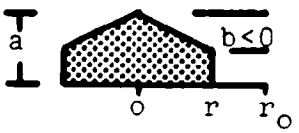

$A_{nominal}$

$\frac{r}{r_o}$	.500	.750	1.000	1.250	1.500	1.750	2.000
.50	.123	.125	.125	.125	.125	.125	.125
.75	.288	.330	.348	.354	.357	.358	.359
.80	.327	.390	.419	.433	.439	.441	.443
.90	.407	.534	.615	.663	.689	.704	.712
1.00	.491	.731	.967	1.200	1.429	1.656	1.880

Table A-2. Film shape effect: A_{max} for b = a/2

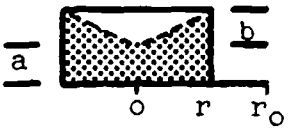

$\underline{A_{nom}}$

$\frac{r}{r_o}$	.500	.750	1.000	1.250	1.500	1.750	2.000
.50	.123	.125	.125	.125	.125	.125	.125
.75	.291	.333	.349	.355	.358	.358	.359
.80	.330	.393	.422	.434	.440	.442	.443
.90	.412	.541	.622	.669	.694	.707	.714
1.00	.498	.745	.991	1.236	1.479	1.721	1.962

Table A-3. Film shape effect: A_{max} for a = 0, b > 0

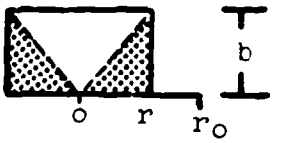

$\underline{A_{nom}}$

$\frac{r}{r_o}$	.500	.750	1.000	1.250	1.500	1.750	2.000
.50	.119	.122	.123	.124	.124	.124	.125
.75	.272	.312	.331	.341	.346	.349	.352
.80	.308	.365	.395	.411	.421	.427	.431
.90	.383	.493	.565	.610	.640	.660	.673
1.00	.462	.662	.842	1.001	1.143	1.269	1.381

Table A-4. Film shape effect: A_{max} for b = -a

A_{nom}

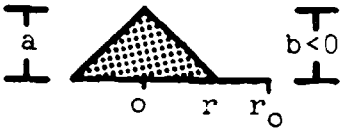

$\frac{r}{r_o}$	.500	.750	1.000	1.250	1.500	1.750	2.000
.50	.106	.112	.115	.117	.118	.119	.120
.75	.228	.263	.283	.296	.305	.312	.317
.80	.257	.302	.330	.349	.362	.372	.380
.90	.317	.394	.447	.485	.513	.536	.554
1.00	.380	.506	.606	.689	.759	.819	.872

Table A-5. Film shape effect: A_{max} for b = 0; uniform thickness.

A_{nom}

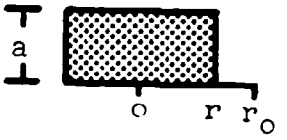

$\frac{r}{r_o}$	.500	.750	1.000	1.250	1.500	1.750	2.000
.50	.123	.125	.125	.125	.125	.125	.125
.75	.292	.334	.350	.356	.358	.359	.359
.80	.332	.395	.423	.435	.440	.442	.443
.90	.414	.594	.625	.671	.696	.709	.715
1.00	.500	.750	1.000	1.250	1.500	1.750	2.000

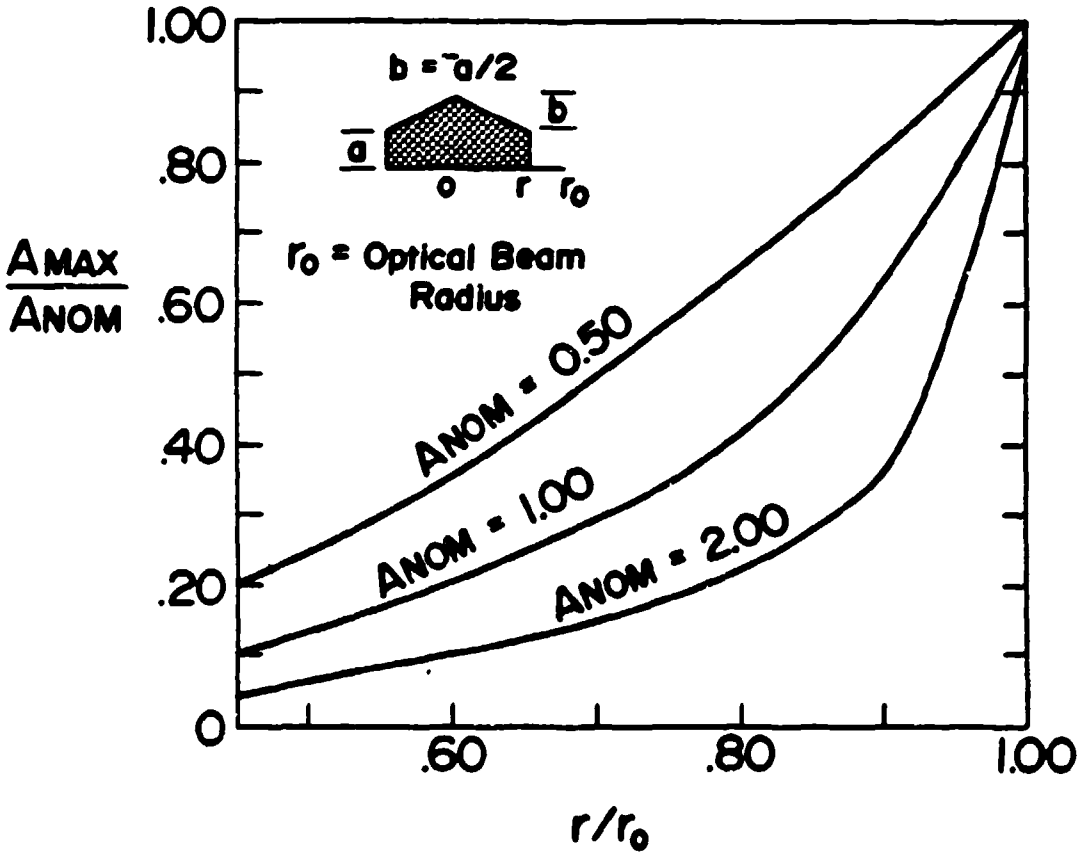

Figure A-1. Effect on the peak amplitude of an optical film which is of non-uniform thickness (shape as indicated) and which fills various amounts of the optical beam.

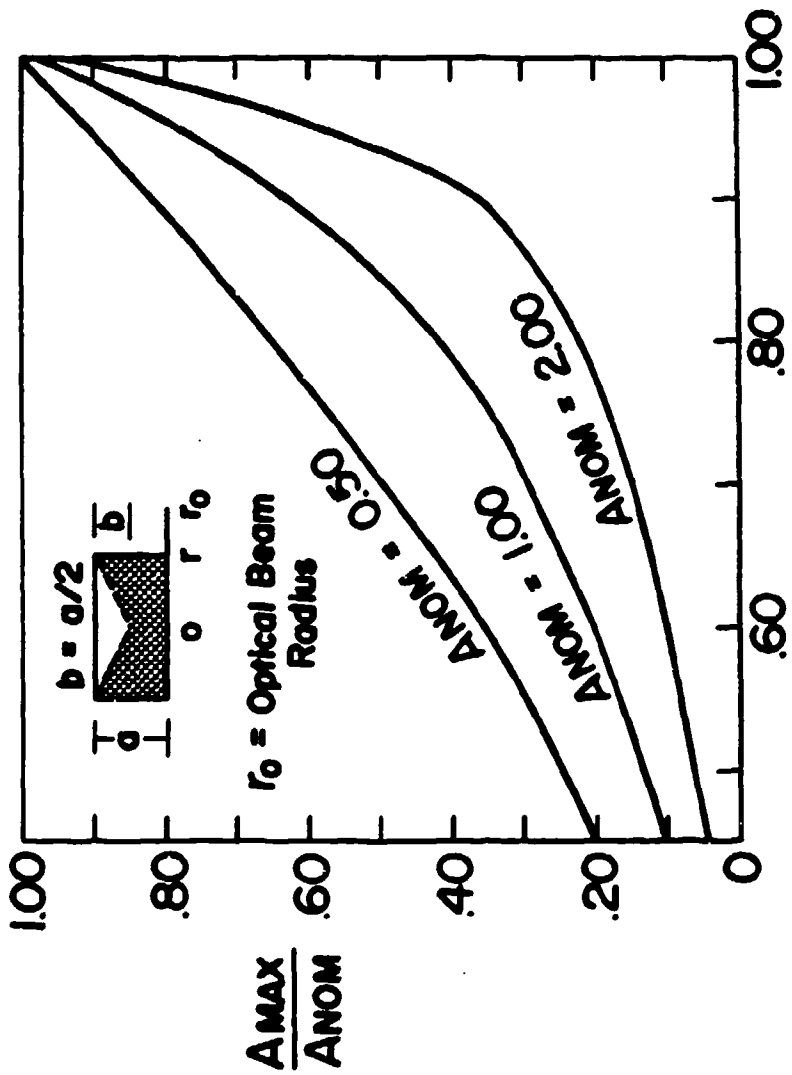

Figure A-2. Effect on the peak amplitude of an optical film which is of non-uniform thickness (shape as indicated) and which fills various amounts of the optical beam.

It is informative to observe the effect of a film of non-uniform thickness on a complete lineshape, not just upon the maximum peak amplitude as in the previous tables and figures. An absorption curve of Lorentzian shape can be described by:

$$g(\omega-\omega_o) = \frac{T_2/\pi}{1 + (\omega-\omega_o)^2 T_2^2} \qquad \text{(A-13)}$$

where ω_o is the angular frequency of the radiation at resonance and T_2 is the spin-spin relaxation time. For the purposes here, the lineshape function can be simplified considerably:

$$Y = Y_{max} \frac{c}{d^2 + (\omega-\omega_o)^2} \qquad \text{(A-14)}$$

where Y_{max} equals A_{nom} when $c = d = 1$. For each incremental step of $(\omega-\omega_o)$ in Equation A-14, Equation A-12 is employed to determine A_{max} for the desired A_{nom} and chosen film geometry. The results are displayed graphically in Figures A-3 and A-4 for nominal absorbances of 1.50 and 2.00, respectively.

The results show that the highest nominal absorbances are affected the most by both irregular film thickness and incomplete coverage of the beam cross section. Films not filling the entire optical beam cross section cause a significant peak broadening with a reduction in amplitude.

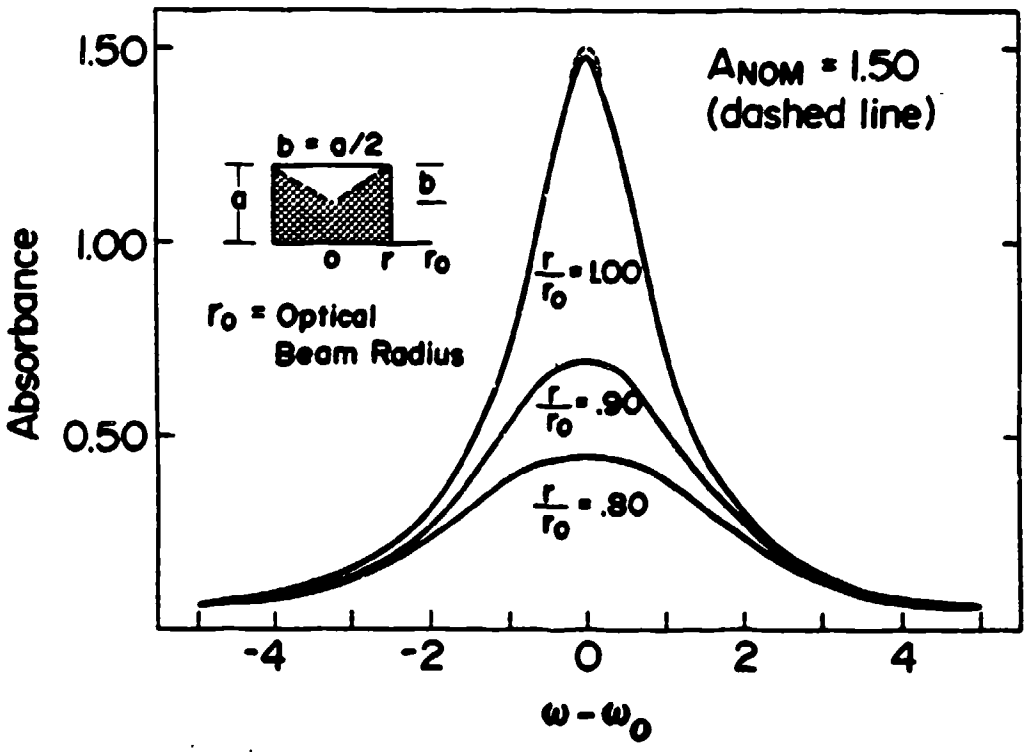

Figure A-3. Effect on a Lorentzian absorption peak with a nominal 1.50 absorbance when the optical film is of non-uniform thickness (shape as indicated) and when it fills various amounts of the optical beam.

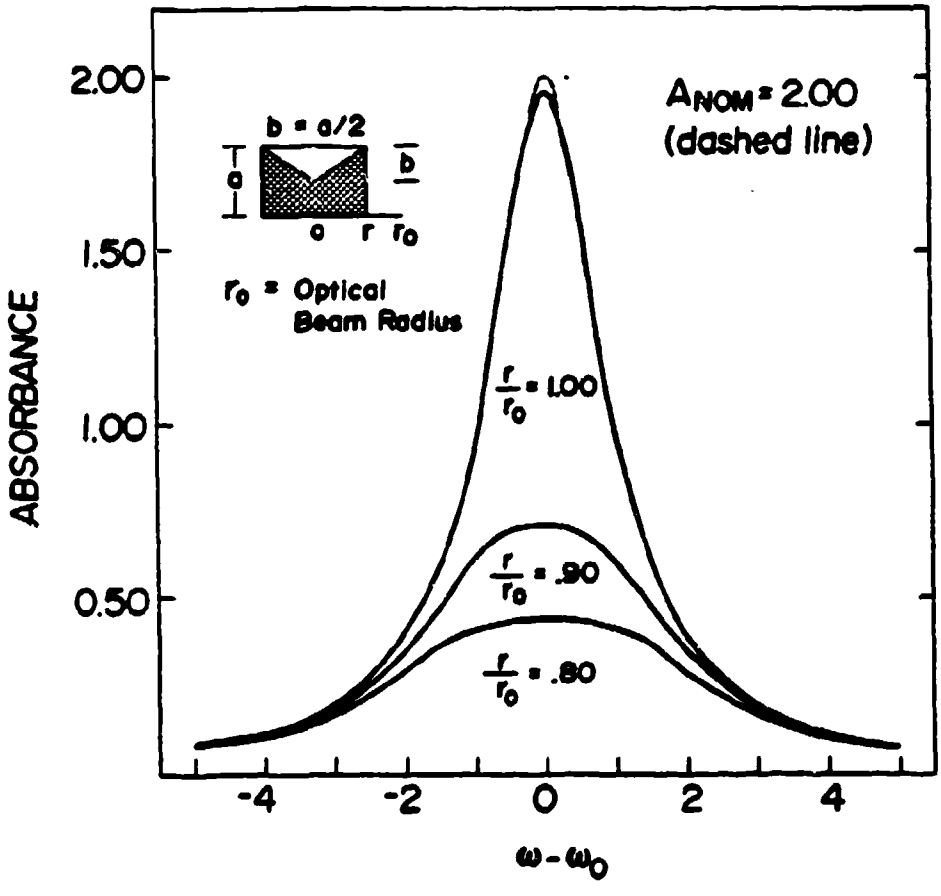

Figure A-4. Effect on a Lorentzian absorption peak with a nominal 2.00 absorbance when the optical film is of non-uniform thickness (shape as indicated) and when it fills various amounts of the optical beam.

However, most films in this study covered much of the optical cell walls, and with the beam passing through two walls, the probability of only 81% or 64% coverage as depicted in Figures A-3 and A-4 seems remote. It is very difficult to judge the uniformity of film thicknesses, so no one geometry in this study should be considered more likely than any other. It should be noted, however, that as films become very thin (the center of the disk for Table A-3 or the edges for Table A-4), the deviations from nominal absorbance become quite large.

BIBLIOGRAPHY

BIBLIOGRAPHY

1. W. Weyl, Ann. Phys., 197, 601 (1863) or Poggendorffs Annln., 121, 601 (1864).

2. J. L. Dye in "Progress in Macrocyclic Chemistry," Vol. 1, J. J. Christensen and R. M. Izatt (eds.), Wiley-Interscience (New York) 1979, Chap. 2.

3. J. L. Dye, M. G. DeBacker and V. A. Nicely, J. Am. Chem. Soc., 92, 5226 (1970).

4. J. L. Dye, M. T. Lok, F. J. Tehan, R. B. Coolen, N. Papadakis, J. M. Ceraso, and M. G. DeBacker, Ber. Bunsenges Phys. Chem., 75, 659 (1971).

5. J. L. Dye in "Electrons in Fluids, Colloque Weyl III," J. Jortner and N. R. Kestner (eds.), Springer-Verlag (Berlin) 1973, p. 77.

6. J. L. Dye, J. M. Ceraso, M. T. Lok, B. L. Barnett and F. J. Tehan, J. Am. Chem. Soc., 96, 608 (1974).

7. T. A. Beckman and K. S. Pitzer, J. Phys. Chem., 65, 1527 (1961).

8. J. A. Vanderhoff, E. W. LeMaster, W. H. McKnight, J. C. Thompson and P. R. Antoniewicz, Phys. Rev. A, 4, 427 (1971).

9. R. L. Schroeder, J. C. Thompson and P. L. Oertel, Phys. Rev., 178, 298 (1969).

10. K. D. Vos and J. L. Dye, J. Chem. Phys., 38, 2033 (1963).

11. R. Catterall, J. Chem. Phys., 43, 2262 (1965).

12. J. C. Thompson, "Electrons in Liquid Ammonia," Clarendon Press (Oxford) 1976.

13. C. A. Hutchison, Jr. and R. C. Pastor, J. Chem. Phys., 21, 1959 (1953).

14. E. Huster, Ann. Phys., 33, 477 (1938).

15. S. Freed and N. Sugarman, J. Chem. Phys., 11, 354 (1943).

16. J. P. Lelieur and P. Rigny, J. Chem. Phys., 59, 1142 (1973).

17. P. R. Marshall, J. Chem. Eng. Data, 7, 399 (1962).

18. W. S. Glaunsinger and M. J. Sienko, J. Chem. Phys., 62, 1883 (1975).

19. F. J. Dyson, Phys. Rev., 98, 349 (1955).

20. G. Feher and A. F. Kip, Phys. Rev., 98, 337 (1955).

21. R. H. Webb, Phys. Rev., 158, 225 (1967).

22. P. P. Edwards, A. R. Lusis and M. J. Sienko, J. Chem. Phys., 72, 3103 (1980).

23. J. R. Buntaine, M. J. Sienko and P. P. Edwards, J. Phys. Chem., 84, 1230 (1980).

24. P. P. Edwards, J. R. Buntaine and M. J. Sienko, Phys. Rev. B, 19, 5835 (1979).

25. R. B. Von Dreele, W. S. Glaunsinger, A. L. Bowman and J. L. Yarnell, J. Phys. Chem., 79, 2992 (1975).

26. W. S. Glaunsinger, J. Phys. Chem., 84, 1163 (1980).

27. In discussion following R. J. Peck and W. S. Glaunsinger, J. Phys. Chem., 84, 1176 (1980).

28. Reference 12, page 265.

29. L. Kevan, J. Phys. Chem., 84, 1232 (1980).

30. G. Dolivo and L. Kevan, J. Chem. Phys., 70, 2599 (1979).

31. L. Kevan, J. Chem. Phys., 56, 838 (1972).

32. L. Kevan, J. Phys. Chem., 79, 2846 (1975).

33. J. Paraszczak and J. E. Willard, J. Chem. Phys., 70, 5823 (1979).

34. J. E. Willard, J. Phys. Chem., 79, 2966 (1975).

35. E. F. Budzinski, W. R. Potter, G. Potienko and H. C. Box, J. Chem. Phys., 70, 5040 (1979).

36. H. C. Box and H. G. Freund, Appl. Spect., 34, 293 (1980).

37. D. F. Feng and L. Kevan, Chem. Rev., 80, 1 (1980).

38. T. Shida, S. Iwata and T. Watanabe, J. Phys. Chem., 76, 3683 (1972).

39. T. Shida, S. Iwata and T. Watanabe, J. Phys. Chem., 76, 3691 (1972).

40. A. Banerjee and J. Simons, J. Chem. Phys., 68, 415 (1978).

41. S. A. Rice, J. Phys. Chem., 84, 1280 (1980).

42. C. Kittel, "Introduction to Solid State Physics," 5th ed., John Wiley & Sons, Inc. (New York) 1976.

43. J. J. Markham, "F-Centers in Alkali Halides," Academic Press (New York) 1966.

44. C. K. Ong and J. M. Vail, Phys. Rev. B, 15, 3898 (1977).

45. R. S. Alger, "Electron Paramagnetic Resonance: Techniques and Applications," John Wiley & Sons, Inc. (New York) 1968.

46. W. Schmitt and U. Schindewolf, Ber. Bunsenges. Phys. Chem., 81, 584 (1977).

47. See, for example, N. F. Mott, Proc. Phys. Soc., A62, 416 (1949); Phil. Mag., 6, 287 (1961); Phil. Mag., 19, 835 (1969); and "Metal-Insulator Transitions," Taylor and Francis (London) 1974.

48. P. P. Edwards and M. J. Sienko, Phys. Rev. B, 17, 2575 (1978).

49. J. Hubbard, Proc. R. Soc., A276, 238 (1963); A277, 237 (1964); and A281, 401 (1964).

50. P. W. Anderson, Phys. Rev., 109, 1492 (1958) and Comments Sol. St. Phys., 1, 190 (1970).

51. B. Dietrich, J. M. Lehn and J. P. Sauvage, Tetrahedron Lett., 34, 2885 (1969).

52. J. M. Lehn and J. P. Sauvage, J. Am. Chem. Soc., 97, 6700 (1975).

53. J. L. Dye, J. Phys. Chem., 84, 1084 (1980).

54. J. L. Dye, Angew. Chem., Int. Ed. Engl., 18, 587 (1979).

55. J. L. Dye, C. W. Andrews and S. E. Mathews, J. Phys. Chem., 79, 3065 (1975).

56. J. L. Dye, J. Chem. Educ., 54, 332 (1977).

57. J. L. Dye, Pure Appl. Chem., 49, 3 (1977).

58. J. L. Dye, M. R. Yemen, M. G. DaGue and J. M. Lehn, J. Chem. Phys., 68, 1665 (1978).

59. F. B. Tehan, B. L. Barnett and J. L. Dye, J. Am. Chem. Soc., 96, 7203 (1974).

60. M. G. DaGue, J. S. Landers, H. L. Lewis and J. L. Dye, Chem. Phys. Lett., 66, 169 (1979).

61. J. L. Dye, M. G. DaGue, M. R. Yemen, J. S. Landers and H. L. Lewis, J. Phys. Chem., 84, 1096 (1980).

62. D. Moras and R. Weiss, Acta Cryst., B29, 400 (1973).

63. J. M. Lehn and F. Montavon, Tetrahedron Lett., 44, 4557 (1972).

64. M. G. DaGue, Ph.D. Dissertation, Michigan State University, 1979.

65. I. Hurley, T. R. Tuttle and S. Golden, J. Chem. Phys., 48, 2818 (1968).

66. Y. M. Cahen, J. L. Dye and A. I. Popov, J. Phys. Chem., 79, 1292 (1975).

67. J. E. Young, Jr., Ph.D. Dissertation, Cornell University, 1970.

68. B. S. Deaver, Jr., C. M. Falco, J. H. Harris and S. A. Wolf (eds.), "Future Trends in Superconductive Electronics (Charlottesville, 1978)," AIP Conference Proceedings No. 44, American Institute of Physics (New York) 1978, p. 59.

69. J. E. Wertz and J. R. Bolton, "Electron Spin Resonance: Elementary Theory and Practical Applications," McGraw-Hill (New York) 1972.

70. Comments by R. Catterall following Reference 61.

71. M. T. Lok, Ph.D. Dissertation, Michigan State University, 1973.

72. M. R. Yemen, private communication.

73. A similar device is depicted in Reference 71, page 179. This apparatus was constructed by Van Eck and Lewis as noted in Reference 74.

74. The hydrogen evolution device was assembled by Mr. Bradley Van Eck and Dr. H. L. Lewis following the method of Dewald and Dye: R. R. Dewald and J. L. Dye, J. Phys. Chem., 68, 128 (1964).

75. F. Feigl and V. Anger (eds.), "Spot Tests in Inorganic Analysis," 6th English Ed., Elsevier Publishing (New York) 1972.

76. H. Aulich, L. Nemec and P. Delahay, J. Chem. Phys., 61, 4235 (1974).

77. D. F. Burow and J. J. Lagowski, J. Phys. Chem., 72, 169 (1968).

78. R. E. Honig and H. O. Hook, RCA Review, 21, 360 (1960); the data for ammonia was based primarily upon R. Overstreet and W. F. Giauque, J. Am. Chem. Soc., 59, 254 (1937).

79. R. E. Rondeau, J. Chem. Eng. Data, 11, 124 (1966).

80. K. Bar-Eli and G. Gabor, J. Phys. Chem., 77, 323 (1973).

81. E. Mei, A. I. Popov and J. L. Dye, J. Am. Chem. Soc., 99, 6532 (1977).

82. B. Bockrath, J. F. Gavias and L. M. Dorfman, J. Phys. Chem., 79, 3064 (1975).

83. C. P. Poole, Jr., "Electron Spin Resonance - A Comprehensive Treatise on Experimental Techniques," Interscience Publishers, Inc. (New York) 1967.

84. N. S. VanderVen, Phys. Rev., 168, 787 (1968).

85. T. Chang and A. H. Kahn, National Bureau of Standards Special Publication 260-59: "Standard Reference Materials: Electron Paramagnetic Resonance Intensity Standard: SRM-2601; Description and Use," U.S. Department of Commerce (Washington, D.C.) 1978.

86. B. G. Segal, M. Kaplan and G. K. Fraenkel, J. Chem. Phys., 43, 4191 (1965).

87. A. H. Morrish, "The Physical Principles of Magnetism," John Wiley & Sons, Inc. (New York) 1965.

88. J. L. Dye and V. A. Nicely, J. Chem. Educ., 48, 443 (1971).

89. W. Wojciechowski, Inorg. Chim. Acta., 1, 319 (1967).

90. T. Oguchi, Prog. Theor. Phys., 13, 148 (1955).

91. H. Ohya-Nishiguchi, Bull. Chem. Soc. Jpn., 52, 3480 (1979).

92. J. C. Thompson, private communication based on reflectance spectra in Reference 8.

93. J. M. Ceraso, P. B. Smith, J. S. Landers and J. L. Dye, J. Phys. Chem., 81, 760 (1977).

94. H. L. Lewis, private communication.

95. E. Mei, L. Liu, J. L. Dye and A. I. Popov, J. Solution Chem., 6, 771 (1977).

96. E. Kaufmann, J. L. Dye, J. M. Lehn and A. I. Popov, J. Am. Chem. Soc., 102, 2274 (1980).

97. M. G. DeBacker and J. L. Dye, J. Phys. Chem., 75, 3092 (1971).